# รายงานการวิจัยฉบับสมบูรณ์

ผลกระทบของโครงสร้างนาโนและสัณฐานของอนุภาคเขม่าต่อเคมีจลศาสตร์

จากการเผาไหม้จากเชื้อเพลิงชีวภาพ

IMPACT OF MORPHOLOGY AND NANOSTRUCTURE ON

PARTICULATE MATTER'S OXIDATION KINETICS FROM

BIOFUEL COMBUSTION

ผศ.ดร. ปรีชา การินทร์

งานวิจัยนี้ได้รับทุนสนับสนุนงานวิจัย
จากงบประมาณเงินรายได้ประจำปีงบประมาณ พ.ศ. 2560
วิทยาลัยนานาชาติ
สถาบันเทคโนโลยีพระจอมเกล้าเจ้าคุณทหารลาดกระบัง

This material is reserved for educational use only, not allowed for commercial use.
Forbidden to modify the content, and cite the document when use.

| | |
|---|---|
| **ชื่อโครงการ** | **ผลกระทบของโครงสร้างนาโนและสัณฐานของอนุภาคเขม่าต่อเคมีจลศาสตร์จากการเผาไหม้จากเชื้อเพลิงชีวภาพ**<br>IMPACT OF MORPHOLOGY AND NANOSTRUCTURE ON PARTICULATE MATTER'S OXIDATION KINETICS FROM BIOFUEL COMBUSTION |
| **แหล่งเงิน** | งบประมาณรายได้ วิทยาลัยนานาชาติ |
| **ประจำปีงบประมาณ** | 2560 จำนวนเงินที่ได้รับการสนับสนุน 100,000 บาท |
| **ระยะเวลาทำการวิจัย** | 1 ปี ตั้งแต่ 1 ตุลาคม 2559 ถึง 31 กันยายน 2560 |
| **หัวหน้าโครงการ** | ผศ.ดร. ปรีชา การินทร์ |
| **หน่วยงานต้นสังกัด** | วิทยาลัยนานาชาติ<br>aeautolab@gmail.com@gmail.com |

King Mongkut's Institute of Technology Ladkrabang

This material is reserved for educational use only, not allowed for commercial use.
Forbidden to modify the content, and cite the document when use.

**RESEARCH REPORT**

# IMPACT OF MORPHOLOGY AND NANOSTRUCTURE ON PARTICULATE MATTER'S OXIDATION KINETICS FROM BIOFUEL COMBUSTION

**ASST. PROF. DR. PREECHAR KARIN**

**FISCAL YEAR 2017**

**INTERNATIONAL COLLEGE**

**KING MONGKUT'S INSTITUTE OF TECHNOLOGY LADKRABANG**

This material is reserved for educational use only, not allowed for commercial use.
Forbidden to modify the content, and cite the document when use.

## ABSTRACT

It is well known that diesel engines have the highest thermal efficiency at same load conditions compared with other internal combustion engines but their disadvantage is Particulate Matter (PM) emission. Since particulate matters can be harmful to human health, it is necessary to be eradicated from exhaust gas before emitted to atmosphere. This research is divided into two parts. The first part relates to effects of combustion characteristics of Biodiesel and Ethanol blended fuel on particulate matter emission. Experimental results show that ethanol-blended fuel helps in further reduction of particulate emission by 58.6% compared with base biodiesel. The second part focuses on properties of particulate matters emitted from combustion. Relationships of PM's morphology, nanostructure, and oxidation kinetics were investigated. Application of Scanning Electron Microscope (SEM), Transmission Electron Microscope (TEM) and Thermo-Gravimetric Analysis (TGA) was adopted in the analysis. From the experiment, shorter carbon crystallite structure in the soot emitted from ethanol-blended fuel shows strong relationship with reduction of soot activation energy at 79 kJ/mol. That means functional groups in the ethanol-blended fuel play an important role in soot oxidation. Results of this research are expected as useful information for further research in fields of biofuel especially ethanol related particulate matters.



Keywords: Particulate Matter (PM), Diesel Engine, Ethanol, Biodiesel,



This material is reserved for educational use only, not allowed for commercial use.
Forbidden to modify the content, and cite the document when use.

## TABLE OF CONTENTS




This material is reserved for educational use only, not allowed for commercial use.

Forbidden to modify the content, and cite the document when use.

This material is reserved for educational use only, not allowed for commercial use.
Forbidden to modify the content, and cite the document when use.

# CHAPTER 1

# INTRODUCTION

## 1.1 Research Background

Nowadays, shortage of energy is one of main problem in the world. The global energy demand, reported by International Energy Agency, has been increasing continuously. The energy demand to year 2030 of transportation sector is growing approximately 1.7% yearly as shown in Fig. 1.1 and the energy from oil is 36 % of global energy usage which the biggest factor as shown in Fig. 1.2. Thus, renewable energy usage is one of solutions for the crisis. It is well known that diesel engines have high thermal efficiency mainly due to high compression ratio compared with other internal combustion engines at the same load. Applying diesel vehicles in transportation sector is an alternative to increase efficiency of limited liquid fossil fuel in the world. However, main pollutants from diesel engines are solid particles (Particulate Matter or PM) and nitrogen oxide (NOx) [1]. Pollutants should be removed from exhaust gas because of their effects on environment and human health, such as lung cancer. Hence, regulations of pollution standard for diesel emission are proper way to control the emission that emitted to the atmosphere.

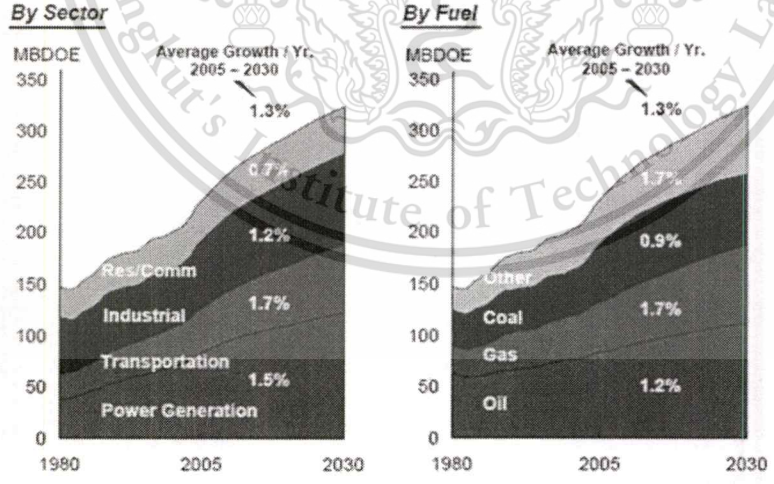


**Figure 1.1** Global energy demands, View to the year 2030 [2]

This material is reserved for educational use only, not allowed for commercial use.
Forbidden to modify the content, and cite the document when use.

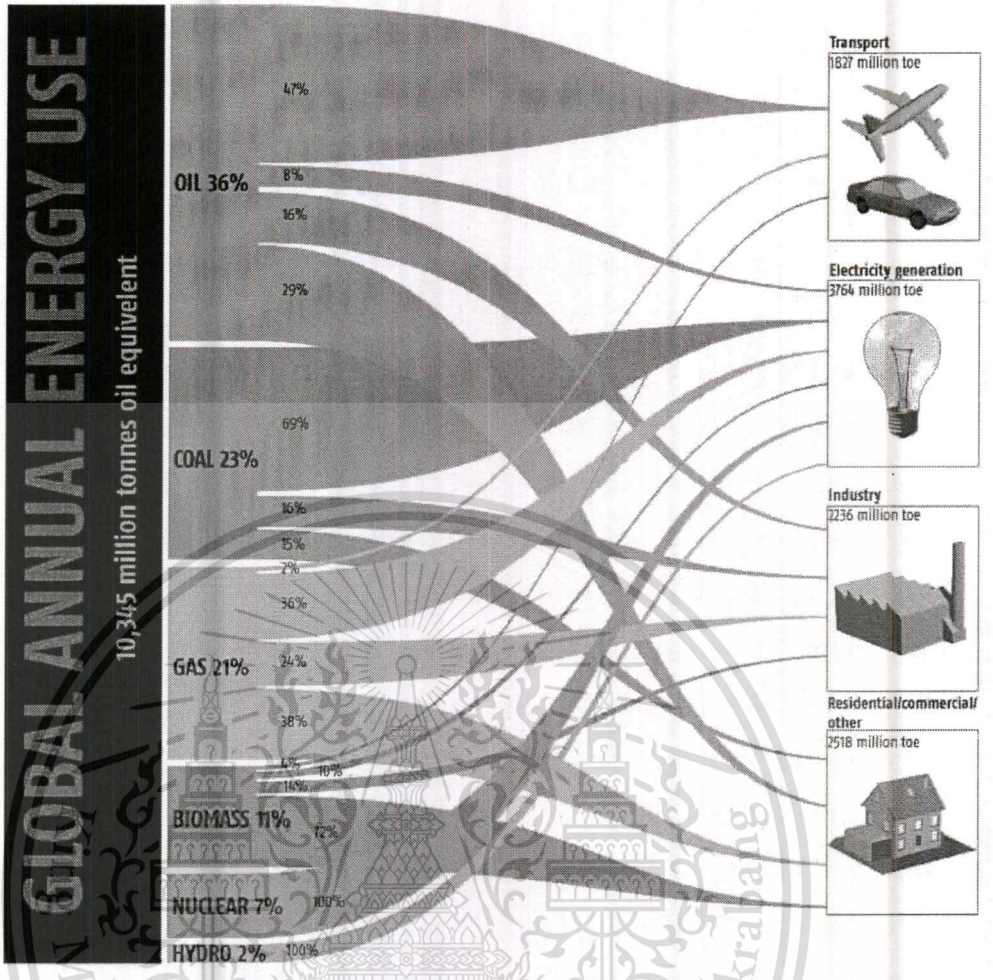


**Figure 1.2** World energy use and the sectorial split of fuel use [3]

Since 2012, Thai government has adopted Thailand Industrial Standard of level 7 (TIS 2160-2543) for small diesel engine vehicles which is equivalent to Euro 4 emission standard in order to control exhaust gas emission from diesel engines especially particulate matter. Figure 1.3 shows EU emission standard for diesel's passenger vehicles. Euro 4 restricts Particulate Matter (PM) emission at less than 0.025 g/km. However, trends of pollutant control in Thailand are going to be more severe in the near future (Euro 5 or Euro 6).

This material is reserved for educational use only, not allowed for commercial use.
Forbidden to modify the content, and cite the document when use.

| Stage | Date | CO | HC | HC+NOx | NOx | PM | PN |
|---|---|---|---|---|---|---|---|
| | | g/km | | | | | #/km |
| **Compression Ignition (Diesel)** | | | | | | | |
| Euro 1† | 1992.07 | 2.72 (3.16) | - | 0.97 (1.13) | - | 0.14 (0.18) | - |
| Euro 2, IDI | 1996.01 | 1.0 | - | 0.7 | - | 0.08 | - |
| Euro 2, DI | 1996.01[a] | 1.0 | - | 0.9 | - | 0.10 | - |
| Euro 3 | 2000.01 | 0.64 | - | 0.56 | 0.50 | 0.05 | - |
| Euro 4 | 2005.01 | 0.50 | - | 0.30 | 0.25 | 0.025 | - |
| Euro 5a | 2009.09[b] | 0.50 | - | 0.23 | 0.18 | 0.005[f] | - |
| Euro 5b | 2011.09[c] | 0.50 | - | 0.23 | 0.18 | 0.005[f] | $6.0\times10^{11}$ |
| Euro 6 | 2014.09 | 0.50 | - | 0.17 | 0.08 | 0.005[f] | $6.0\times10^{11}$ |

**Figure 1.3** EU Emission Standards for Diesel passenger cars [4]

Source: https://www.dieselnet.com/standards/eu/ld.php#intro

The biofuel such as biodiesel or bioethanol have been often discussed as alternatives for diesel fuel replacement since they are obtained from renewable sources and can be re-produced faster than fossil fuel. Biodiesel consists of alkyl monoesters of fatty acids derived from vegetable oil or animal fats. Since its similar physical properties to diesel fuel, there is no need to modify the engine when the engine is fueled with the blends [JSAE 2-4, 5-7]. Regarding biodiesel situation in Thailand, Thai government are promoting usage of biodiesel in transportation sectors since it can be produced with domestic agriculture product of palm oil, jatropha oil, and etc.

Another benefit of biodiesel in diesel replacement is emission reduction. Biodiesel has low sulfur and aromatic hydrocarbon content. Besides, biodiesel has oxygen atoms in fuel molecules and also acts like environmental friendly fuel. Oxygen content in biodiesel fuel promotes more complete combustion than fossil fuel that means it emit low amount of particulate matter. Referred from KMITL previous researches, they are in accord with above statement that biodiesel contribute in less particulate matter emission. Figure 1.4 and Figure 1.5 show that use of biodiesel can substantially produce less smoke emission compared with diesel.

Bioethanol or ethanol is a low cost oxygenated fuel with comparatively high oxygen content. It is composed of the homogeneous chemical compound ($C_2H_5OH$) whether it is produced from sugar-based feedstock or from agricultural residues [(https://energy.gov/eere/energybasics/articles/ethanol-fuel-basics), 8]. Ethanol is a high-octane fuel. So, it obviously cannot be replaced with diesel. However, it can be applied in forms of blend, dual injection, or ethanol fumigation into the intake port. In

This material is reserved for educational use only, not allowed for commercial use.
Forbidden to modify the content, and cite the document when use.

terms of emission reduction, especially particulate matter, high oxygen content is being considered to bring some PM reduction [(https://www.dieselnet.com/tech/fuel_ediesel.php), 9].

From above advantages of biofuels regarding emission reduction, this research aimed to study effects of ethanol on further reduction of particulate matter from biodiesel in order to prepare for more severe emission control standard.

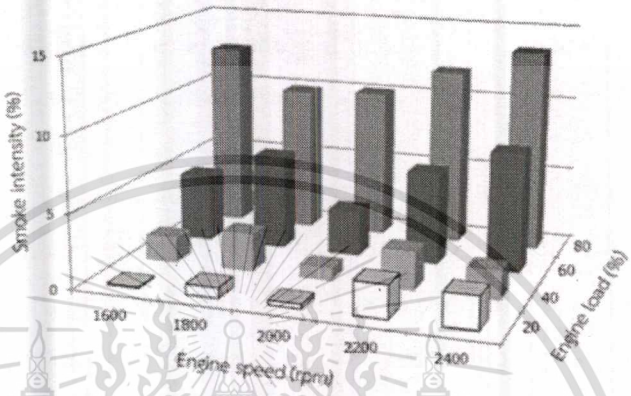


(a) Diesel engine's particulate matters

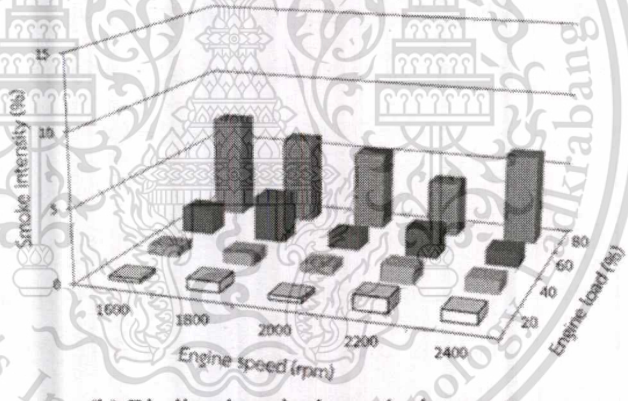


(b) Biodiesel engine's particulate matters

**Figure 1.4** Quantity of (a) Diesel engine's PMs and (b) Biodiesel engine's PMs using opacity smoke meter in each engine load and engine speed operation condition

[Source : International Journal of Automotive Technology, Vol. 18, No. 1, pp. 31−40 (2017) DOI 10.1007/s12239−017−0003−y, 10]

This material is reserved for educational use only, not allowed for commercial use.
Forbidden to modify the content, and cite the document when use.

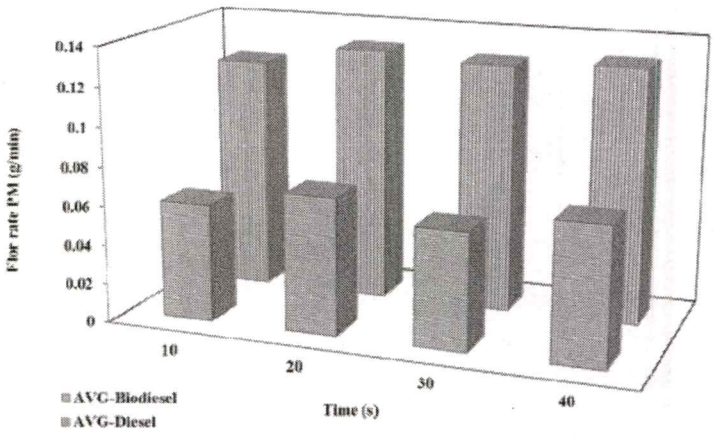


**Figure 1.5** Average particulate matter flow rate of diesel (blue) and biodiesel (red)

[Source : **JSAE 20159821 / SAE 2015-32-0821, 11]**

King Mongkut's Institute of Technology Ladkrabang

This material is reserved for educational use only; not allowed for commercial use.
Forbidden to modify the content, and cite the document when use.

## 1.2 Objectives

- To clarify impact of ethanol on diesel engine's Particulate Matter(PM) emission quantity
- To compare PM's morphology and nanostructure produced from ethanol-blended biodiesel fuel and biodiesel fuel (and diesel fuel)
- To explain relationships between PM's morphology/nanostructure and oxidation kinetics of ethanol-blended biodiesel fuel and to compare with biodiesel and diesel

## 1.3 Scope of work

This research focuses on effects of bio-oxygenated fuel, especially ethanol, on combustion and Particulate Matter (PM) emission characteristics in a small diesel engine. Since unique properties compared with conventional diesel fuel, few percentage of ethanol was blended with palm biodiesel to keep compatibility in fuel properties with biodiesel and diesel fuel. Engine performance and in-cylinder combustion behavior e.g. combustion pressure and heat release rate were investigated. Then, PM analysis was conducted in terms of emission quantity and PM morphology. PM morphology was investigated up to nanostructure level. In the final part, PM was analyzed in a viewpoint of oxidation kinetics by TGA method. Highlight of this research is aimed to get insights of relationships between PM nanostructure and oxidation kinetics i.e. roles of biofuel's PM nanostructure, especially ethanol on the oxidation reactivity.

This material is reserved for educational use only, not allowed for commercial use.
Forbidden to modify the content, and cite the document when use.

# CHAPTER 2

# RESEARCH THEORY AND LITERATURE REVIEW

## 2.1 Diesel engine

A conventional internal combustion diesel engine works on "Diesel Cycle". In the simple diesel engines, an injector injects fuel into the combustion chamber above the piston directly. Diesel engines are also commonly known as Compression-Ignition engines; since the diesel is burned due to hot compressed air. The temperature of the air inside the combustion chamber rises to above 400°c to 800°c, which in turn, ignites the diesel which was injected into the combustion chamber. The 'Diesel Cycle' does not use an external mechanism such as a spark-plug to ignite the air-fuel mixture. The principle of diesel cycle can be divided in to 4 stoke, as shown in figure2.1.

1. Suction – With pistons moving downwards and opening of the inlet valve creates suction of clean air into the cylinders.

2. Compression – With closing of Inlet valve the area above the piston gets closed. The piston moves up resulting in compression of the air in a confined space under higher compression-ratio.

3. Combustion – At this stage the injector sprays the diesel into the combustion chamber. The rise in temperature of the air caused by its compression; results in instantaneous burning of diesel with in an explosion. This causes heat to release resulting in generation of expanding forces known as power. These forces again push the pistons downwards resulting in their reciprocating motion.

4. Exhaust– On their way up, the pistons push the exhaust gases above them thru' the exhaust valve which opens during exhaust stroke.

This material is reserved for educational use only, not allowed for commercial use.
Forbidden to modify the content, and cite the document when use.

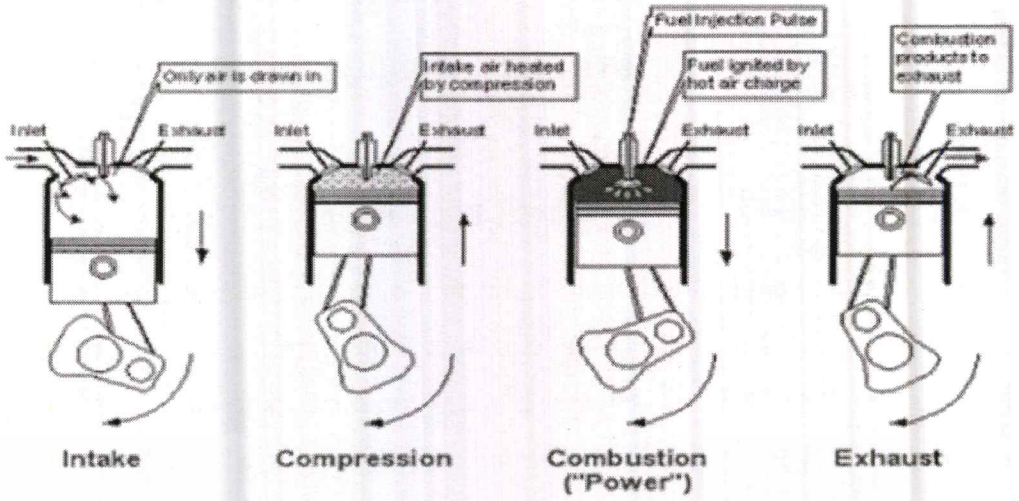


**Figure 2.1** Diesel cycle [12]

The heat release rate as shown in Fig. 2.2 in the combustion stoke of diesel cycle has 4 stage which consist of ignition delay phase, premixed combustion phase, mixing-controlled combustion phase and late combustion phase. The heat release rate explain the process as

- Ignition Delay Phase, a - b is the time period since the start of fuel injection in the combustion chamber until the fuel ignited.

- Premixed Combustion Phase, b - c is the time duration of the premixed fuel combustion after ignition delay phase which will initiate the rapid auto - ignition and increase heat release rate.

- Diesel Fuel Performance Mixing Combustion Phase, c - d is occurred in combustion chamber after the completely burned of premixed fuel. The combustion rate will be controlled by the formation rate of mixture between air - fuel that ready to be burned.

- Late Combustion Phase, d - e is the period that the heat release rate is low during the exhaust stroke. It is the combustion of the rest of the fuel and carbon residue which previously generated from the rich mixture.

This material is reserved for educational use only, not allowed for commercial use.
Forbidden to modify the content, and cite the document when use.

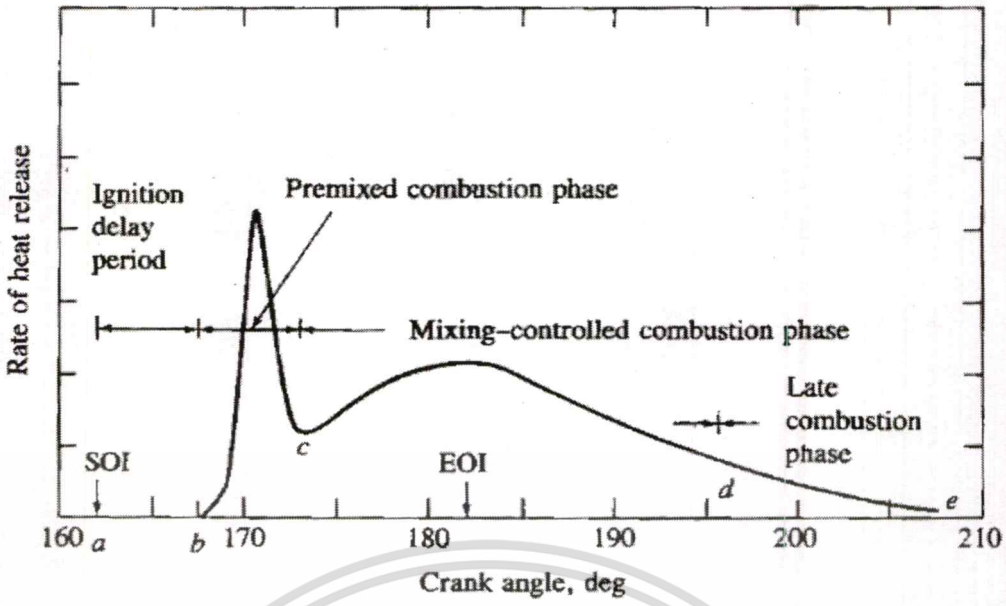


**Figure 2.2** Stage of heat release rate [13]

## 2.2 Emission of diesel engine

Diesel engines convert the chemical energy contained in the fuel into mechanical power. Diesel fuel is injected under pressure into the engine cylinder where it mixes with air and where the combustion occurs. The exhaust gases which are discharged from the engine contain several constituents that are harmful to human health and to the environment. By the emission of diesel engine consist of CO, HC, NOx, SO2 and particulate matter as shown on eqn. 2.1 [14] and Fig. 2.3 shows the combustion phenomena in combustion chamber.

$$C_xH_y + AIR \rightarrow aCO_2 + bH_2O + cCO + dC_{(s)} + mHC_{(l)} + nNO_x \quad (2.1)$$

This material is reserved for educational use only, not allowed for commercial use.
Forbidden to modify the content, and cite the document when use.

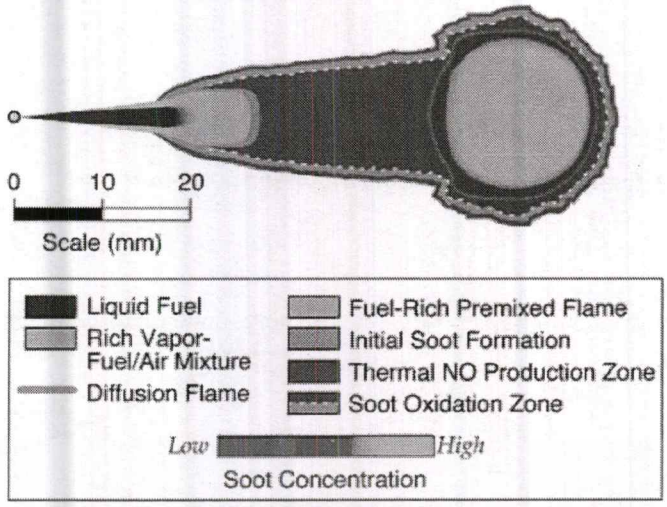


**Figure 2.3** Diesel combustion flame zone [14]

Carbon monoxide (CO), hydrocarbons (HC), and aldehydes are generated in the exhaust as the result of incomplete combustion of fuel. A significant portion of exhaust hydrocarbons is also derived from the engine lube oil. When engines operate in enclosed spaces, such as underground mines, buildings under construction, tunnels or warehouses, carbon monoxide can accumulate in the ambient atmosphere and cause headaches, dizziness and lethargy. Under the same conditions, hydrocarbons and aldehydes cause eye irritation and choking sensations. Hydrocarbons and aldehydes are major contributors to the characteristic diesel smell. Hydrocarbons also have a negative environmental effect, being an important component of smog.

Nitrogen oxides (NOx) are generated from nitrogen and oxygen under the high pressure and temperature conditions in the engine cylinder. NOx consist mostly of nitric oxide (NO) and a small fraction of nitrogen dioxide (NO2). Nitrogen dioxide is very toxic. NOx emissions are also a serious environmental concern because of their role in the smog formation.

Sulfur dioxide (SO2) is generated from the sulfur present in diesel fuel. The concentration of SO2 in the exhaust gas depends on the sulfur content of the fuel. Low sulfur fuels of less than 0.05% sulfur are being introduced for most diesel engine applications. Sulfur dioxide is a colorless toxic gas with a characteristic, irritating odor. Oxidation of sulfur dioxide produces sulfur trioxide which is the precursor of sulfuric acid which, in turn, is responsible for the sulfate particulate matter emissions.

This material is reserved for educational use only, not allowed for commercial use.
Forbidden to modify the content, and cite the document when use.

Sulfur oxides have a profound impact on environment being the major cause of acid rains.

Particulate matter (PM) is a complex aggregate of solid and liquid material. Its origin is carbonaceous particles generated in the engine cylinder during combustion. The primary carbon particles form larger agglomerates and combine with several other, both organic and inorganic, components of diesel exhaust.

## 2.3 Particulate matter

Particulate matter (PM) is the most important characteristics of diesel emissions which is responsible for black smoke traditionally associated with diesel powered vehicles. Diesel particulate matter emission is usually abbreviated as PM or DPM. Size of PM particles can be classified into various categories. Particles which normally found in atmosphere are called PM10, diameter (D) < 10 μm; fine particles, D < 2.5 μm; ultrafine particles, D < 0.10 μm; and nanoparticles, D < 50 nm [15, (D. B. Kittelson, 1998)]. Detailed information of particulate matter is to be referred in the literature review session of "2.6.2 Particulate matter morphology and nanostructure".

## 2.4 Alternative fuel

Renewable bio-oxygenated fuels – liquid and gaseous fuels derived from organic matter – can play an important role in reducing CO2 emissions (greenhouse gas effect and global warming) because of bio-fuels is the carbon neutral, as shown in Fig 2.4.

To reduce dependency on oil and to contribute to growing efforts to decarbonize the transport sector, bio-fuels release shifting to low-carbon, non-petroleum fuels, often with minimal changes to vehicle stocks and distribution infrastructure. While improving vehicle efficiency is by far the most important low-cost way of reducing CO2 emissions in the transport sector, bio-fuels will need to play a significant role in replacing liquid fossil fuels suitable for planes, marine vessels and other heavy transport modes that cannot be electrified. Production and use of bio-fuel can also provide benefits such as increased energy security, by reducing dependency on oil imports, and reducing oil price volatility. In addition, bio-fuels can

This material is reserved for educational use only, not allowed for commercial use.
Forbidden to modify the content, and cite the document when use.

support economic development by creating new sources of income in rural areas, as shown in Fig 2.5.

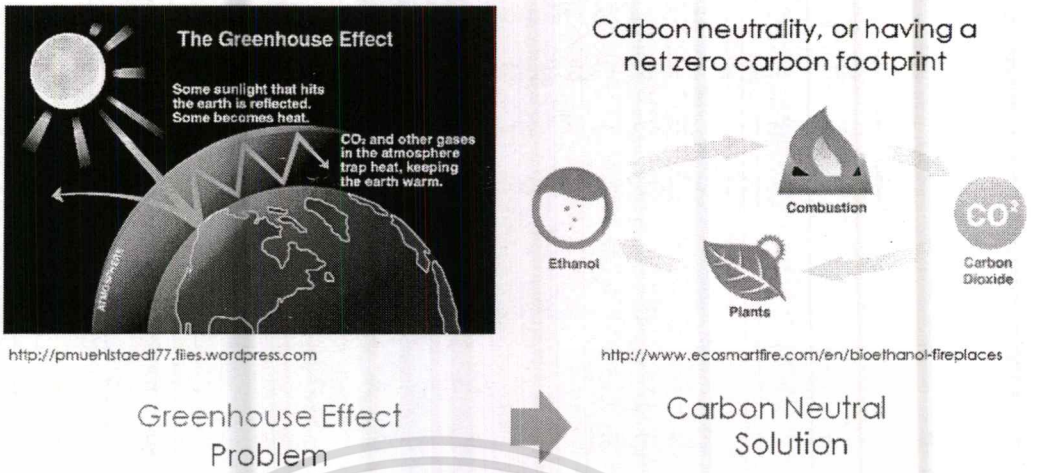


**Figure 2.4** The greenhouse effect (Carbon dioxide) and the concept of carbon neutral of renewable bio-oxygenated fuels [16]

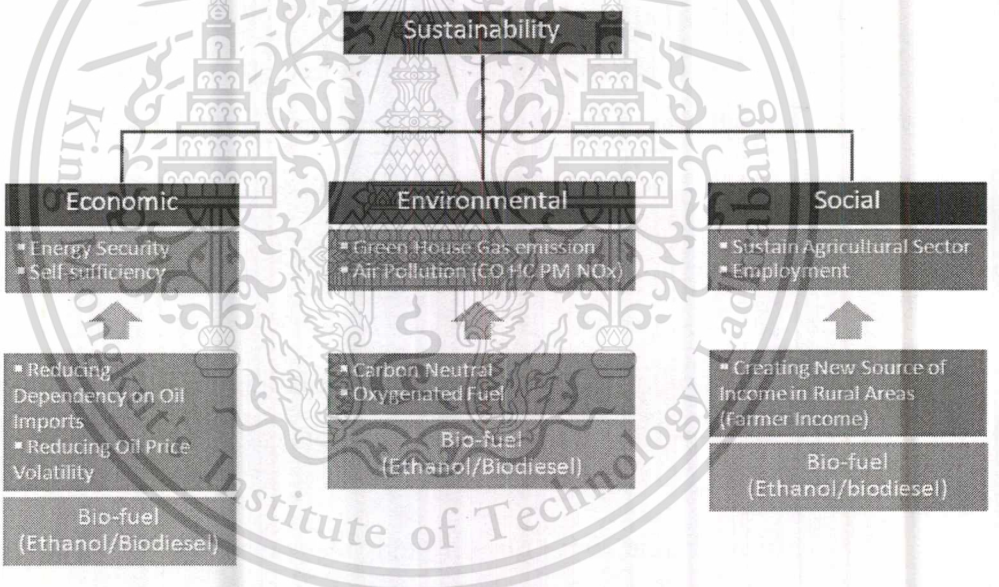


**Figure 2.5** Summary of influent of renewable bio-oxygenated fuel (Ethanol and Biodiesel) for economic, environmental and social [17]

2.4.1 Biodiesel

Biodiesel is an alternative fuel for diesel engines that is produced by chemically reacting a vegetable oil or animal fat with an alcohol such as methanol. The reaction requires a catalyst, usually a strong base, such as sodium or potassium hydroxide, and produces new chemical compounds called methyl esters. It is these esters that have come to be known as biodiesel. Because its primary feedstock is a

This material is reserved for educational use only, not allowed for commercial use.
Forbidden to modify the content, and cite the document when use.

vegetable oil or animal fat, biodiesel is generally considered to be renewable. Since the carbon in the oil or fat originated mostly from carbon dioxide in the air, biodiesel is considered to contribute much less to global warming than fossil fuels. Diesel engines operated on biodiesel have lower emissions of carbon monoxide, unburned hydrocarbons, particulate matter, and air toxics than when operated on petroleum-based diesel fuel. Biodiesel is produced through a process known as transesterification, as shown in Fig 2.6. By R1, R2, and R3 are long hydrocarbon chains, sometimes called fatty acid chains. There are only five chains that are most common in soybean oil and animal fats (others are present in small amounts) [18].

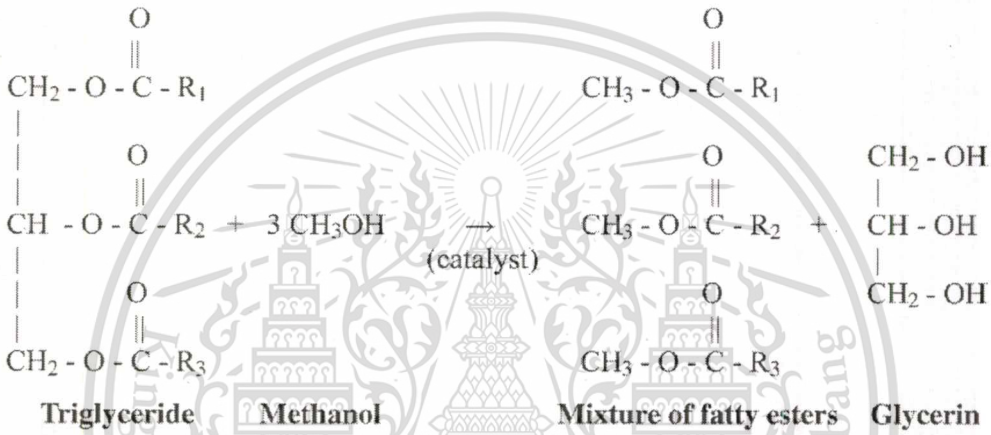


**Figure 2.6** Transesterification of Vegetable Oil to Biodiesel [18]

2.4.2 Ethanol

Ethanol is a clear liquid alcohol that is made by the fermentation of different biological materials. This alcohol is known to have many uses, but one in particular is becoming more popular. Ethanol, the most widely used biofuel, is made in a process similar to brewing beer. The ethanol in the end is blended with gasoline to improve vehicle performance and reduce air pollution. Ethanol is the most important member of a large group of organic compounds that are called alcohols. Alcohol is an organic compound that has one or more hydroxyl (OH) groups attached to a carbon atom. Alcohol is shown as: C-O-H or C-OH. What is attached to the carbon at the three remaining bonds or locations determines the particular kind of alcohol. Ethanol has hydrogen present at two sites while the remaining site holds another carbon atom. This carbon atom, in turn, holds three more hydrogen atoms. It may be shown as Fig. 2.7.

This material is reserved for educational use only, not allowed for commercial use.
Forbidden to modify the content, and cite the document when use.

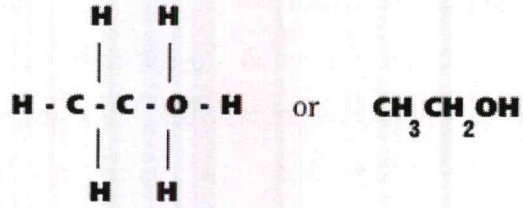


**Figure 2.7** Chemical formula of ethanol [19]

## 2.5 Technical analysis

2.5.1 Scanning electron microscope

The scanning electron microscope (SEM) uses a focused beam of high-energy electrons to generate a variety of signals at the surface of solid specimens. The signals that derive from electron-sample interactions reveal information about the sample including external morphology (texture), chemical composition, and crystalline structure and orientation of materials making up the sample. In most applications, data are collected over a selected area of the surface of the sample, and a 2-dimensional image is generated that displays spatial variations in these properties. Areas ranging from approximately 1 cm to 5 microns in width can be imaged in a scanning mode using conventional SEM techniques (magnification ranging from 20X to approximately 30,000X, spatial resolution of 50 to 100 nm). The main SEM components include: Source of electrons, Column down which electrons travel with electromagnetic lenses, Electron detector, Sample chamber and Computer and display to view the images as shown in Fig. 2.8. Electrons are produced at the top of the column, accelerated down and passed through a combination of lenses and apertures to produce a focused beam of electrons which hits the surface of the sample. The sample is mounted on a stage in the chamber area and, unless the microscope is designed to operate at low vacuums, both the column and the chamber are evacuated by a combination of pumps. The level of the vacuum will depend on the design of the microscope. The position of the electron beam on the sample is controlled by scan coils situated above the objective lens. These coils allow the beam to be scanned over the surface of the sample. This beam scanning, as the name of the microscope suggests, enables information about a defined area on the sample to be collected. As a result of the electron-sample interaction, a number of signals are produced. These signals are then detected by appropriate detectors.

This material is reserved for educational use only, not allowed for commercial use.
Forbidden to modify the content, and cite the document when use.

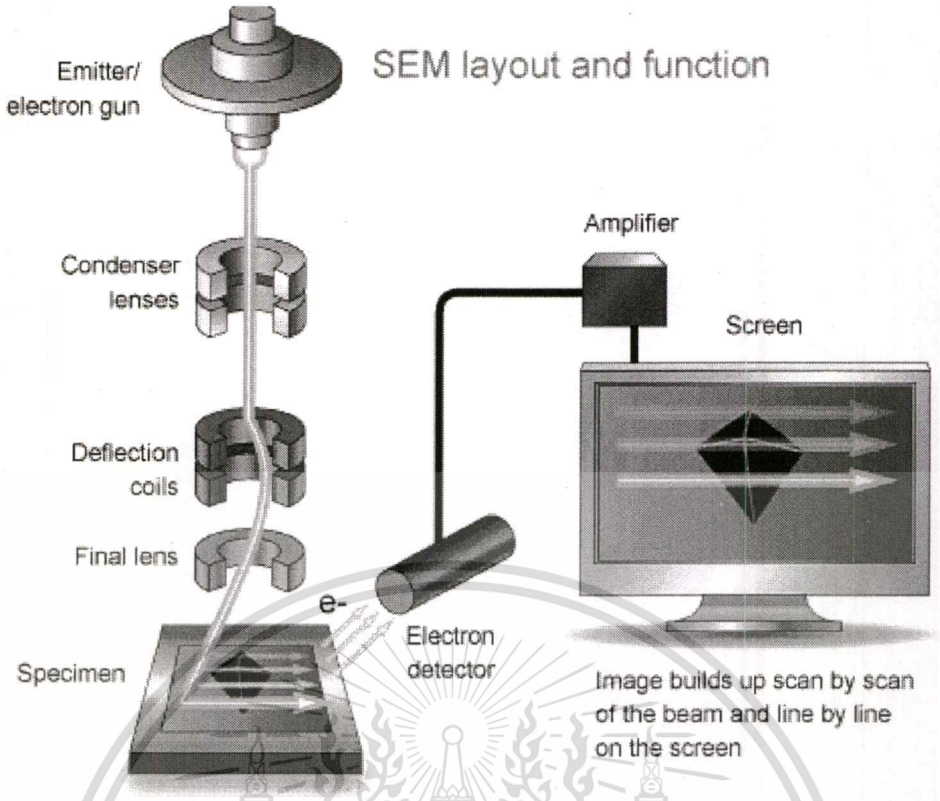


**Figure 2.8** Schematics of scanning electron microscopy operation [20]

2.5.2 Transmission electron microscope

The transmission electron microscope (TEM) is a very powerful tool for material science. Figure 2.9 shows schematic of transmission electron microscopy operation by a high energy beam of electrons is shone through a very thin sample, and the interactions between the electrons and the atoms can be used to observe features such as the crystal structure and features in the structure like dislocations and grain boundaries. Chemical analysis can also be performed. TEM can be used to study the growth of layers, their composition and defects in semiconductors. High resolution can be used to analyze the quality, shape, size and density of quantum wells, wires and dots. The TEM operates on the same basic principles as the light microscope but uses electrons instead of light. Because the wavelength of electrons is much smaller than that of light, the optimal resolution attainable for TEM images is many orders of magnitude better than that from a light microscope. Thus, TEMs can reveal the finest details of internal structure - in some cases as small as individual atoms.

This material is reserved for educational use only, not allowed for commercial use.
Forbidden to modify the content, and cite the document when use.

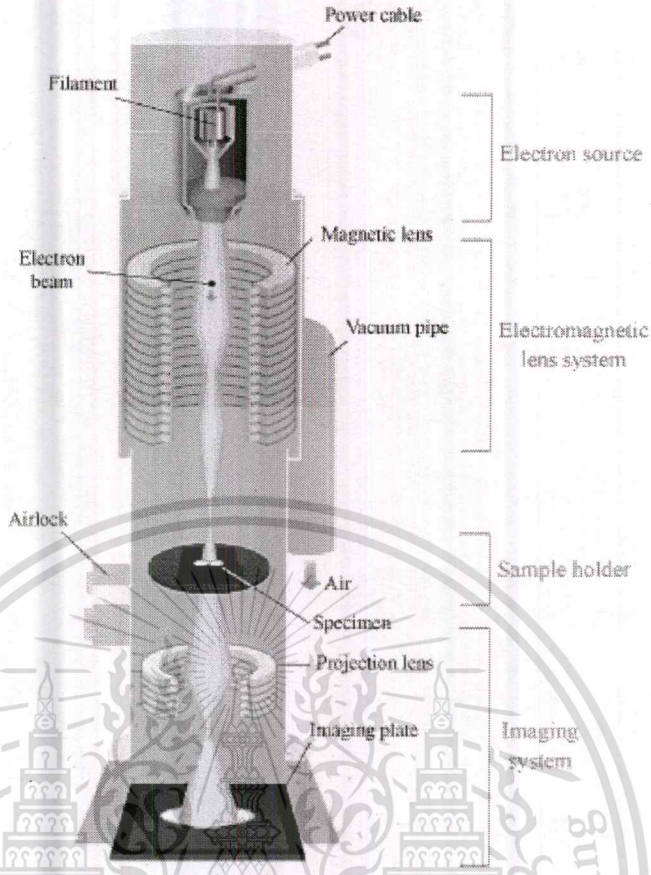


**Figure 2.9** Schematics of transmission electron microscopy operation [21]

In the TEM, when a beam of electrons of high energy strikes a thin sample then most of the electrons pass through it. These are called transmitted electrons and include both undeflected and deflected electrons. The beam of electrons which passes through the sample without any deflection from its original direction is focused at the back focal plane (BFP) of the objective lens parallel to the optical axis and is called direct beam as shown in Fig. 2.10 [22]. The other electrons which are scattered at certain angles are focused off-axis at the BFP of the lens and they are called diffracted beams.

In order to form images in the TEM from transmitted electrons, either the central bright spot, or some or all of the scattered electrons can be used. Electrons scattered at a specific angle can thus be selected by inserting an aperture into the BFP of the objective lens. This aperture is called the objective aperture. If the direct beam is selected, the resultant image is called bright-field (BF) image, and if scattered

This material is reserved for educational use only, not allowed for commercial use.
Forbidden to modify the content, and cite the document when use.

electrons are selected then the micrograph is called dark-field (DF) image. Typical magnification ranges of these modes are 25,000x-100,000x.

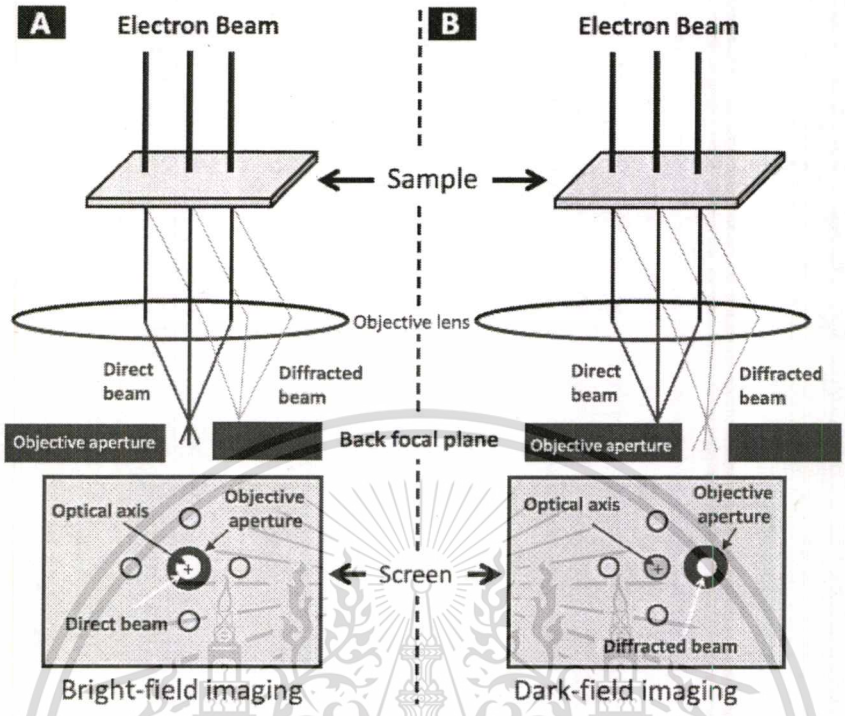


**Figure 2.10** Schematic diagrams of how the direct and diffracted beams can be selected to form an image on TEM. [22]

2.5.3 Thermogravimetric analysis

Thermogravimetric Analysis or Thermal Gravimetric Analysis (TGA) is a type of testing that is performed on samples to determine changes in weight in relation to change in temperature. Such analysis relies on a high degree of precision in three measurements: weight, temperature, and temperature change. As many weight loss curves look similar, the weight loss curve may require transformation before results may be interpreted. A derivative weight loss curve can be used to tell the point at which weight loss is most apparent. Again, interpretation is limited without further modifications and deconvolution of the overlapping peaks may be required. Typically TGA analysis has 2 types; Isothermal TGA and Non Isothermal TGA. Isothermal TGA works at constant temperature and weight loss is recorded with time, meanwhile Non isothermal TGA performs on continuous increasing temperature with time. Also, weight change is recorded. [(http://pakinfohub.com/types-of-thermo-gravimetric-analysis-tga/), 23] TGA is commonly employed in research and testing to determine characteristics of materials such as polymers, to determine degradation temperatures,

This material is reserved for educational use only, not allowed for commercial use.
Forbidden to modify the content, and cite the document when use.

absorbed moisture content of materials, the level of inorganic and organic components in materials, decomposition points of explosives, and solvent residues. It is also often used to estimate the corrosion kinetics in high temperature oxidation. Simultaneous TGA-DTA/DSC measures both heat flow and weight changes (TGA) in a material as a function of temperature or time in a controlled atmosphere. Simultaneous measurement of these two material properties not only improves productivity but also simplifies interpretation of the results. The complementary information obtained allows differentiation between endothermic and exothermic events which have no associated weight loss (e.g., melting and crystallization) and those which involve a weight loss (e.g. degradation). Figure 2.11 shows schematics of Thermogravimetric Analysis operation.

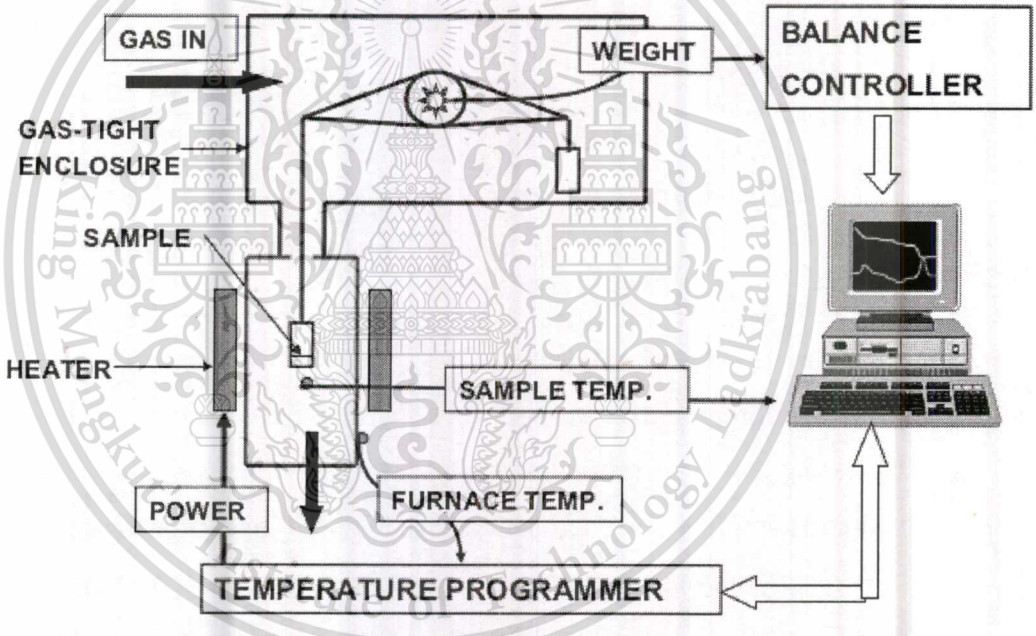


**Figure 2.11** Schematics of thermogravimetric analysis operation [23]

This material is reserved for educational use only, not allowed for commercial use.
Forbidden to modify the content, and cite the document when use.

## 2.6 Literature reviews

### 2.6.1 Biofuel's effect on diesel engines

Appropriate biofuels which are appropriate for diesel engines in this research field are considered as biodiesel and ethanol. For ethanol, fuel in a form of mixture with conventional diesel as blend might have a concern of miscibility limit. K. Cheenkachorn et al. [24] has researched about miscibility among ethanol, biodiesel, and diesel as following. He explained that miscibility limit occur due to difference in chemical structures and characteristics between ethanol and diesel. Therefore, an effective emulsification technique is necessary for being an emulsion. These two liquid fuels can be efficiently emulsified into a heterogeneous mixture of one micro-particle liquid phase dispersed into another liquid phase by mechanical blending in cooperation with suitable emulsifiers. The emulsifier would reduce the interfacial tension force and increase the affinity between the two liquid phases, leading to emulsion stability [4 of K. Cheen, 25]. A suitable emulsifier for ethanol and diesel fuel is suggested to contain both lipophilic part (non-polar) for matching with diesel molecules and hydrophilic part (polar) for matching with ethanol molecules in order to obtain an emulsion of diesohol. And such chemical structures can be found in biodiesel, as shown in Fig. 2.12.

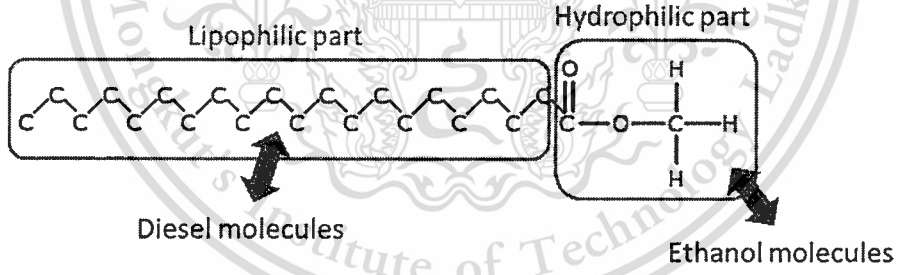


**Figure 2.12** Biodiesel chemical structure

According to fuel miscibility, P. Kwanchareon et al. [26] have performed experiments of three phase diagram of diesel - palm biodiesel - ethanol at different conditions of temperature and purity of ethanol. Overall results show that biodiesel could be used as an effective additive for ethanol-diesel emulsions. Intersolubility of the components of diesel–biodiesel–ethanol system decreased with decreasing temperature. However, at temperatures above 20 degree Celsius, there was no problem with phase separation. Figure 2.13 shows a three phase diagram of ethanol 99.5%-biodiesel-diesel at 20°C.

This material is reserved for educational use only, not allowed for commercial use.
Forbidden to modify the content, and cite the document when use.

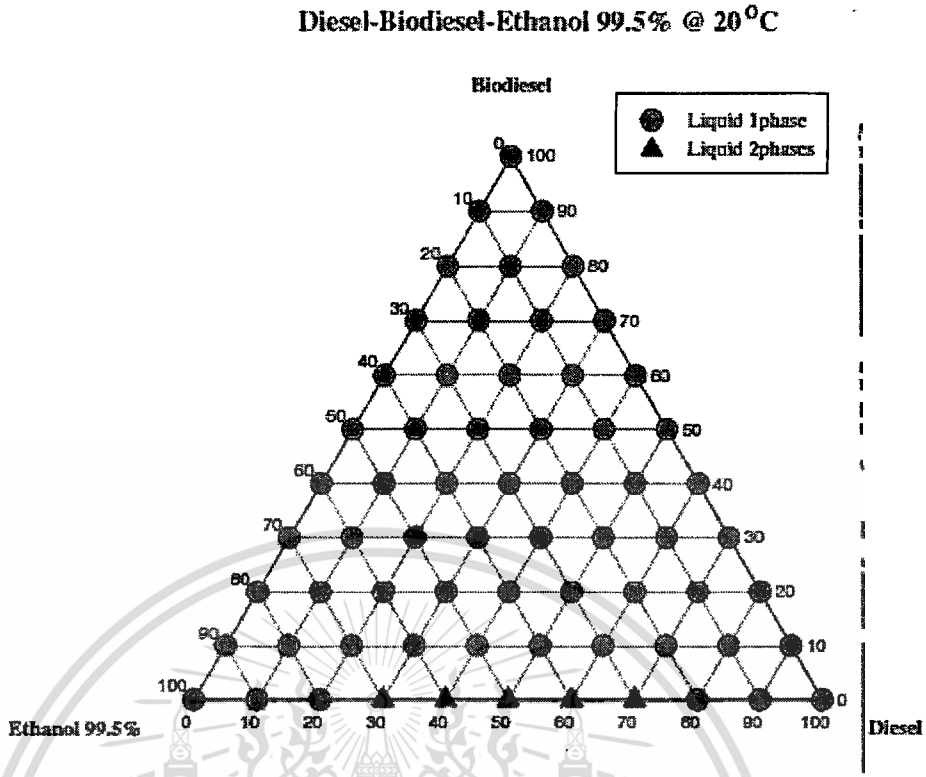


**Figure 2.13** Phase behavior of diesel–biodiesel–ethanol 99.5% at 20°C [26]

In terms of engine performance, combustion characteristics, and emission, following researchers have done experiments and discussed in various interesting points.

D. B. Hulwan et al. [27] performed experiments with blended fuels of biodiesel (B), ethanol (E), and diesel (D) with ratio of D70/E20/B10, D70/E30/B20, D50/E40/B10, and D100. Fuels were supplied to a 3-cylinders diesel engine with adjustable injection timing. At low load of 0.2 MPa BMEP, low speed of 1200 RPM, and injection timing of 13 bTDC (timing range from 13 to 21 bTDC), fuel with ethanol content show obvious combustion delay represented as pressure and heat release graphs with respect to crank angle represented as Fig 2.14. In addition, fuel consumption increases as ethanol proportion in the fuel as shown in Fig. 2.15. Regarding emission gas and smoke, smoke reduced remarkably for blends especially at medium and high loads of both speeds and all injection timings. NO emission does not show obvious trend while CO emission is drastically increased at low loads and decreased slightly at high loads for the blends.

This material is reserved for educational use only, not allowed for commercial use.
Forbidden to modify the content, and cite the document when use.

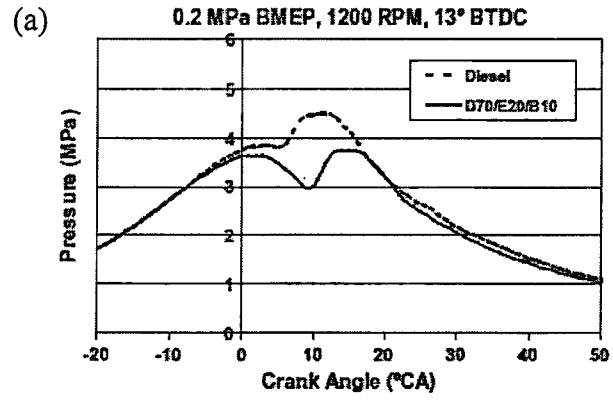


**Figure 2.14** (a) Pressure–Crank angle diagram, (b) Net heat release rate at 1200 RPM [27]

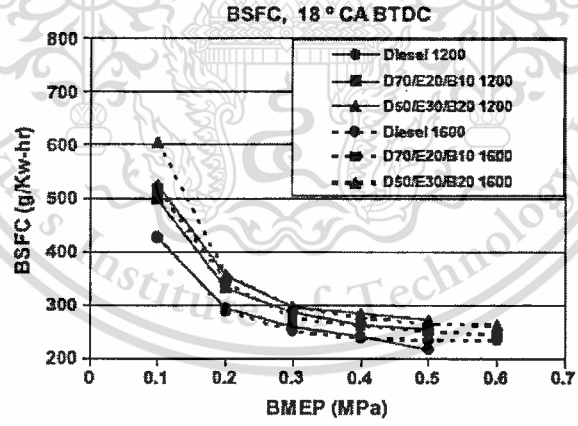


**Figure 2.15** Brake specific fuel consumption [27]

W. Tutak et al. [28] compared combustion effect between diesel-ethanol (DE) mixture and biodiesel-ethanol (BE) mixture on a small diesel engine. Compared to the BE blend, diesel engine powered by the DE blend is characterized by higher values of IMEP and thermal efficiency (Fig. 2.16). However, as increasing ethanol content, obvious combustion delay can be observed as represented in Fig. 2.17

This material is reserved for educational use only, not allowed for commercial use.
Forbidden to modify the content, and cite the document when use.

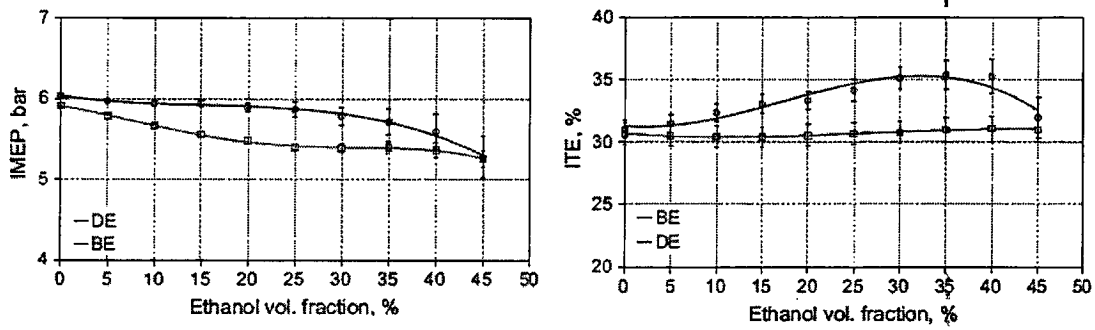


**Figure 2.16** Indicated mean effective pressure and indicated thermal efficiency [28]

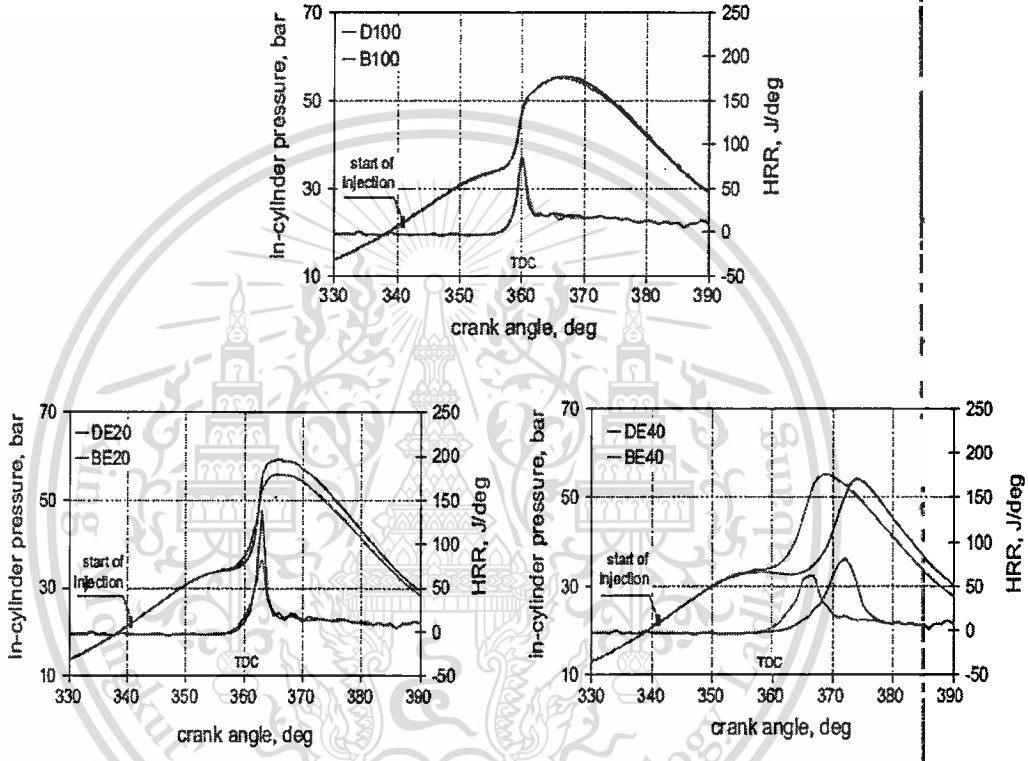


**Figure 2.17** Pressure and heat release of engine by diesel-ethanol (DE) and biodiesel-ethanol (BE) at various ethanol ratio [28]

L. Zhu et al. [29] investigated combustion performance and emission characteristics of a DI diesel engine fueled with ethanol–biodiesel blends (BE). Figure2.18 shows results of engine performance which indicate that when compared with Euro V diesel, thermal efficiency of biofuels has improved significantly and BE5 has highest thermal efficiency. On the whole, compared with Euro V diesel fuel, the BE blends could lead to reduction of both NOx and particulate emissions of the diesel engine as shown in Fig 2.19.

This material is reserved for educational use only, not allowed for commercial use.
Forbidden to modify the content, and cite the document when use.

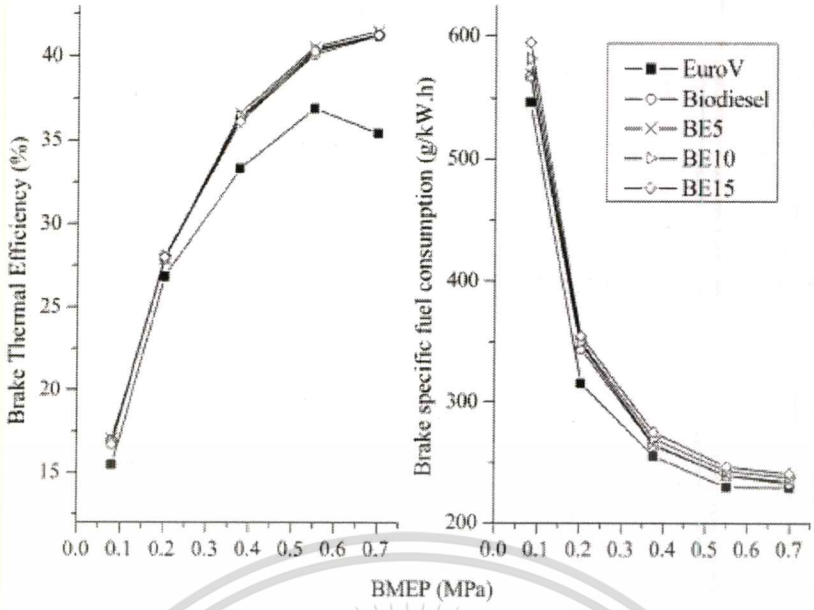


**Figure 2.18** Brake thermal efficiency and brake specific fuel consumption[29]

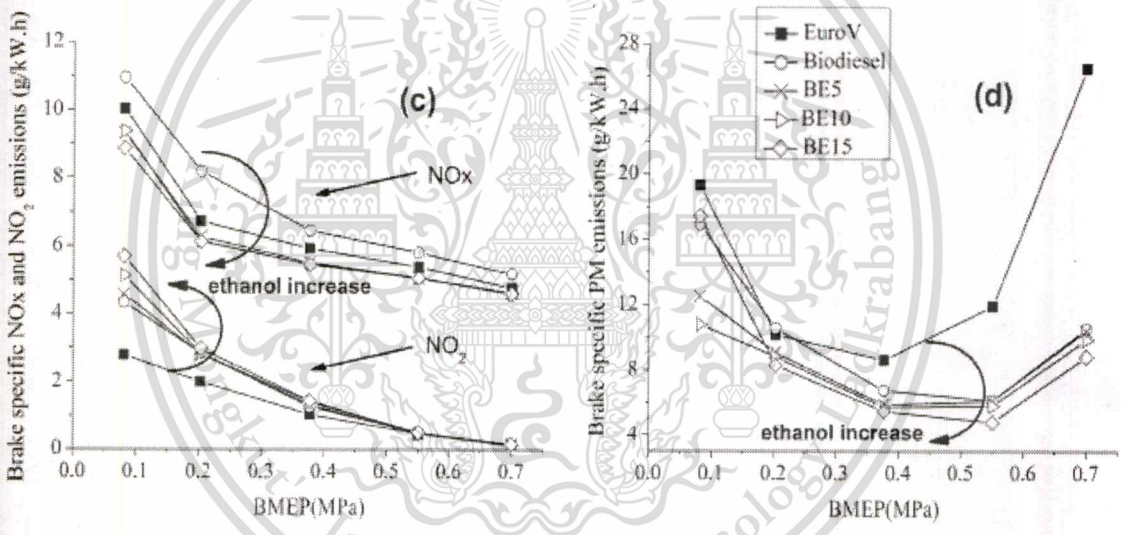


**Figure 2.19** Brake specific emissions [29]

2.6.2 Particulate matters morphology and nanostructures

Particles of particulate matters can be divided into 3 modes of size range according to exhaust stream of a motor vehicle: Nucleation mode, Accumulation mode, and Coarse mode as shown in Fig 2.20 [Ford, 30]. Nucleation mode is so far obscure. Most researchers suggested that nucleation mode particles consist of volatile material i.e. appear in spherical shapes, while others proclaimed nucleation mode particles are in fact solid.

Accumulation mode particles consist of many **primary particles** or **spherules**. Spherules are porous carbonaceous shells formed in pyrolysis of gaseous

This material is reserved for educational use only, not allowed for commercial use.
Forbidden to modify the content, and cite the document when use.

fuels or volatile components of liquid or solid fuels. Size range of spherules is typically 20-50 nm. Agglomerate sizes arbitrarily depend on number of the spherules. Number of the spherules in agglomerate has not been revealed in clear relationship to other factors yet.

Coarse mode is formed at combination of the accumulation and the nucleation mode which particles include abnormal rust and scale. Processes in the coarse mode were reported as random and unpredictable manner.

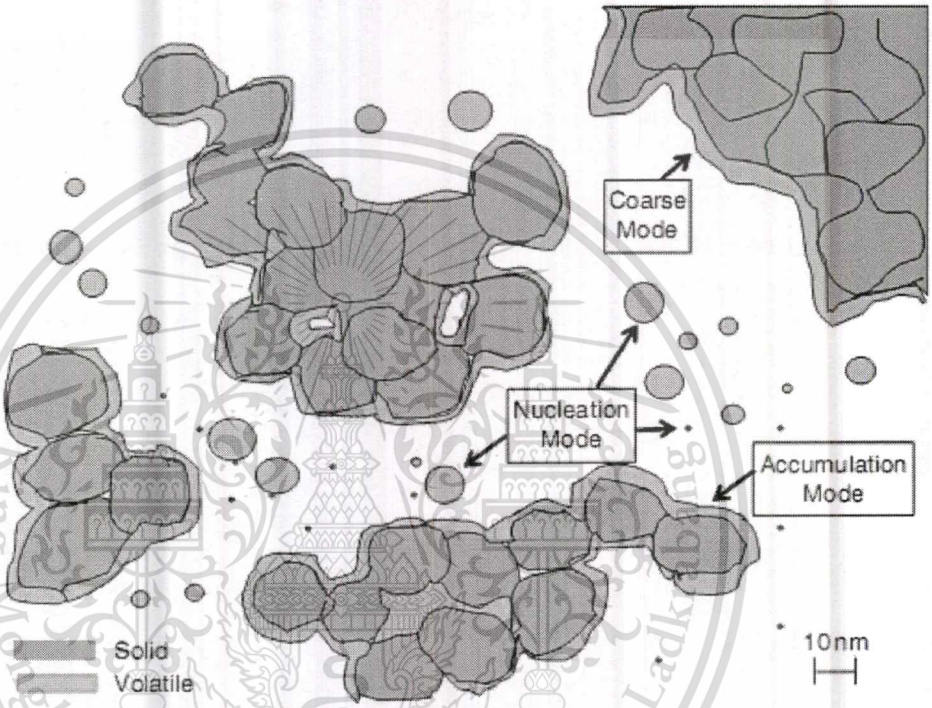


**Figure 2.20** Schematic diagram of particles in coarse mode (largest, shown in part), accumulation mode (middling), and nucleation mode (smallest) [Ford, 30]

M. M. Maricq (2007) [31] proposed characteristics of particulate matters from diesel engine. Figure 2.21 shows the diesel particulate matter consists of two types of particles: (a) fractal-like agglomerates of primary particles 15–30 nm in diameter, composed of carbon and traces of metallic ash, and coated with condensed heavier end organic compounds and sulfate; (b) nucleation particles composed of condensed hydrocarbons and sulfate.

This material is reserved for educational use only, not allowed for commercial use.
Forbidden to modify the content, and cite the document when use.

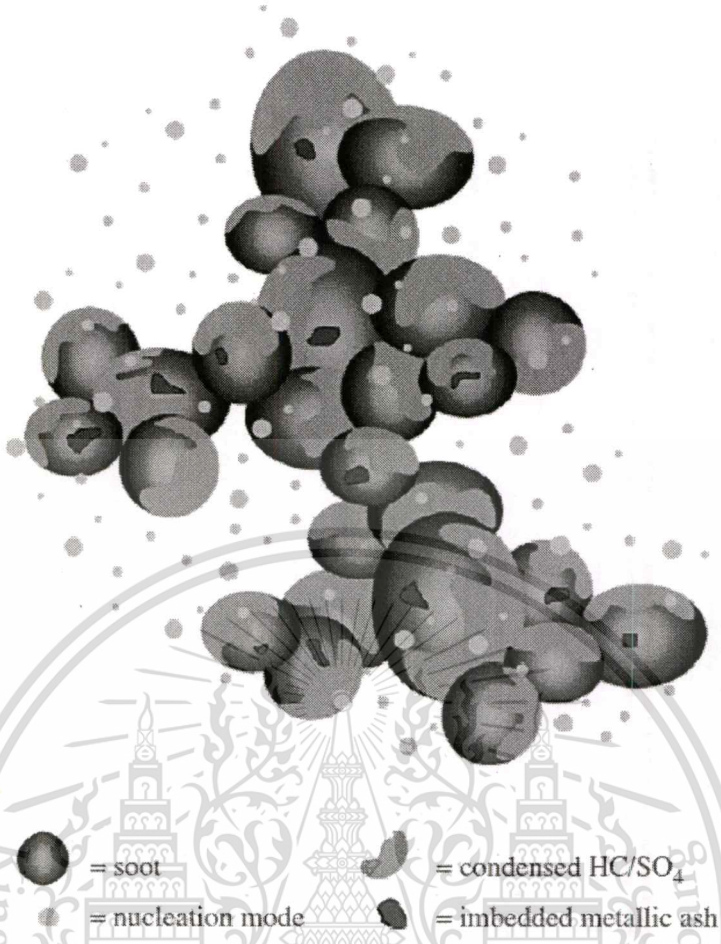


**Figure 2.21** Artist's conception of diesel particulate matter [31]

D. B. Kittelson [32] proposes a model of size distributions for typical particles emitted from internal combustion engines as shown in Fig. 2.22. The size distributions were plotted according to 3 measurement aspects: number, area, and mass distribution. For nucleation mode, particles range from few nanometers to less than 50 nm and become larger by accumulation mode in the range of 0.1 – 0.3 micron. Coarse mode which consists of nucleation mode and accumulation mode formation represents further larger size.

This material is reserved for educational use only, not allowed for commercial use.
Forbidden to modify the content, and cite the document when use.

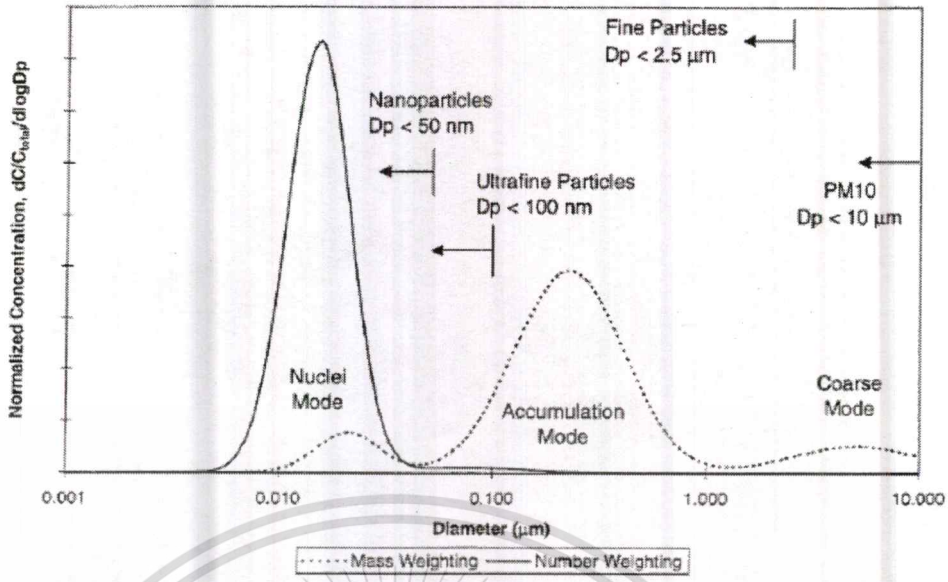


**Figure 2.22** Particle size distribution of soot from a diesel engine [32]

Referred from P. Eastwood [30], particulate matters composition can be categorized into 2 main groups as; volatile or soluble group, and non-volatile or insoluble group. **Volatile** matters consist of **sulphate fraction and organic fraction**. **Non-volatile** matters consist of **carbonaceous fraction or "Soot"** in this research, and **ash fraction**. Soot and ash are generated in the engine, while other volatile substances form later. Four main sources of particulate matter's emergence are fuel, lubricant, air, and material breakdown. Fuel contributes mainly to carbonaceous fraction and organic fraction, while other agents contribute to ash and sulphate fraction. Particulate matter formation starts with the earliest process in the combustion chamber. Carbonaceous fraction or soot forms within the engine. Ash fraction probably forms before exhaust valve open depending on the source of emergence. Organic and sulphate fraction which is considered as volatile are suggested to form at final stage, probably at the cold end of the exhaust system.

Since carbonaceous fraction is considered to be the best explanation for the particulate formation, this research focuses on the mechanisms of carbonaceous or **Soot formation**.

Soot formation start with fuel molecules in the combustion chamber with lack of oxygen. At high temperature and low oxygen condition, **pyrolysis** breaks down fuel molecules with high molecular weight into **Soot precursor** molecules as

This material is reserved for educational use only, not allowed for commercial use.
Forbidden to modify the content, and cite the document when use.

represented in Fig. 2.23. Precursor molecules are hold and undergo **Nucleation** to form the first discernable particle or **Nuclei** at less than 3 nm. which Wang H. [Ford P.68 ,33] proclaimed as acetylene (C2H2) and polycyclic aromatic hydrocarbons (PAH). Nuclei begin to increase their mass but keep unchanged number of particles in **Surface growth.** At this process, spherules are generated by carbon added but hydrogen is removed so that ratio of C/H reduces and isolated spherule particles are formed with size range of 20 – 50 nm. During this growth, spherules collision due to free movement sticks particles together in **Agglomeration** process. Concurrent surface growth and agglomeration lead to bigger particles with familiar identities. Particle number decreases with mass unchanged in this process. Agglomeration is more physical while nucleation and surface growth is rather chemical process.

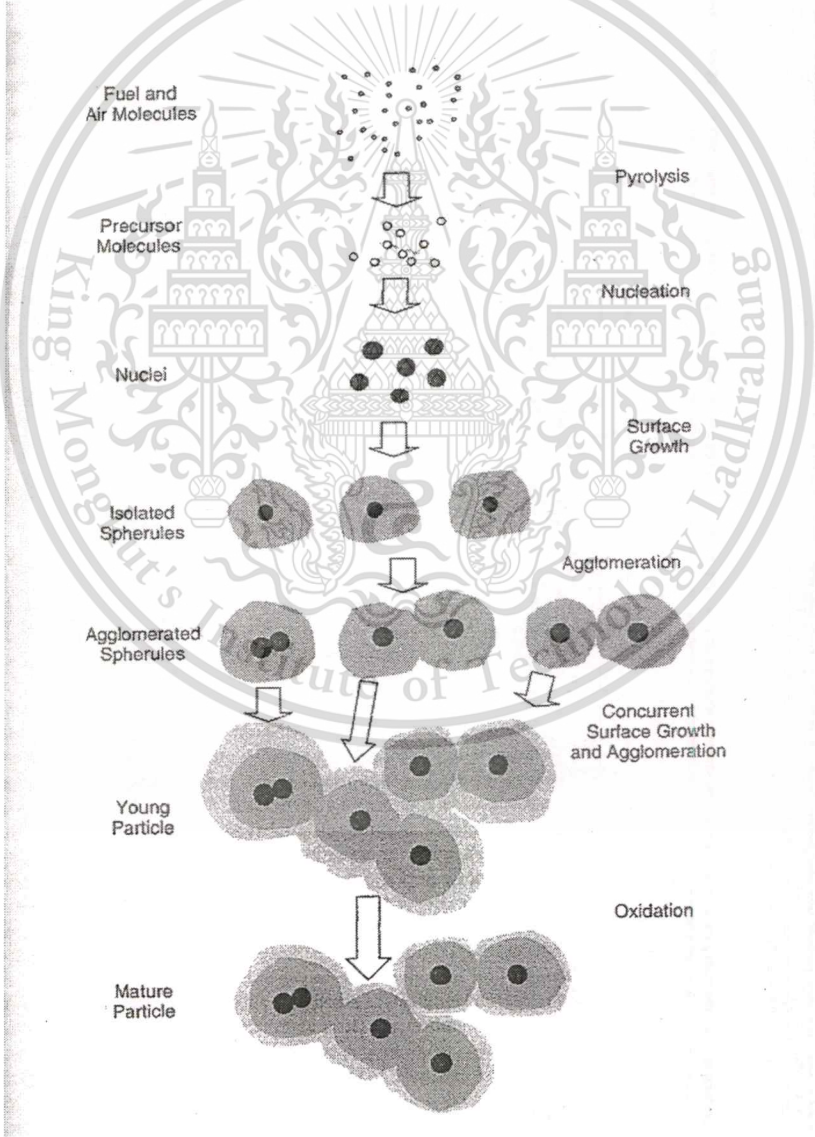


**Figure 2.23** Conceptual scheme for soot formation [30]

This material is reserved for educational use only, not allowed for commercial use.
Forbidden to modify the content, and cite the document when use.

**Oxidation** is a converse process since it reverses the process of soot production and stops the growth in any formation stage. There are two aspects in explanation of restricted spherule diameters even across different combustion. First, common termination of surface growth due to supply of soot precursors is exhausted. Second is oxidation of the spherule surface stops the particle's growth. Oxidation is a chemical rather than physical. Responsible oxidant is suggested as O, OH, H, CO2, CO, H2O, and O2. Predominant oxidant are proclaimed as OH and O2 [34, (Smith O. I. , Ford P80)]. Clustered morphology tends to be less oxidized than chain. Disorder amorphous structure tends to be more oxidative which take place on surface as expressed as surface recession.

To visualize the conceptual scheme of soot, P. Karin et al. [35] investigated physical characterization of diesel particulate matters by SEM and TEM. Figure2.24 shows SEM image of diesel agglomerated PMs. The agglomerate particle size is about 100 to 600 nm and much amount number of particles is in range of 100 to 300 nm

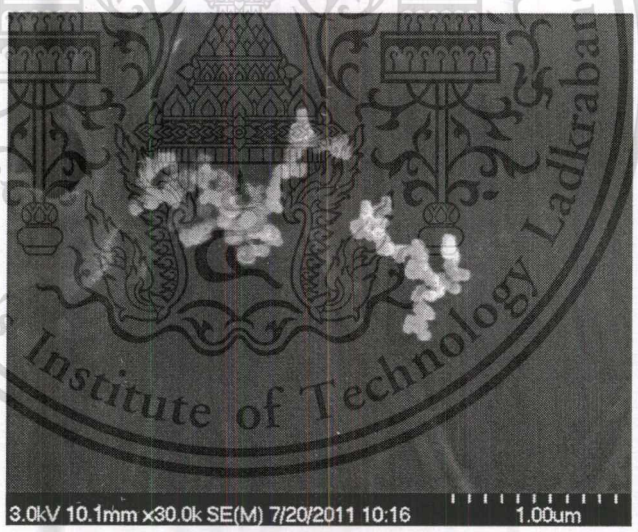


**Figure 2.24** SEM image of fine agglomerated PM from a small diesel engine [35]

Figure 2.25 shows TEM image of diesel primary particle PMs. The particle size was about 20 to 80 nm. The different size of a primary particle might be depends on not only amount of carbon atoms accumulation but also the oxidation of PM's surface during fuel combustion process. Detailed primary particles as shown in Fig. 2.26 are nearly spherical shape even though surfaces are not so smooth. The image

This material is reserved for educational use only, not allowed for commercial use.
Forbidden to modify the content, and cite the document when use.

also shows structure of inner core zone and outer shell zone of PMs. The inner core diameters are approximately 5 to10 nm.

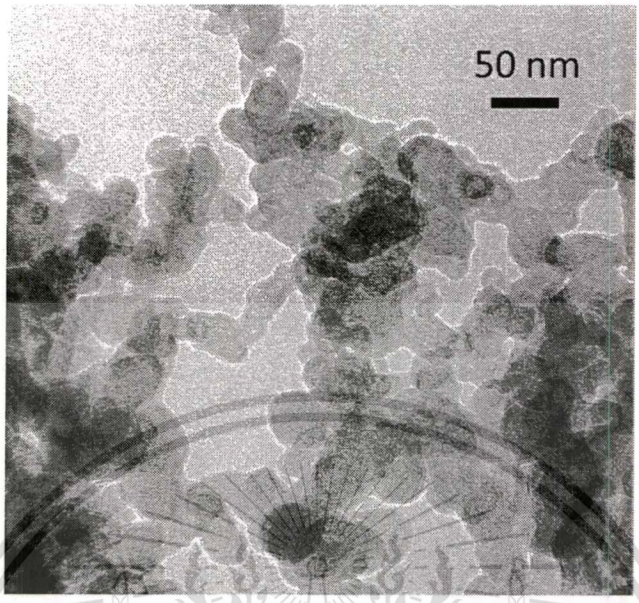


**Figure 2.25** TEM image of fine agglomerated PM from a small diesel engine [35]

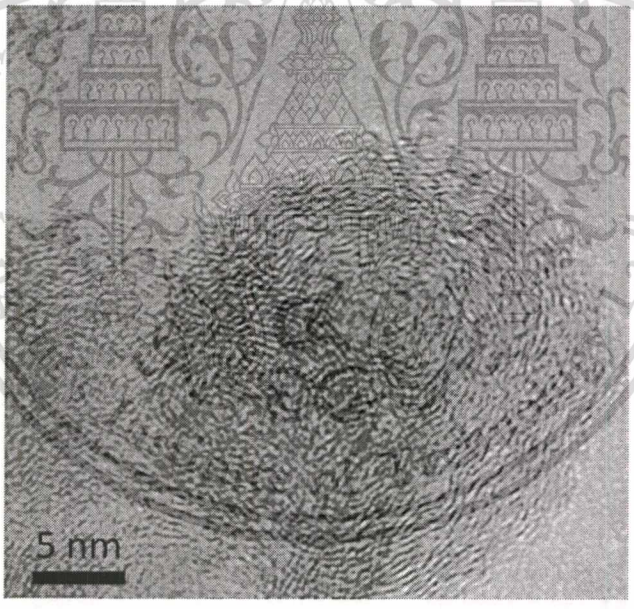


**Figure 2.26** TEM image of fine agglomerated PM from a small diesel engine [35]

Since basic structure unit of the carbonaceous fraction is spherule or primary particle, examining particles in nanostructure detail might help to get more insight of soot. Lipkea et al. [36, Ford P214] proposed well-accepted conceptual models of spherule nanostructure as shown in Fig. 2.27. On an ascending dimensional scale, a primary particle's nanostructure components start from carbon atoms arranged in

This material is reserved for educational use only, not allowed for commercial use.
Forbidden to modify the content, and cite the document when use.

repeating six-membered rings with covalent bond, forming planar hexagonal arrays. Two hexagonal arrays are chemically bonded, forming parallel with 0.35 – 0.36 nm apart, face-centered layers or **platelets**. Two to five platelets are stacked, forming commonly oriented **crystallites**. This interlayer bonding is weaker, relying on Van der Waal's forces. Crystallites are stacked in various orientations, forming completed spherules. Naturally, a spherule contains ~10^5 to 10^6 carbon atoms into ~10^3 to 10^4 crystallites.

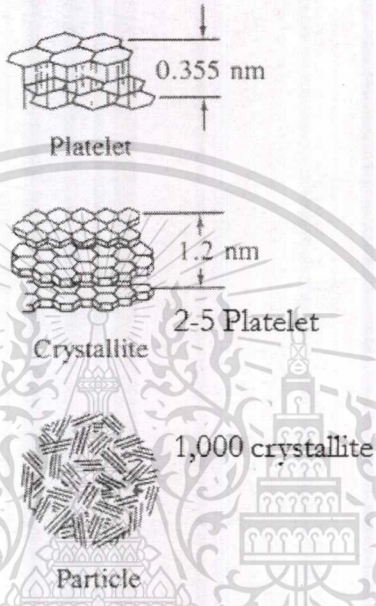


**Figure 2.27** TEM image of fine agglomerated PM from a small diesel engine [36]

Braun et al. [Frod P214, 37] claimed from the experimental observation that hexagonal ordered microstructure can be referred as graphite or the arrays of **graphene sheets**. V. Fernandez-Alos et al. [38] represented soot and char molecular models derived from High Resolution TEM lattice fringe images. Soot images were image-processed to generate the lattice fringe format. It was assumed that each fringe length is as long as it is deep in depth dimension so that a graphene sheet is form in the shape of a hexagon which depend on sizes of polyaromatic hydrocarbon (PAH) molecules. The longer fringes are inferred as larger aromatic structures of varying carbon numbers (numbers of hexagonal rings). Figure 2.28 show schematic diagram of relationships between number of hexagon rings and amount of carbon atoms contained in the graphene sheet.

This material is reserved for educational use only, not allowed for commercial use.
Forbidden to modify the content, and cite the document when use.

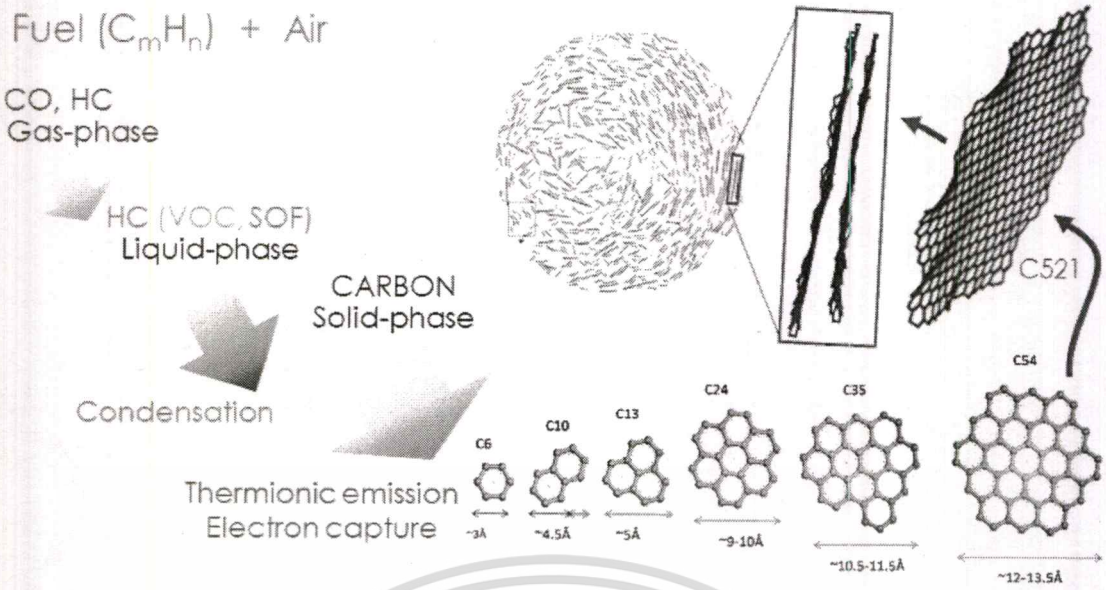


**Figure 2.28** Relationship between number of hexagon rings and carbon atoms in graphene sheet of soot particle [38]

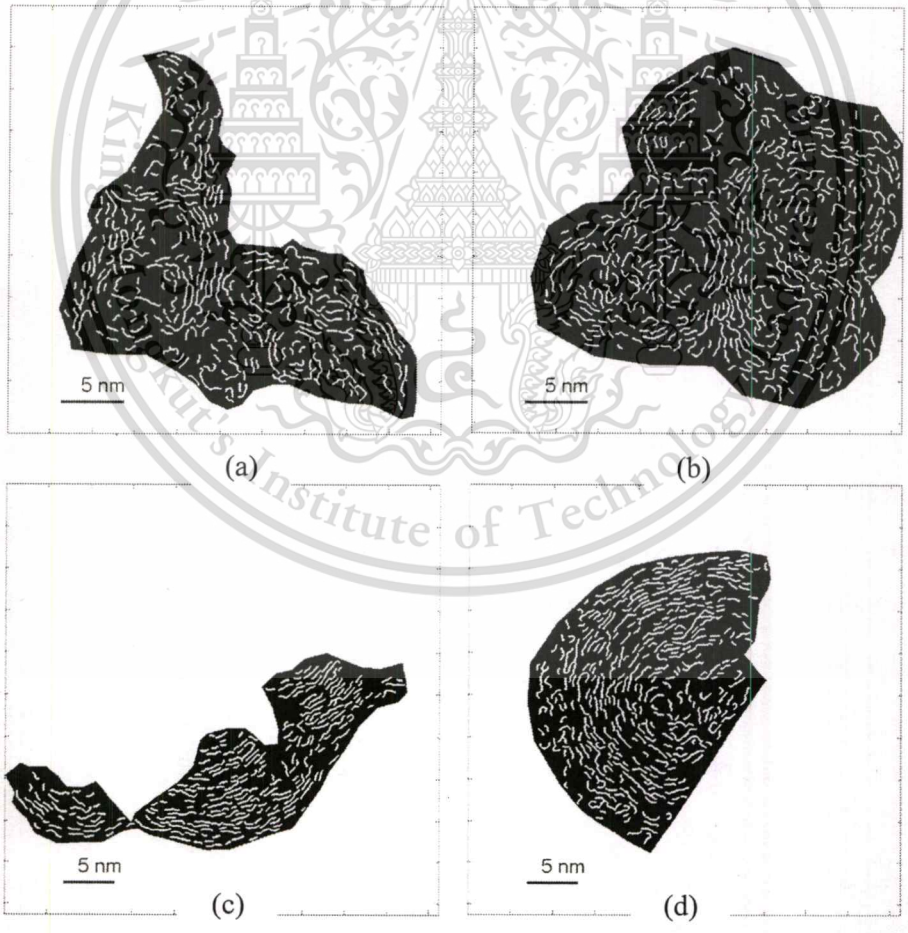


**Figure 2.29** Skeletonized images on the selected region of four TEM images of soot (a, b) High-efficiency clean combustion, (c, d) conventional diesel combustion [39]

This material is reserved for educational use only, not allowed for commercial use.
Forbidden to modify the content, and cite the document when use.

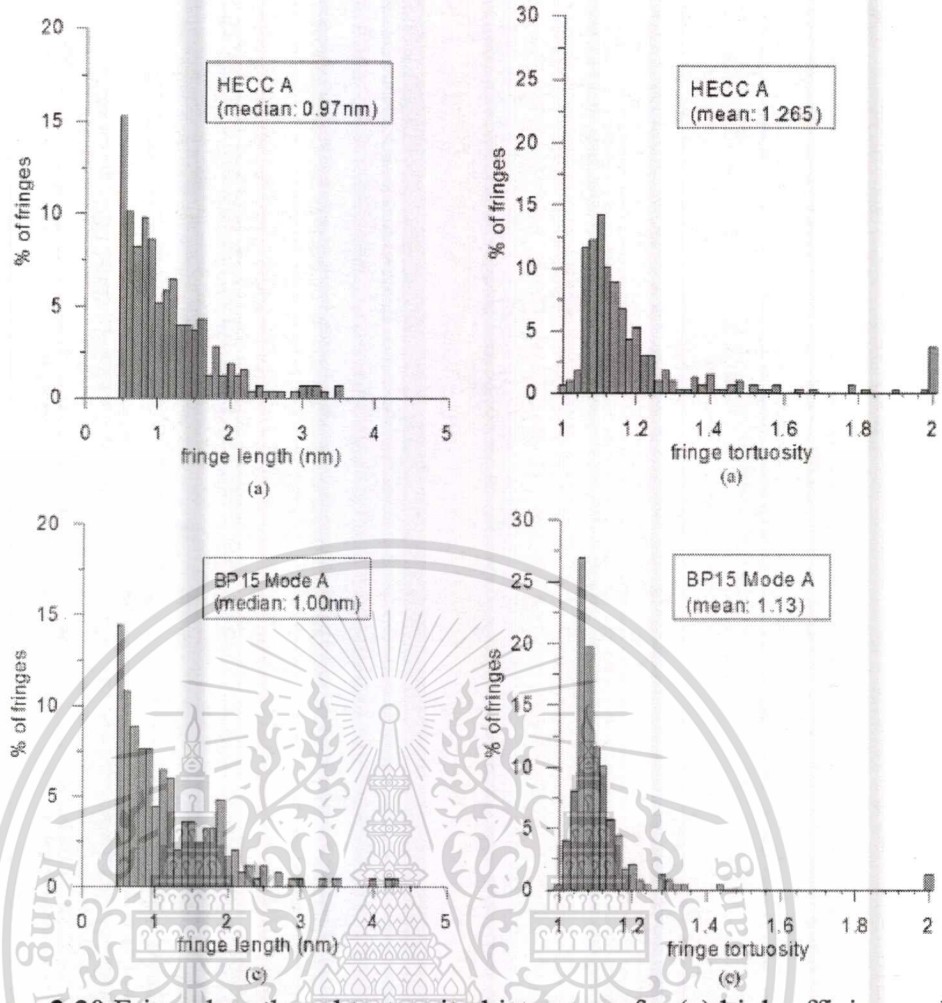


**Figure 2.30** Fringe length and tortuosity histograms for (a) high-efficiency clean combustion and (c) conventional diesel combustion condition [39]

K. Yehliu et al. [39] investigated characterization of soot nanostructure generated by a turbodiesel engine in different operating conditions. There is comparison of fringe length and tortuosity. Results on Fig 2.29 and Fig. 2.30 show that conventional diesel combustion condition contributes well-organized soot nanostructure with more portions of long fringe length but low fringe tortuosity compared with high-efficiency clean combustion condition.

As continued investigation of P. Karin [35], they estimated carbon atom density of diesel and biodiesel's PMs with the information of carbon platelet length derived from image processing of soot's TEM images. The estimation applies concepts of "the molecule of carbon-6 (C6) is the possible smallest size" / "there are 3 layers arranged to be a platelet". Results show that PMs contain approximately 600-900 carbon atoms/nm^3.

This material is reserved for educational use only, not allowed for commercial use.
Forbidden to modify the content, and cite the document when use.

2.6.3 Oxidation kinetics

Particulate matter's oxidation kinetics usually applies TGA experimental data for analysis. A. Williams et al. [40] investigated different fuel property effects on particulate matter reactivity. Biodiesel - diesel blend or B20 and decanol ($C_{10}H_{21}OH$) – diesel blend or D23 which have same percent oxygen content were compared in the experiment. From Fig. 2.31, TGA results of soot created by combustion of the B20 and D23 shows that D23's soot are more reactive. They suggested that the oxygen in decanol is more available for incorporation into the soot as reactive surface oxygen.

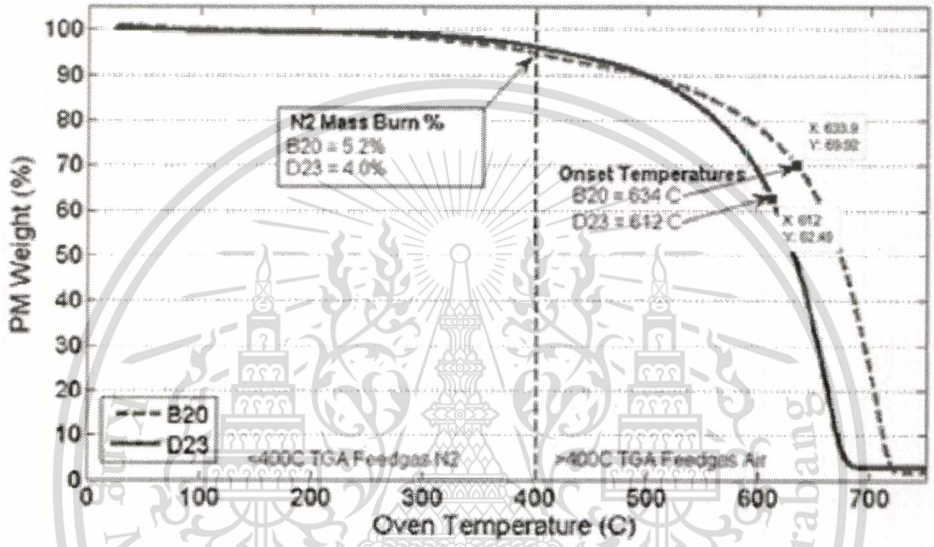


**Figure 2.31** Fuel Oxygen Group – TGA Results [40]

J. P. A. Neeft et al. [41] reported on kinetics of the oxidation of diesel soot. They performed TGA experiments on comparison between carbon black soot and diesel soot to determine many oxidation kinetics parameters e.g. reaction rate, reaction order in carbon, reaction order in oxygen, activation energy, and pre-exponential factors. Oxidation kinetics models often used to describe the reaction rate of carbonaceous materials have a general form as Eqn. 2.2

$$r = N_t \cdot k(T) \cdot f(p_{O2}, p_{H2O}, \dots) \tag{2.2}$$

where r is the reaction rate, $N_t$ is the total number of active sites, k(T) is a temperature-dependent reaction rate constant, and $f(p_{O2}, p_{H2O}, \dots)$ is a function that describes the dependence of the reaction rate on the partial pressure of the various

This material is reserved for educational use only, not allowed for commercial use.
Forbidden to modify the content, and cite the document when use.

reactants and gas-phase components. The total number of active sites $N_t$ is often described by Eqn. 2.3

$$N_t = \lambda \cdot S_a \tag{2.3}$$

where $\lambda$ is the surface concentration of active sites and $S_a$ is the specific surface area. As it is generally accepted that the specific surface area $S_a$ is a function of conversion $\xi$ (the fraction of carbon that is oxidized), kinetic models describe the dependence of $N_t$ as a function of conversion. A simple approach is to use an $n^{th}$ order of $(1- \xi)$ as Eqn. 2.4

$$S_a = S_{a,0} \cdot (1 - \xi)^{n_\xi} \tag{2.4}$$

where $S_{a,0}$ is the initial surface area (at $\xi = 0$) and $n_\xi$ is the reaction order in carbon. With increasing conversion, the model predicts a decrease in $N_t$ and therefore, in the reaction rate. However, for highly porous carbons, such as soot and activated carbons, $S_a$ can actually increase as a function of conversion, due to pore growth and opening of concluded pore space. Several models have been proposed to account for these phenomena.

The temperature dependence of the reaction rate is usually described by the Arrhenius equation as Eqn. 2.5

$$k(T) = k_0 \cdot \exp(-\frac{E_a}{RT}) \tag{2.5}$$

where T is the absolute temperature, $k_0$ is the pre-exponential factor, R is the molar gas constant, and $E_a$ is the activation energy.

The function that describes the influence of the partial pressures of the gas-phase components on the reaction rate is usually limited to the influence of the oxygen partial pressure, described by the $n_{th}$ order expression as Eqn. 2.6

$$f(p_{O2}, p_{H2O}, \dots) = p_{O2}^{n_{O2}} \tag{2.6}$$

This material is reserved for educational use only, not allowed for commercial use.
Forbidden to modify the content, and cite the document when use.

where $p_{O2}$ is the partial pressure of oxygen and $n_{O2}$ is the order in the oxygen partial pressure.

P. Karin [42] studied PM oxidation kinetics on conventional cordierite diesel particulate filters (DPF) powders mixed with biodiesel's PM and diesel's PM by TGA. The calculated activation energies of biodiesel's PM in oxidation are lower than that of the diesel engine's PM and carbon black because of unburned oxygenated molecule. The activation energy of biodiesel's PM and diesel's PM on the DPF powders are in the range of 109 ~ 131 kJ/mole and 117 ~ 130 kJ/mole, respectively.

J. Hamada et al. [43] studied on effects of engine operating condition on PM structure and oxidation rate. Different combustion conditions produce soot with different oxygen (O) per carbon (C) ratio. Results show that soot with higher O/C ratio tends to have lower activation energy as shown in Fig. 2.32. The mechanism is assumed that soot has oxygen connected to edge of the graphite crystallite (Fig. 2.33). The smaller graphite structure, more oxygen connected due to more surface area. As a result, Soot with small graphite is easier to oxidize than the bigger graphite which is lack of oxygen at central part.

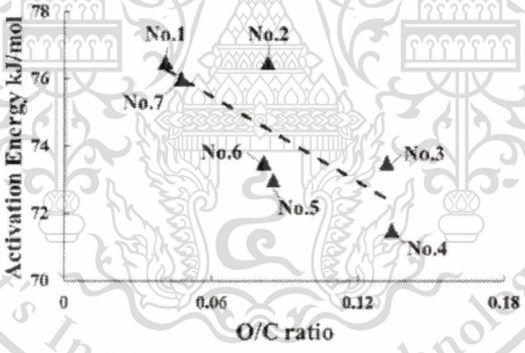


**Figure 2.32** Relationships between O/C ratio and activation energy [43]

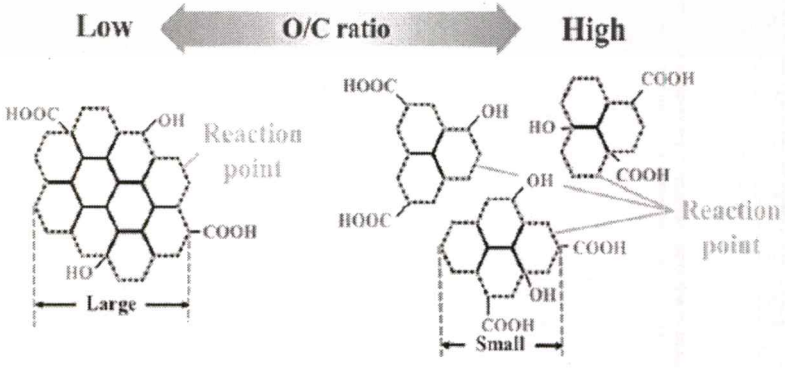


**Figure 2.33** Relationships between O/C ratio and activation energy [43]

This material is reserved for educational use only, not allowed for commercial use.
Forbidden to modify the content, and cite the document when use.

# CHAPTER 3

# RESEARCH METHODOLOGY

## 3.1 Experimental equipment

3.1.1 Diesel engine specification

There are two small diesel engine used in PM related research as shown in Fig. 3.1). The engine A which was applied in previous research (Biodiesel-Diesel) comes up with single cylinder of 638 $cm^3$ displacement. The engine B which was applied in present research (Ethanol-Biodiesel) is also a single cylinder engine with 709 $cm^3$ displacement. Engine specification of both engine are represented in Table 3.1 and Table 3.2.

**Table 3.1** "A" engine specification

| Items | Details |
|---|---|
| Engine type | 1-cylinder, Natural aspirated, Direct injection, Compression Ignition Engine |
| Bore x Stroke | 92 mm x 96mm |
| Displacement | 638 cm3 |
| Compression ratio | 16.1:1 |
| Rated power | 7.7 kW @ 2400 rpm |
| Injection timing | 19° CA bTDC |
| Injection pressure | 20 MPa |

**Table 3.2** "B" engine specification

| Items | Details |
|---|---|
| Engine type | 1-cylinder, Natural aspirated, Direct injection, Compression Ignition Engine |
| Bore x Stroke | 97 mm x 96mm |
| Displacement | 709 cm3 |
| Compression ratio | 18:1 |
| Rated power | 9.2 kW @ 2400 rpm |
| Injection timing | 19° CA bTDC |
| Injection pressure | 22 MPa |

This material is reserved for educational use only, not allowed for commercial use.
Forbidden to modify the content, and cite the document when use.

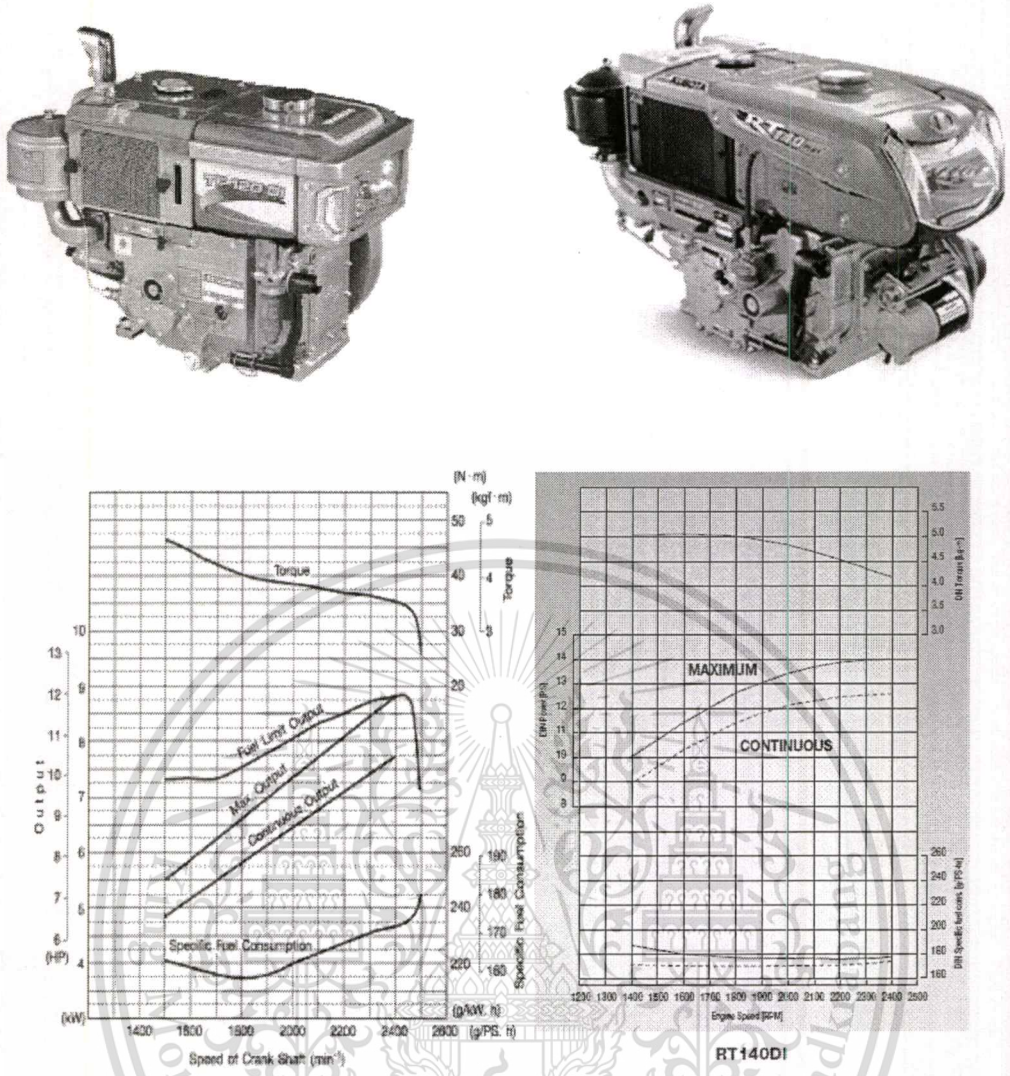


**Figure 3.1** Diesel engine A (left) and engine B (right) specification

3.1.2 Eddy Current Engine Dynamometer

The engine dynamometer as shown in Fig. 3.2, Tokyo Plant model ED-60-Horizontal, was used in the experiment for applying a load on the tested engine and also measuring force, moment of force (torque) and power that the tested engine can produce against the load. The type of the engine dynamometer is Eddy current with external water cooling systems. Eddy current dynamometer can provide a quick load change rate for rapid load setting. Eddy current dynamometer consists of an electrically conductive core moving across a magnetic field to produce resistance to movement. The magnetic field is generated by using variable electromagnets that can change the magnetic field strength to control the amount of braking. The electromagnet voltage is control by a desktop computer, using changes in the magnetic field to match the power output.

This material is reserved for educational use only, not allowed for commercial use.
Forbidden to modify the content, and cite the document when use.

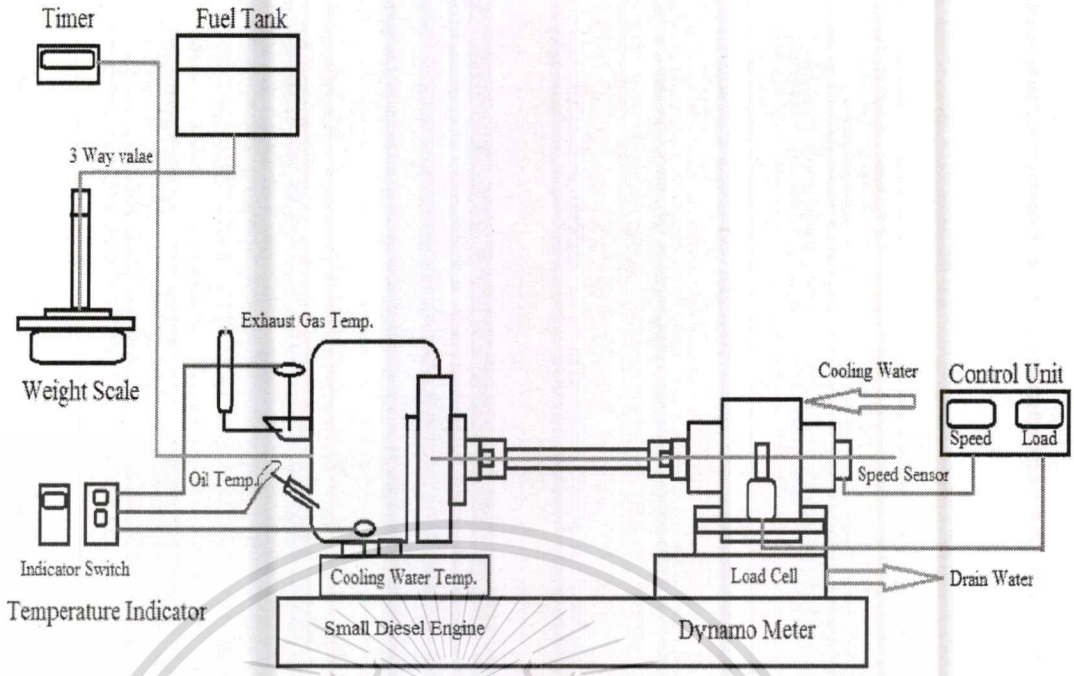


**Figure 3.2** Schematic diagram of engine dynamometer

3.1.3 Fuel specification

The fuels used in this experiment are biodiesel (B100) and ethanol-biodiesel blend. The blended fuels contain 10% and 20% by weight of ethanol, and are identified as BE10 and BE20 respectively. The biodiesel was produced from palm-olein (B100-TIS2313-2549). The ethanol was used as anhydrous ethanol 99.8%. For the blended fuel and ethanol, properties of calorific value, heat of vaporization, carbon content, hydrogen content, oxygen content, stoichiometric air-fuel ratio, and density were estimated by interpolation as shown in Table 3.2. Also, Distillation graph of each based fuel is represented in Fig. 3.3.

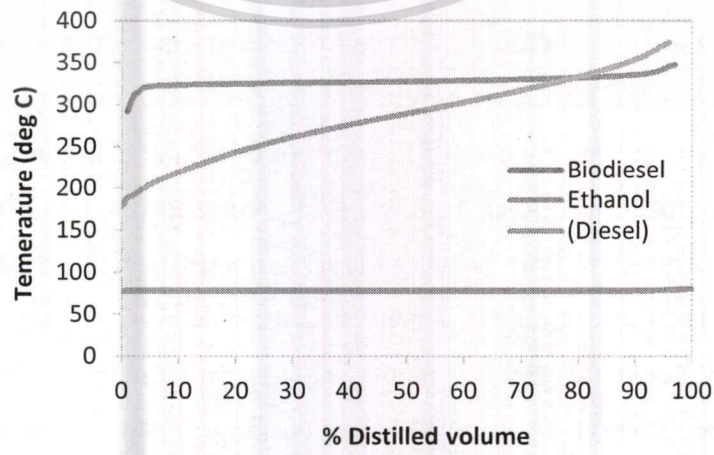


**Figure 3.3** Distillation of diesel, biodiesel, and ethanol

This material is reserved for educational use only, not allowed for commercial use.
Forbidden to modify the content, and cite the document when use.

**Table 3.2** Ethanol and Blended fuel properties

| Fuel Properties | (Diesel) | Biodiesel | Ethanol | BE10 | BE20 |
|---|---|---|---|---|---|
| Chemical formula | $C_{14.2}H_{28}$ | $C_{14.9}H_{29.9}O_{1.9}$ | $C_2H_6O$ | - | - |
| Auto ignition temperature (°C) | 288 | 294 | 365 | - | - |
| Calorific Value (kJ/kg) | 46180 | 39525 | 28329 | 38405 | 37285 |
| Heat of vaporization (kJ/kg) | 250 | 300 | 840 | 354 | 408 |
| Viscosity @ 40°C ($mm^2/s$) | 3.0 | 4.5 | 1.2 | - | - |
| Carbon (% mass) | 85.1 | 74.5 | 52.2 | 72.3 | 70.0 |
| Hydrogen (% mass) | 14.0 | 12.5 | 13.0 | 12.5 | 12.6 |
| Oxygen (% mass) | 0.9 | 13.0 | 34.8 | 15.2 | 17.4 |
| Stoichiometric Air fuel ratio | 14.7 | 12.3 | 9.0 | 11.9 | 11.6 |
| Density @ 25°C ($kg/m^3$) | 844.8 | 875.3 | 789.0 | 866.7 | 858.0 |

Figure 3.3 explains about the distillation curve of fuels in the researches. Ethanol can be distilled easier at low temperature than biodiesel and diesel because it has much smaller molecule sizes. Diesel which is considered as derived from petroleum has wide range of fuel molecules. Therefore, small-size molecules start to vaporize since less than 180°C whereas bigger molecules eventually vaporize at more than 350°C. For biodiesel, according to production process, it is considered as more homogeneous which can be distilled in narrow range of temperature 300~350°C

3.1.4 Black smoke meter

Particulate matter emitted from engine combustion is measured in black smoke's intensity percentage. The smoke meter is applied to measure particulate matter's concentration between particulate matter in exhaust gas before trapping and after trapping in particulate filter by light emitting method. The 0 percentage black smoke means no particulate matter detected on filter, while 100 percentage means the filter be covered with particulate matter at full scale of intensity. This smoke meter

This material is reserved for educational use only, not allowed for commercial use.
Forbidden to modify the content, and cite the document when use.

percentage can be summarized that the filtration efficiency of particulate filter. The smoke meter for the present research, model : Okuda DSM - 240, is shown in figure3.4 .

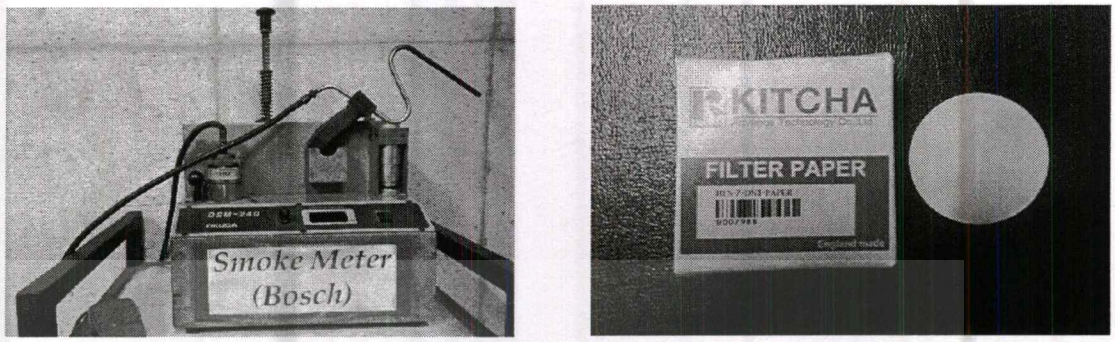


**Figure 3.4** Smoke meter

3.1.5 Pressure sensor

Pressure sensor is used to measure pressure variation in the combustion chamber which is the most important parameter to be analyzed in combustion characteristics. The sensor type "Kistler 6052C31-piezoelectric crystal" represented as Fig. 3.5 is mounted on the cylinder head of the engine B.

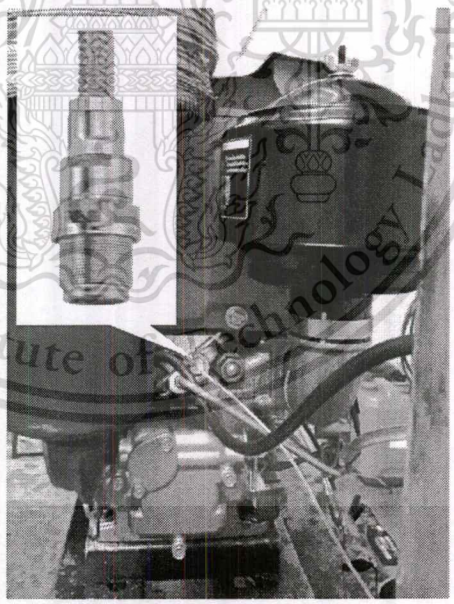

**Figure 3.5** Pressure sensor connect inside cylinder

This material is reserved for educational use only, not allowed for commercial use.
Forbidden to modify the content, and cite the document when use.

3.1.6. Crank angel encoder

Crank angle encoder is used to measure real-time crankshaft position for matching with the pressure parameter as well as to calculate combustion chamber volume. The encoder type "CA-RIE-360" represented as Fig. 3.6 was applied and mounted on the end of dynamometer for serviceability. Resolution of the encoder is 1 degree. The function is based on transmission light principle. An infrared beam is emitted and received at the sensor unit. The customized marker disk (with slits) is mounted in-between the sensors gate. The slits will interrupt the infrared beam; the receiver transforms the light to voltage signal.

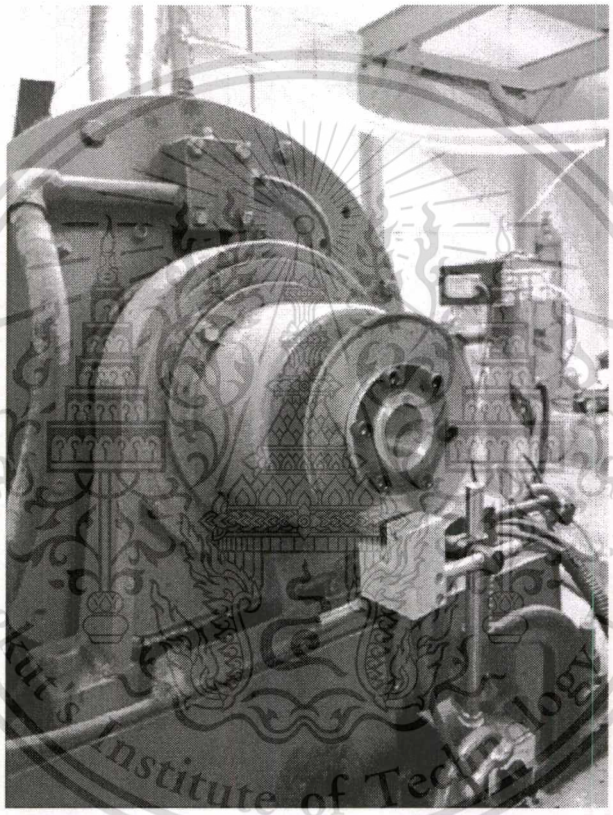

**Figure 3.6** Crank angle encoder at end of engine dynamometer

3.1.7. Data acquisition system

Data acquisition system as shown in orange-highlight portion of Fig. 3.7 is used to integrate signals from both pressure sensor and crank angle encoder. Then it processes data based on crank angle domain so that user can obtain results of Pressure-Volume, Pressure-Crank angle, Rate of heat release-Crank angle, Pressure derivative-Crank angle, Cumulative heat release-Crank angle, and etc. Figure 3.8 – Figure 3.10 shows details of the data acquisition unit "DEWESoft SIRIUSi-HS-CA" for this research.

This material is reserved for educational use only, not allowed for commercial use.
Forbidden to modify the content, and cite the document when use.

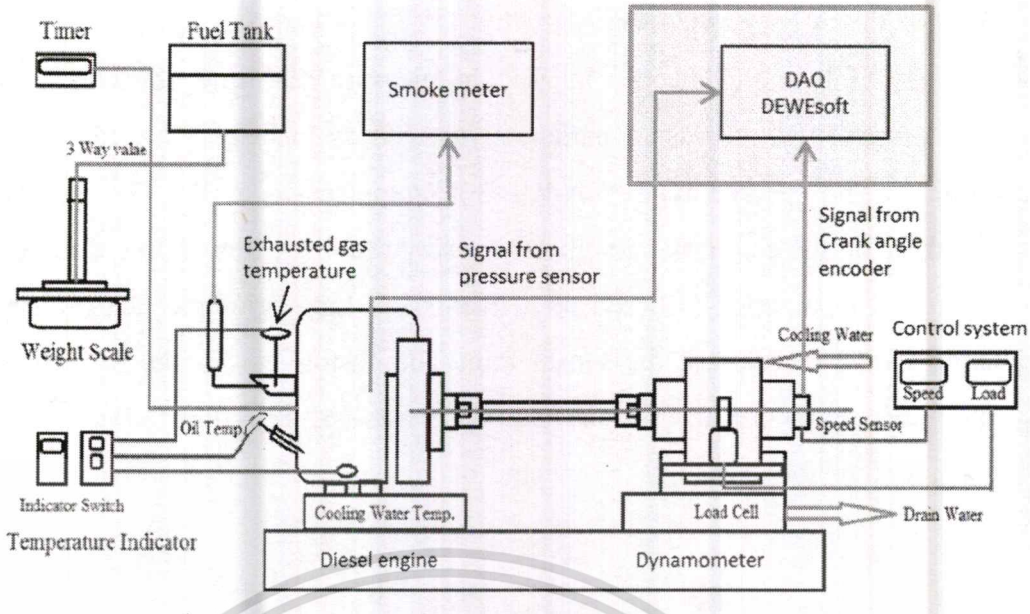


**Figure 3.7** Schematic diagram of data acquisition unit connected to Pressure and Crank angle encoder

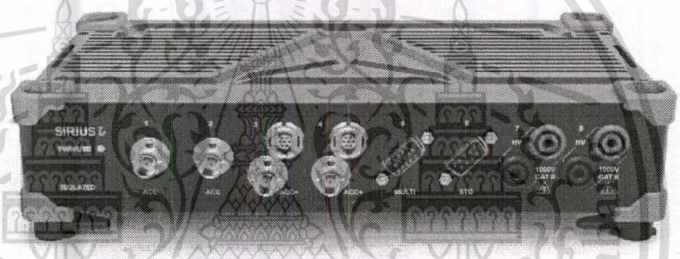

**Figure 3.8** Data Acquisition Unit (DAQ) DEWEsoft SIRIUSi-HS-CA

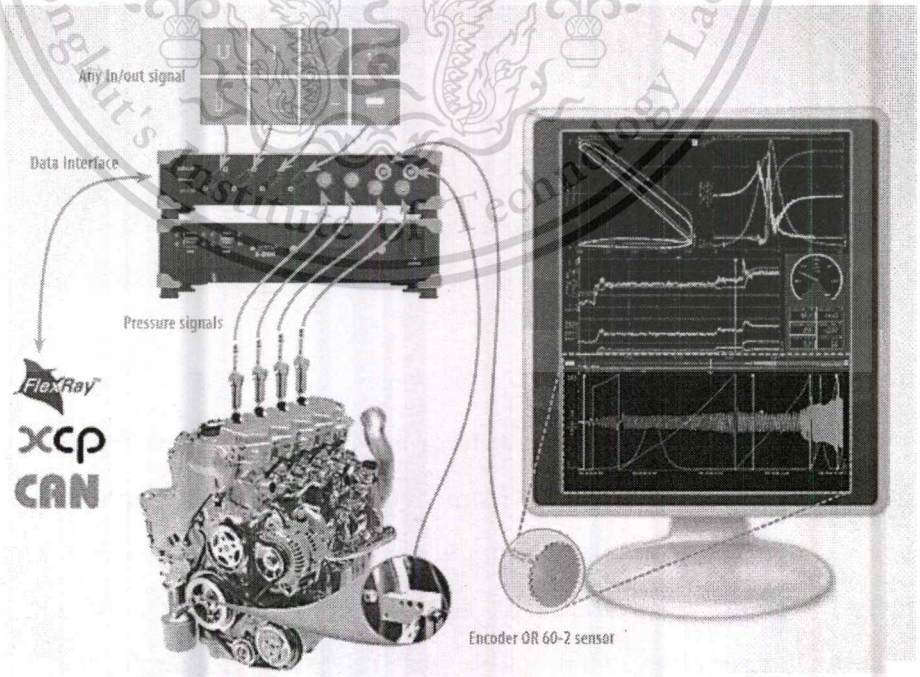


**Figure 3.9** Data Acquisition Unit (DAQ) DEWEsoft

This material is reserved for educational use only, not allowed for commercial use.
Forbidden to modify the content, and cite the document when use.

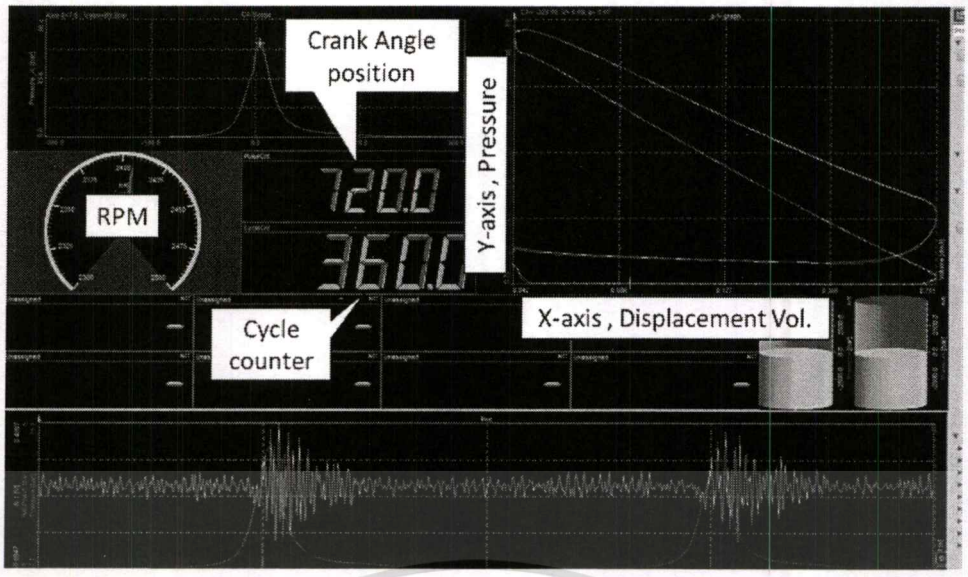


**Figure 3.10** Data acquisition interface

## 3.2 Experimental procedure

This research, biodiesel (B100) and ethanol-blended biodiesel (BE10 and BE20) were supplied in the diesel engine's combustion chamber to produce particulate matter. Combustion characteristics, PM quantity emission, PM morphology, and PM oxidation kinetics will be analyzed through the research.

3.3.1 Combustion characteristics

First, engine performance for each type of fuel was investigated to see overall scope of the experiment. The test was performed at Wide Opened Throttle (WOT) condition varying from 1400 RPM to 2400 RPM. Then, fuel consumption as well as exhaust gas temperature were measured to investigate fuel effect on engine's Brake Thermal Efficiency (BTE). The test was done at constant engine speed of 2000 RPM by varying from no load to 80% load. To be comparable with other research work, load conditions for the combustion analysis were converted to Brake Mean Effective Pressure (BMEP). Then, in-cylinder combustion parameter such as 'Pressure VS Crank angle' and 'Rate of heat release VS Crank angle' were investigated to see combustion characteristics. The test was performed at constant engine speed of 2400 RPM by varying load at 0.2MPa, 0.4MPa, and 0.6MPa of BMEP.

This material is reserved for educational use only, not allowed for commercial use.
Forbidden to modify the content, and cite the document when use.

3.3.2 Particulate matter quantity emission

The particulate matter quantities were investigated by percentage intensity of smoke on filter paper as shown in figure 3.11. The particulate matter was trapped by the smoke meter device and filtered while it suspended in exhaust gas in condition. White filter paper was used to trap particulate matter in exhaust gas to be measured by light emitting method. Results of the present research i.e. PM intensity from B100, BE10, and BE20 were compared with the results from previous research (B100 and diesel) in order to see effect of ethanol on PM emission reduction.

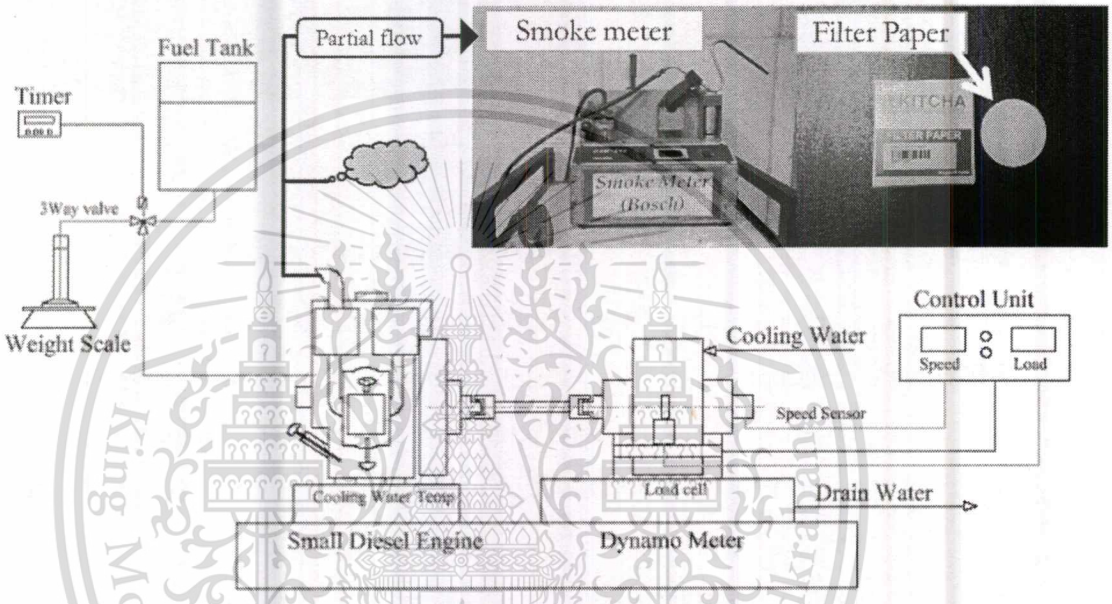


**Figure 3.11** Schematic diagram of PM intensity measurement by smoke meter

3.3.3 Particulate matter morphology

PM emitted from each type of fuel was investigated in viewpoint of morphology. There are two methods for PM collection in this research. First method is PM collection on filter paper which is similar to PM intensity measurement in the section 3.3.2. PM dispersed on filter paper was investigated by Scanning Electron Microscope (SEM) as shown in Fig. 3.12 to see morphology of agglomerated particles. Second method collected PM as powder (trapping equipment is shown as Fig. 3.13). This method, PM was investigated into more detail of morphology by Transmission Electron Microscope (TEM) as shown in Fig. 3.14. Therefore, details of PM nanostructure e.g. primary particle's morphology and of graphite crystallite can be obtained. The engine operating condition for PM collection was controlled at 80% load.

This material is reserved for educational use only, not allowed for commercial use.
Forbidden to modify the content, and cite the document when use.

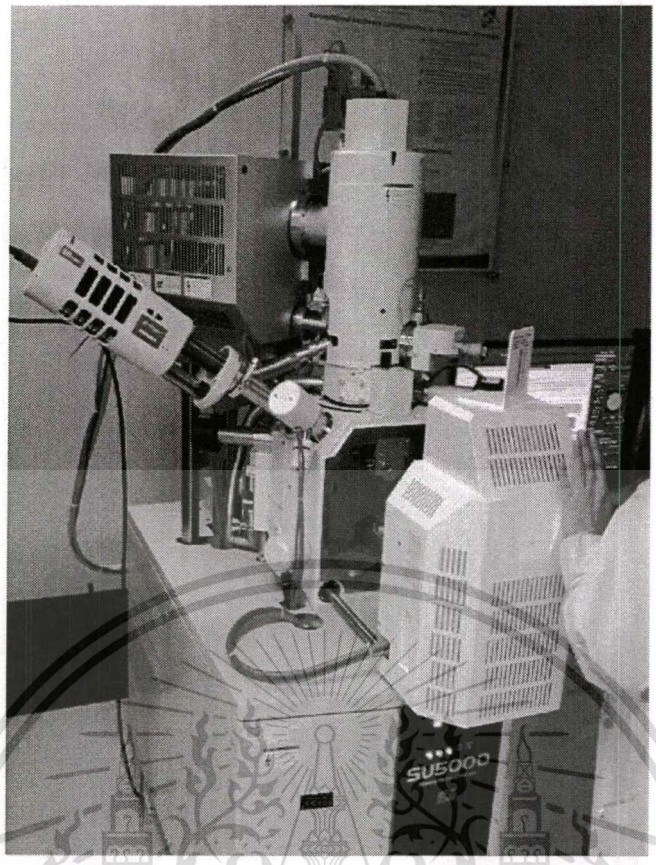


**Figure 3.12** Scanning Electron Microscope for agglomerated particle investigation

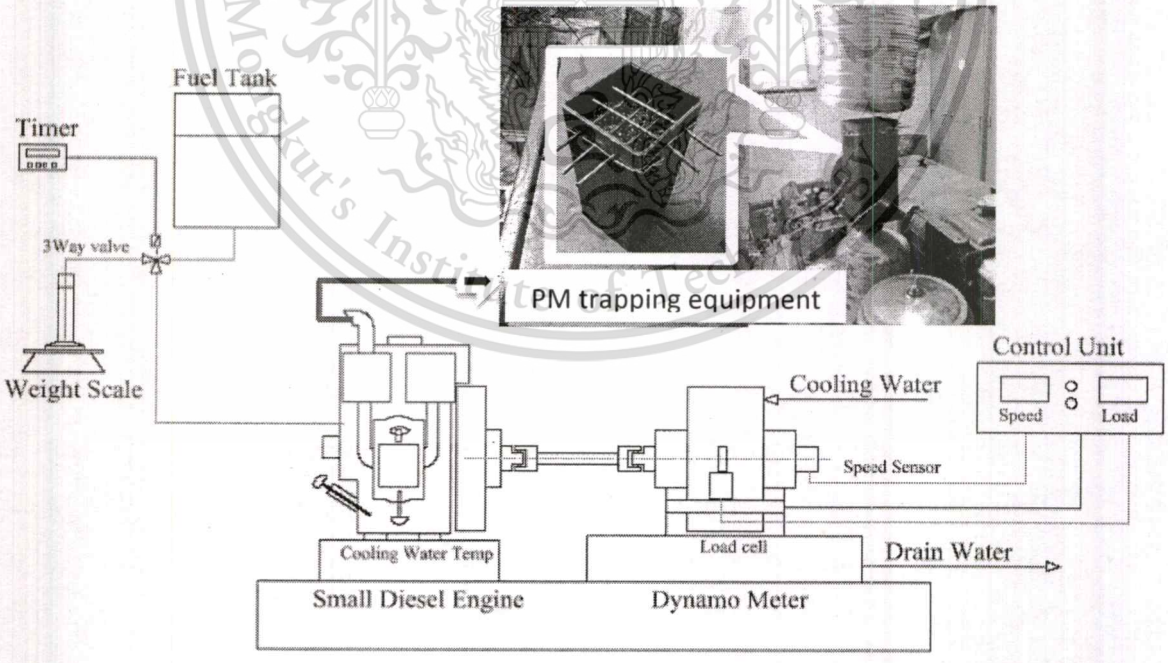


**Figure 3.13** Schematic diagram of PM collection for investigation via Transmission Electron Microscope

This material is reserved for educational use only, not allowed for commercial use.
Forbidden to modify the content, and cite the document when use.

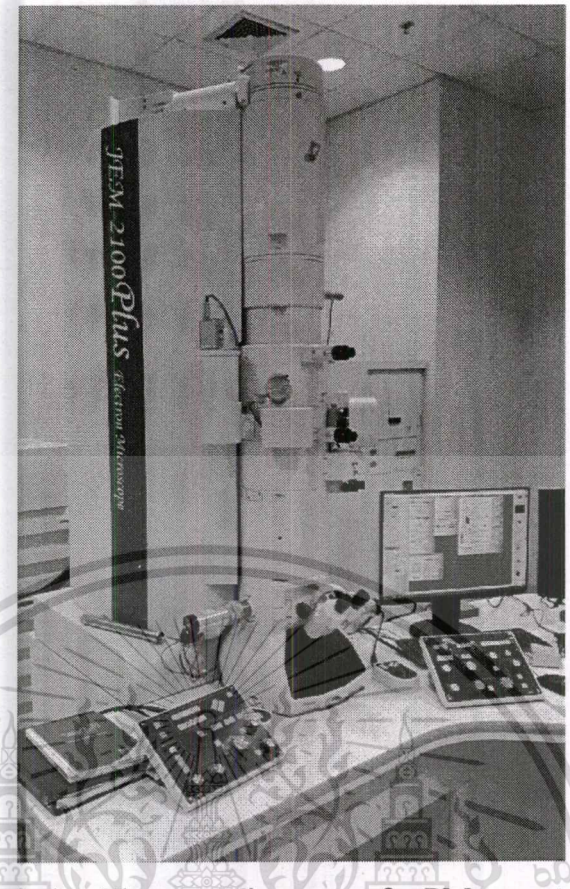


**Figure 3.14** Transmission Electron Microscope for PM nanostructure investigation

3.3.4 Particulate matter oxidation kinetics

The particulate matter powder from each fuel's combustion in section 3.3.3 was brought to analyze by Thermo Gravimetric Analysis (TGA) with isothermal method. The TGA equipment and PM sample for this research is shown in Fig. 3.15. Mass reduction rate together with temperature results from TGA were investigated into oxidation kinetics and chemical consistent. Isothermal TGA applied in this research has temperature range from 425 ℃ to 625 ℃ depending on sources of PM. Before reaching isothermal stage, temperature of all types of PM sample were controlled with the increment rate of 100 ℃ per minute from room temperature (30 ℃). While the ramping up from 30 ℃ to isothermal stage, nitrogen gas was released to prevent the oxidation of particulate matter and after that air was release to oxidize with particulate matter. For the chemical consistent, the moisture, unburned hydrocarbon and carbon fraction inside the particulate matter from each type of fuel was determined from the oxidation temperature. Moisture and hydrocarbon are oxidized in first phase at low temperature. Carbon or soot is expected to be oxidized in the isothermal phase.

This material is reserved for educational use only, not allowed for commercial use.
Forbidden to modify the content, and cite the document when use.

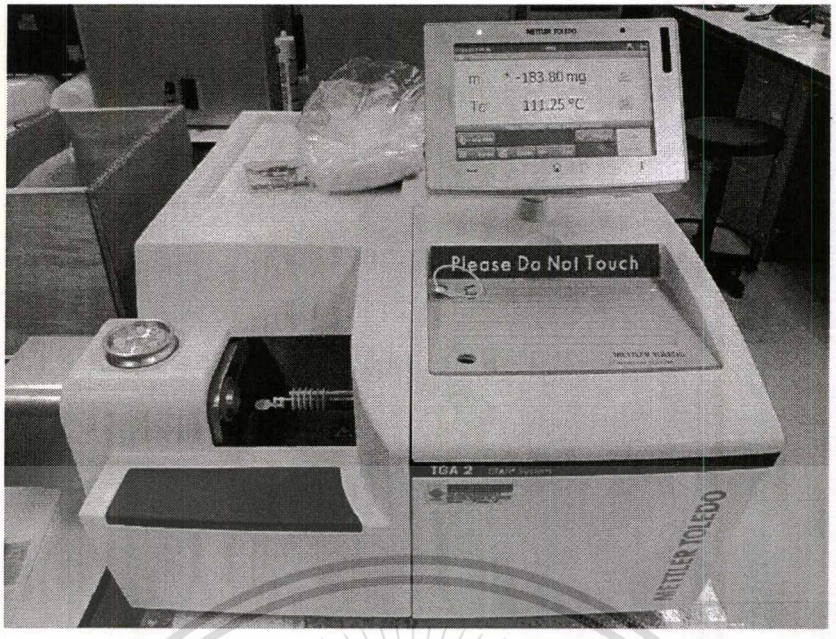


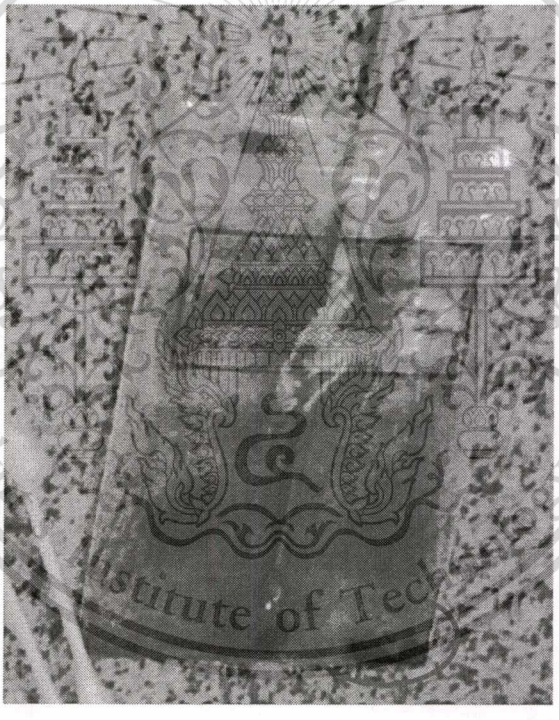

**Figure 3.15** TGA Analyzer and PM sample for oxidation kinetics investigation

This material is reserved for educational use only, not allowed for commercial use.
Forbidden to modify the content, and cite the document when use.

# CHAPTER 4

# RESULTS AND DISCUSSIONS

## 4.1 Engine performance

The engine B's performance curve of biodiesel (B100), ethanol blended biodiesel (BE10 and BE20), and diesel (as reference) is plotted in Fig. 4.1. **(In chapter 4, diesel's test result and diesel's analysis data that are put in parenthesizes are results from previous PM research. They are used as reference for this research)** Engine load drops as increasing engine speed for all fuels. The ethanol blended fuel (BE10 and BE20) produces lower load due to lower calorific value as well as lower stoichiometric air-fuel ratio i.e. leaner combustion compared with biodiesel and diesel. The engine load shows significant drop at higher speed and more ethanol blended ratio.

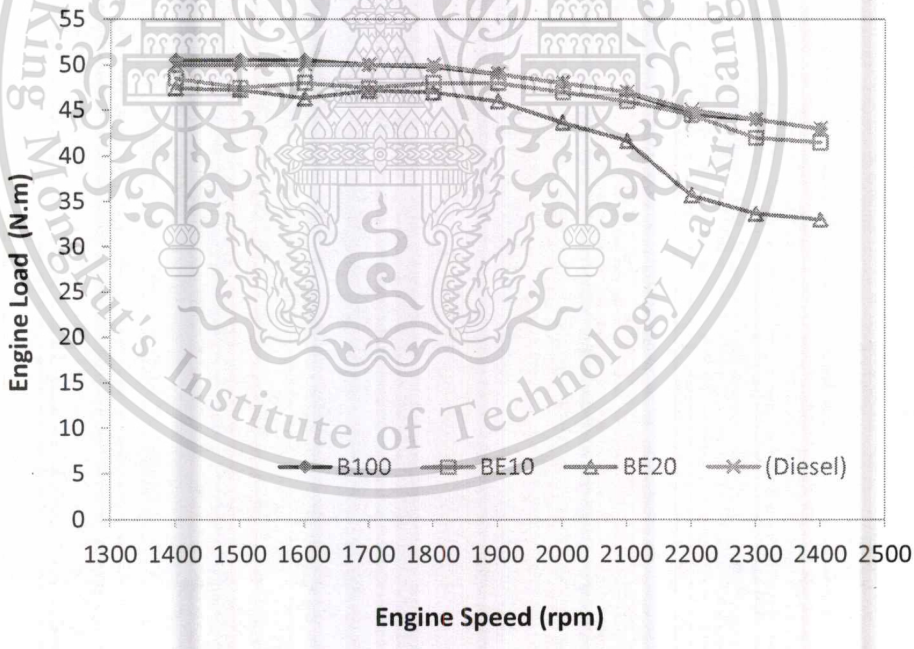


**Figure 4.1** Engine performance curve

This material is reserved for educational use only, not allowed for commercial use.
Forbidden to modify the content, and cite the document when use.

## 4.2 Brake specific fuel consumption (BSFC), Brake thermal efficiency (BTE), and Exhausted gas temperature (EGT)

Brake specific fuel consumption (BSFC), Exhausted gas temperature (EGT), and Brake thermal efficiency (BTE) with respect to engine load are shown in Fig. 4.2, Fig. 4.3, and Fig. 4.4 respectively. BSFC of the ethanol blended fuels, are higher than that of biodiesel at all load conditions due mainly to the lower calorific value of ethanol. (This phenomenon agrees with diesel fuel as well). Thus, the amount of fuel supply into the engine must be greater. The trend shows decrease in the BSFC as the engine load increase. It can be explained as; when the engine load increases, combustion temperature which is implied from the rise of EGT increases as well. Reactivity of fuel and oxygen activates conversion of combustion heat to mechanical work much more than amount of energy from the fuel input. That is why the BSFC decreases as the engine load increases.

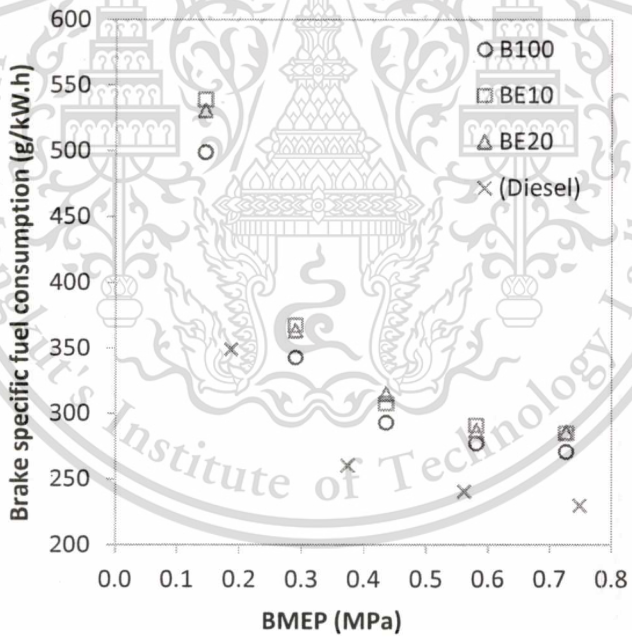


**Figure 4.2** Engine performance curve

This material is reserved for educational use only, not allowed for commercial use.
Forbidden to modify the content, and cite the document when use.

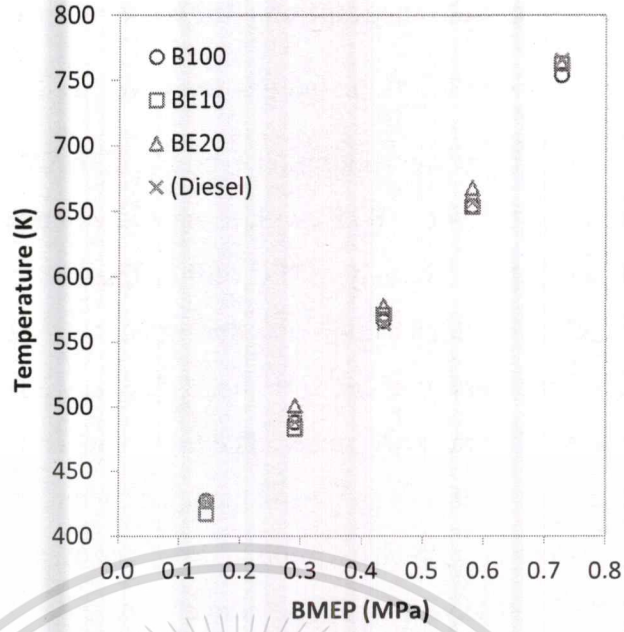


**Figure 4.3** Exhausted gas temperature

BTE plots show that as the engine load increases, the engine produces more thermal efficiency for all fuels. BTEs are not significantly different among fuels because fuels with higher BSFC such as BE20 or BE10 compensates their lower calorific values, compared with B100 or diesel.

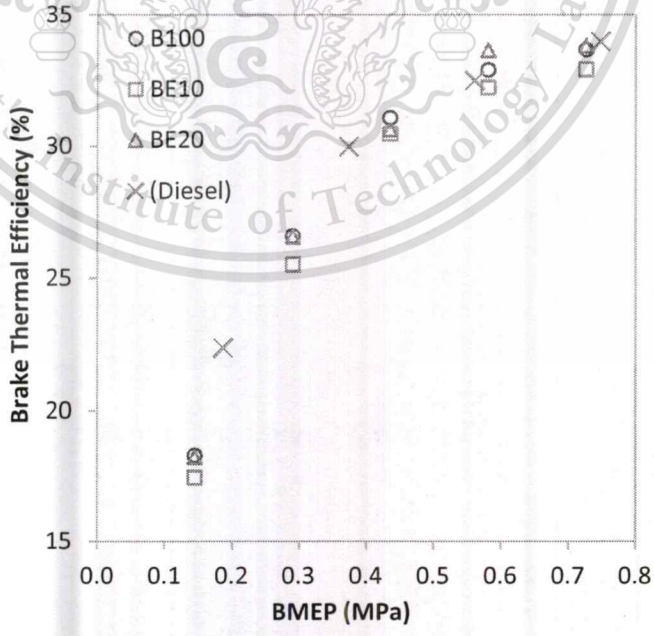


**Figure 4.4** Brake thermal efficiency

This material is reserved for educational use only, not allowed for commercial use.
Forbidden to modify the content, and cite the document when use.

### 4.3 Combustion characteristics

For the engine B's combustion characteristics, in-cylinder pressure variation with respect to crank angle is shown in Fig. 4.5 and heat release rate in Fig. 4.6 for B100, BE10, BE20, and diesel. The engine load was varied in the range of 0.2 MPa, 0.4 MPa, and 0.6 MPa at constant engine speed of 2400 rpm. Peak pressures of all fuels increase with the increasing engine load. Considering at the ethanol blended fuels, at low load of 0.2MPa, the peak pressure occurs after the biodiesel and diesel's peak for 10 to 15 crank angle degrees. At the low load condition, low combustion temperature causes ethanol blended fuel which has higher heat of vaporization as well as high auto ignition temperature delay in the start of combustion. Therefore, the peak pressure occurs further away from top dead center. At higher engine load, the increment of combustion temperature cause better fuel vaporization which leads to less combustion delay in the ethanol blended fuel and the peak pressures increase as well.

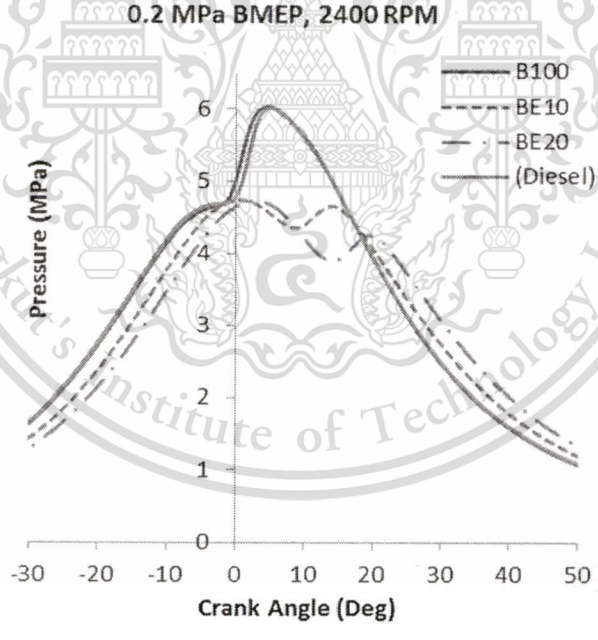


**Figure 4.5a** In-cylinder pressure versus crank angle at 0.2MPa BMEP and engine speed of 2400 rpm

This material is reserved for educational use only, not allowed for commercial use.
Forbidden to modify the content, and cite the document when use.

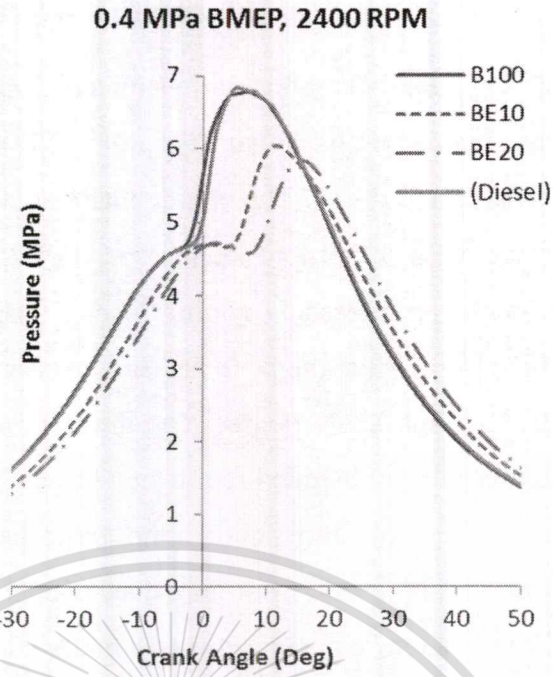


**Figure 4.5b** In-cylinder pressure versus crank angle at 0.4MPa BMEP and engine speed of 2400 rpm

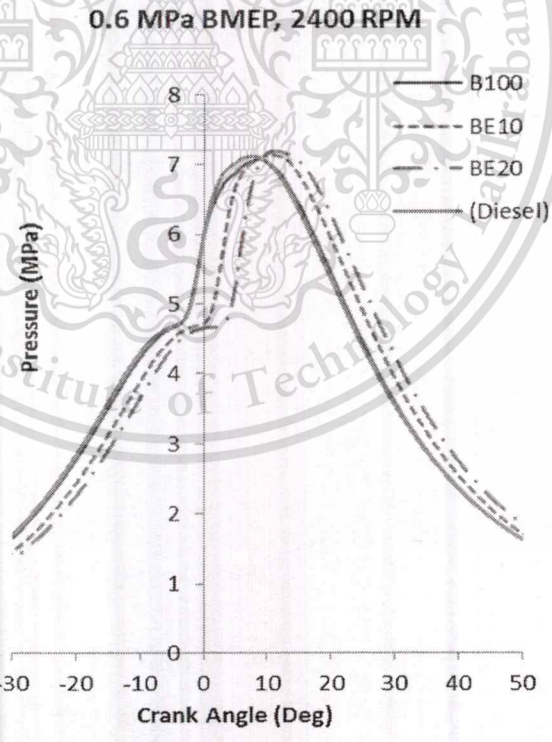


**Figure 4.5c** In-cylinder pressure versus crank angle at 0.6MPa BMEP and engine speed of 2400 rpm

This material is reserved for educational use only, not allowed for commercial use.
Forbidden to modify the content, and cite the document when use.

Heat release rate plots in Fig. 4.6 show that combustion processes of all fuels start with premixed combustion phase followed by diffusion combustion phase. At low engine load (Fig. 4.6a), the fuel with more ethanol content which is BE20 has more significant ignition delay than B100 which effects on retarded premixed combustion phase, while a higher peak of the heat release can be observed on higher load (Fig. 4.6c). (The result of high peak in heat release has less effect when compared with diesel because diesel also has a little retarded combustion behavior compared with B100) The reason is that low temperature in the low load condition causes the ethanol blended fuel need more time for fuel atomization due to higher heat of vaporization of ethanol and auto ignition temperature as explained above. After enough fuel atomization and mixing with oxygen, rapid combustion produces high peaks of heat release rate as shown in the Fig. 4.6c. However, at the higher engine load, higher combustion temperature makes better fuel vaporization and fuel atomization as well. Therefore, there is less retarded combustion for the ethanol blended fuels and stronger premixed combustion leads to higher peak of heat release rate. Although the ethanol blended fuels have more delay in premixed combustion compared with B100 and diesel, their combustion processes or diffusion combustion zone tends to finish earlier. That means the diffusion combustion time for the ethanol blend is reduced because of better fuel atomization, better fuel mixing , and more oxygen content in the fuels promote more complete combustion.

This material is reserved for educational use only, not allowed for commercial use.
Forbidden to modify the content, and cite the document when use.

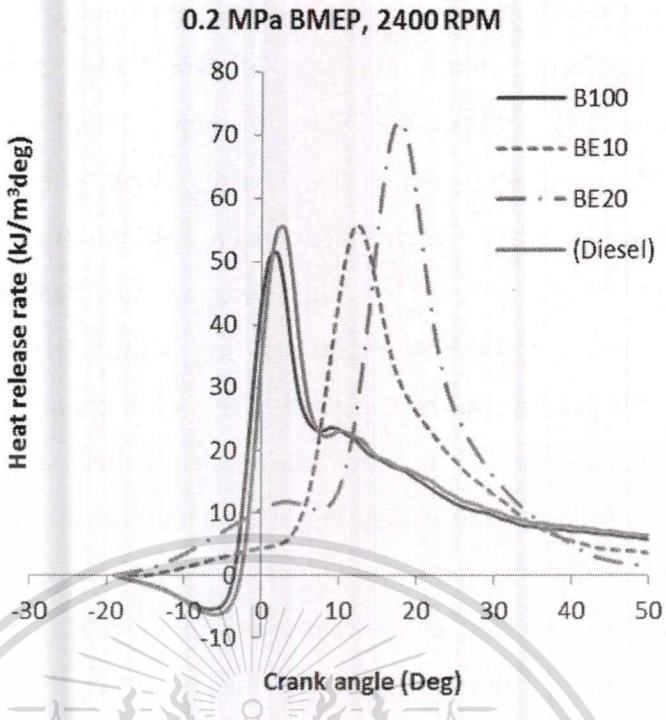


**Figure 4.6a** Heat release rate versus crank angle at 0.2MPa BMEP and engine speed of 2400 rpm

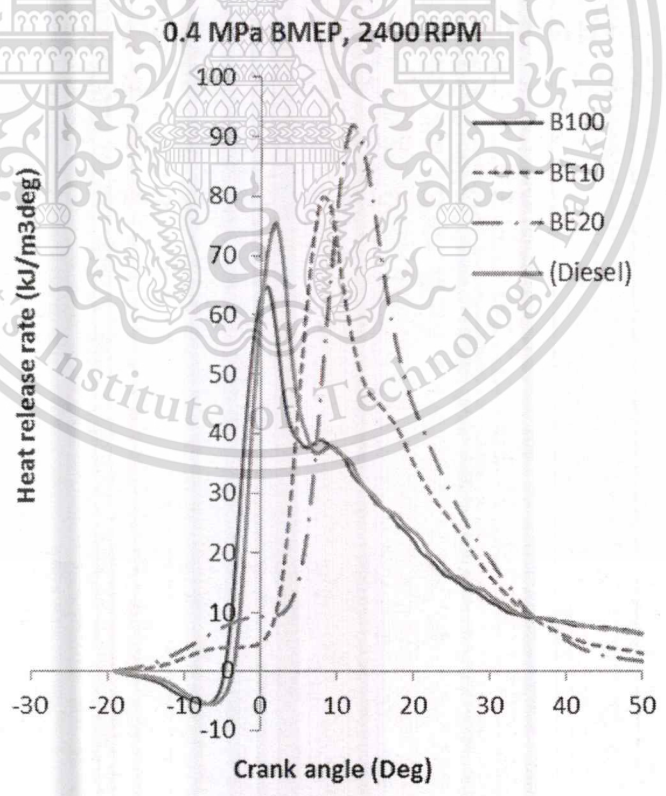


**Figure 4.6b** Heat release rate versus crank angle at 0.4MPa BMEP and engine speed of 2400 rpm

This material is reserved for educational use only, not allowed for commercial use.
Forbidden to modify the content, and cite the document when use.

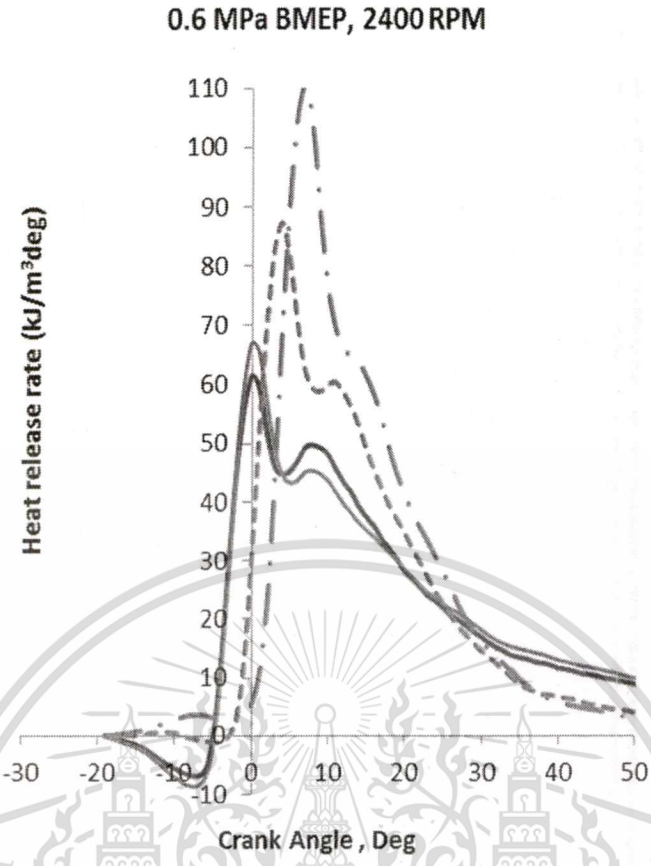


**Figure 4.6c** Heat release rate versus crank angle at 0.6MPa BMEP and engine speed of 2400 rpm

This material is reserved for educational use only, not allowed for commercial use.
Forbidden to modify the content, and cite the document when use.

### 4.4 Particulate matter's quantity emission

Figure 4.7a shows a result of the previous research in smoke intensity comparison between biodiesel and diesel combustion. The study was found that the intensity be strongly dependent on the engine load. The more engine load, the greater smoke intensity due to more fuel supply for combustion. Biodiesel emits approximately 50% smoke intensity less than diesel combustion overall operating conditions. The reason was referred as oxygen fraction in biodiesel's fuel molecules which promotes complete combustion. Surely, the smoke intensity measurement can express trends of smoke quantity, however it is difficult to interpret accurate PM's quantity since it is possible that PM covered by colorless volatile or hydrocarbon might not reflect actual measurement result.

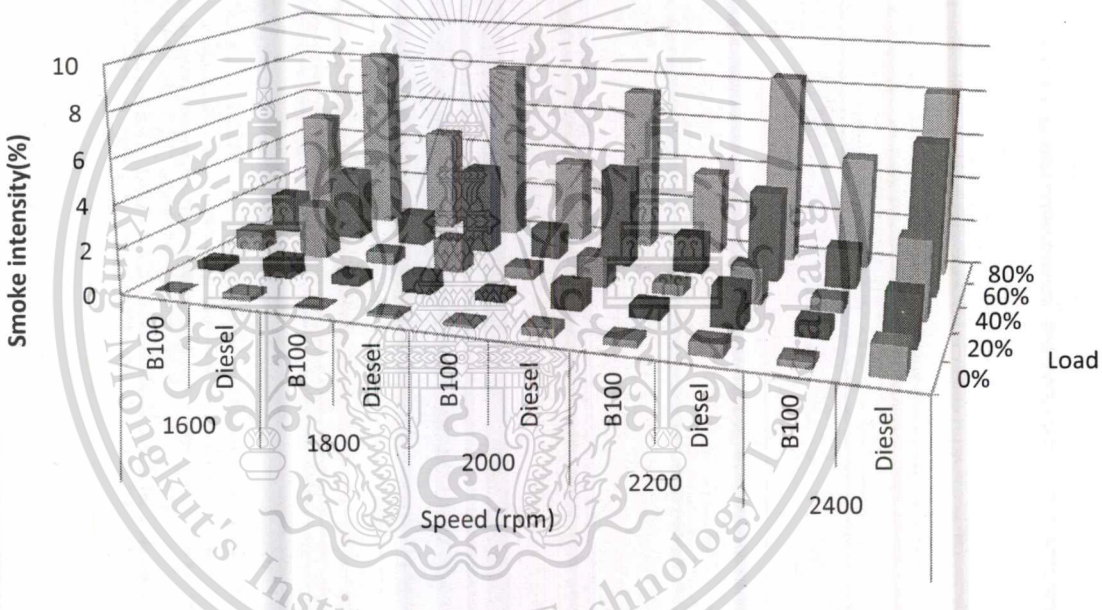


**Figure 4.7a** Smoke intensity comparison between diesel and biodiesel combustion (Previous research)

In the present research, comparison of smoke intensity between ethanol blended fuels and biodiesel is shown as Fig. 4.7b aimed to see effects of ethanol on smoke intensity emission. Ethanol blended fuels (BE10 and BE20) produce less smoke at almost all engine operating conditions compared with biodiesel. Average smoke reduction for BE10 and BE20 is 27.2% and 58.6% respectively. It can be explained into 2 main aspects. First reason which is similar to the research in Fig. 4.9a is that more oxygen fraction in ethanol plays a key role in promoting complete

This material is reserved for educational use only, not allowed for commercial use.
Forbidden to modify the content, and cite the document when use.

combustion. Second, retarded combustion characteristics of the BE10 and BE20 provide enough time for fuel atomization as well as extreme peak of heat release contributes better fuel-oxygen's reactivity i.e. more complete combustion.

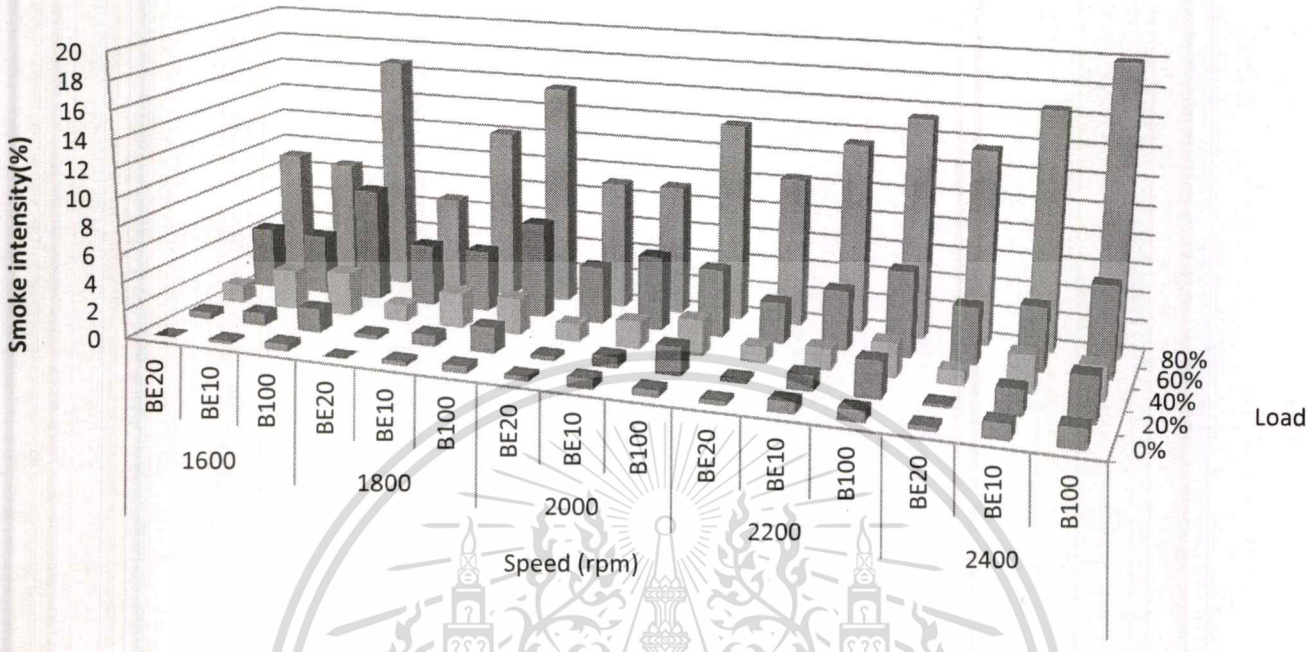


**Figure 4.7b** Smoke intensity comparison among B100, BE10, and BE20 (Present research)

This material is reserved for educational use only, not allowed for commercial use.
Forbidden to modify the content, and cite the document when use.

### 4.5 Particulate matter's morphology and nanostructure

The particulate matter from B100 and BE20's combustion was investigated for PM morphology and nanostructure in the present research. Results were also to be compare with former research (diesel-biodiesel). PM morphology and nanostructure can be analyzed via images derived from modern electron microscopes i.e. Scanning Electron Microscope (SEM) and Transmission Electron Microscope (TEM) techniques.

For SEM images, PM with a level of **agglomerated particles** can be investigated. Figure 4.8a and Figure 4.8b show samples of SEM images of PM derived from B100 and BE20 respectively. They are composed of groups of agglomerated particles gathered on paper filter. Sizes of these agglomerated particle groups vary from hundreds nanometers to few microns. Fine particles or PM2.5 as shown as red mark on Fig 4.8a can be observed. Bigger groups or PM10 is shown as red mark on Fig.4.8b. However, there is no obvious relationship between agglomerated particle's size, appearance, and combustion of each type of fuel.


**Figure 4.8a** SEM images of B100's particulate matter

This material is reserved for educational use only, not allowed for commercial use.
Forbidden to modify the content, and cite the document when use.


**Figure 4.8b** SEM images of BE20's particulate matter

To see more detail of the PM, investigation of PM morphology up to Nano scale is necessary. TEM images were applied to show details of agglomerated particles, **single particles or primary particles**, up to level of graphite crystallite structure. Figure 4.9a and Figure 4.9b show TEM images of agglomerated particles from B100 and BE20 respectively. Both of them look similar in appearance. However, detailed morphology and nanostructure were to be analyzed by image processing with software called "Image J" to measure quantitative data of particles such as particle's size, particle's surface, or graphite crystallite

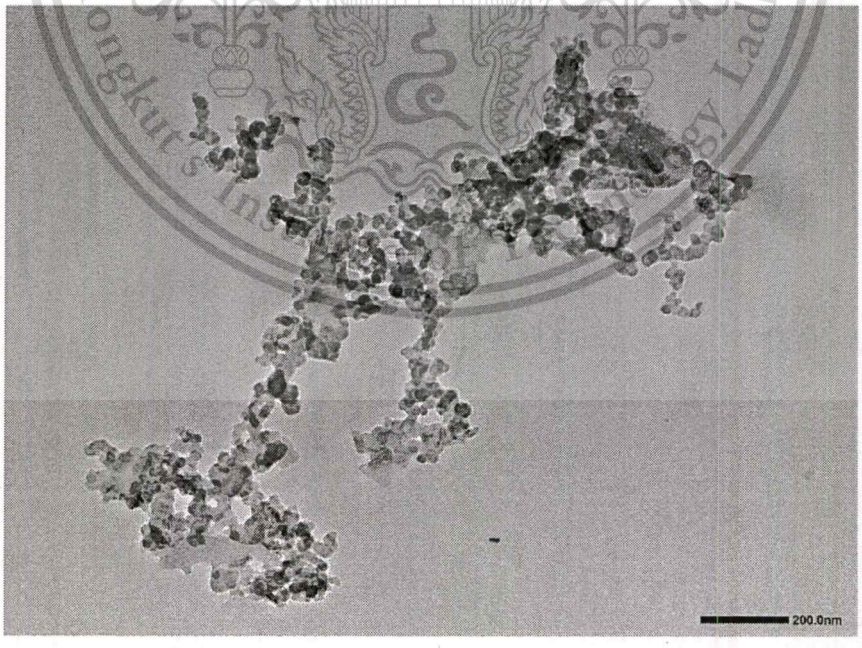


**Figure 4.9a** TEM image of B100's agglomerated particle

This material is reserved for educational use only, not allowed for commercial use.
Forbidden to modify the content, and cite the document when use.

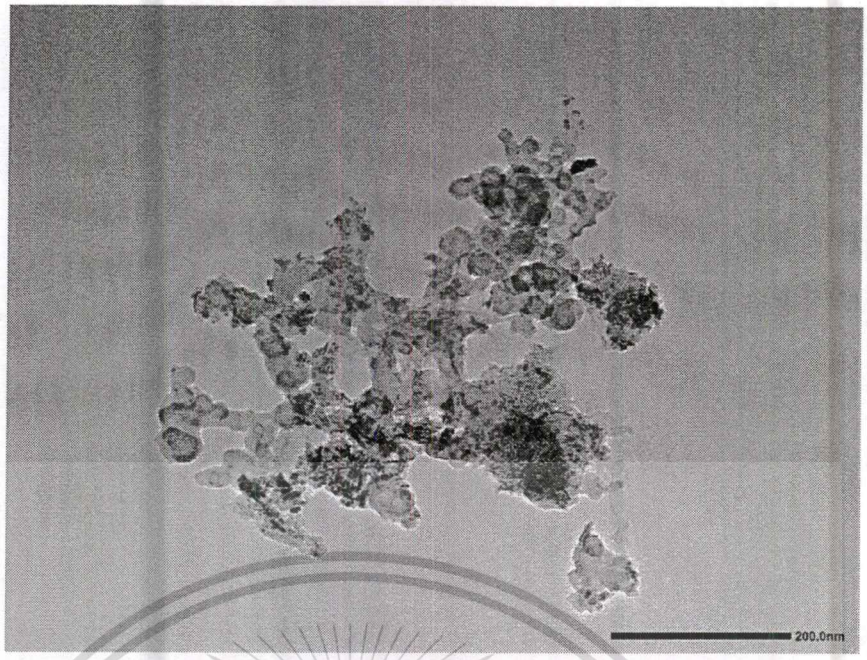


**Figure 4.9b** TEM image of BE20's agglomerated particle

4.5.1 Primary particle's morphology

Figure 4.10a – figure 4.10c show measurement of PM's primary particle size from B100, BE20, and diesel respectively. (**Diesel's particle was also measured as reference results for BE20's and B100's particle analysis**) The measurement applies particle's perimeter approach to determine particle's section area and then to calculate equivalent diameter. Sampling rate is approximately 50-60 per PM types. Figure 4.11a – Figure 4.11d shows measurement result of primary particle's size distribution of fuel B100, BE20, and diesel respectively. B100's particles show size distribution in narrow range compared with BE20's and diesel's particles (Standard deviation of B100's, BE20's, and diesel's particle size is 7.4, 8.6, 8.8 nm, respectively). It means B100's particles are most uniform in size. Average primary particle size of **B100** also is smallest **of 27.0 nm**, followed by **BE20 of 29.1 nm** and **Diesel of 29.8nm**. Therefore, it can be estimated that B100's particles have more reactive external surface area than BE20's particle for 7.7% and 11.1% more compared with diesel's particles. For the effects of primary particle sizes on other PM characteristics will be discussed in Oxidation Kinetics section.

This material is reserved for educational use only, not allowed for commercial use.
Forbidden to modify the content, and cite the document when use.

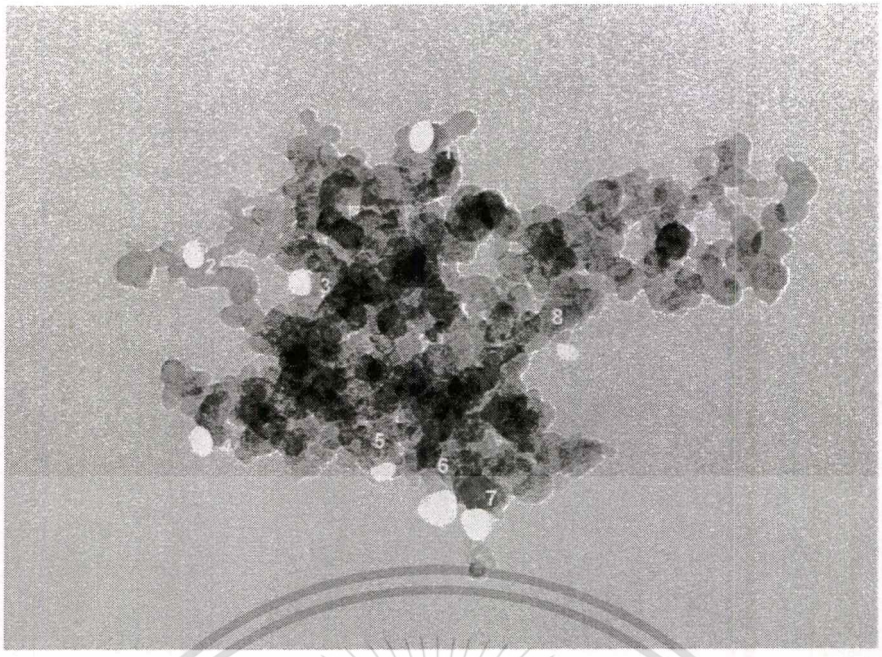

**Figure 4.10a** Sample of B100's primary particle's measurement


**Figure 4.10b** Sample of BE20's primary particle measurement

This material is reserved for educational use only, not allowed for commercial use.
Forbidden to modify the content, and cite the document when use.

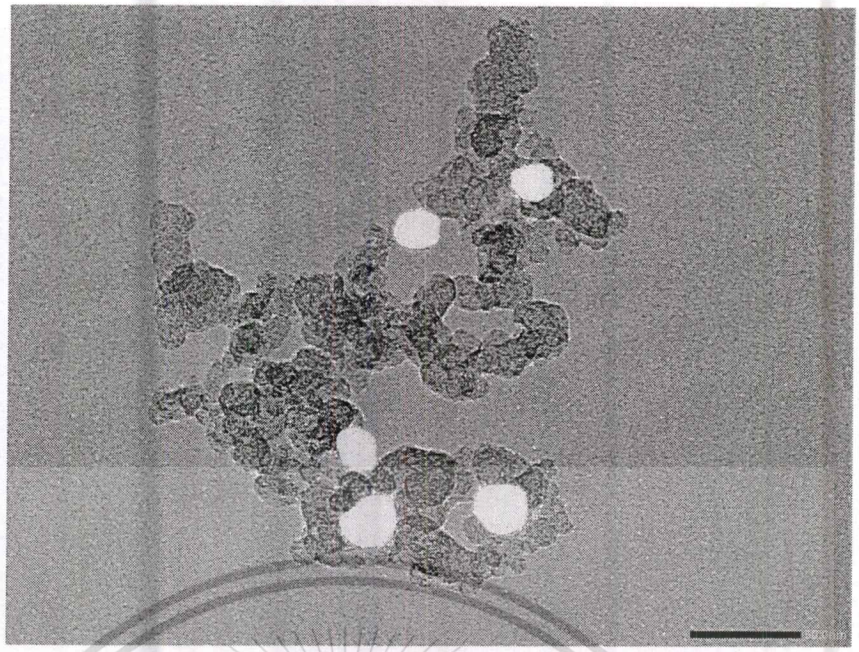

**Figure 4.10c** Sample of diesel's primary particle's measurement

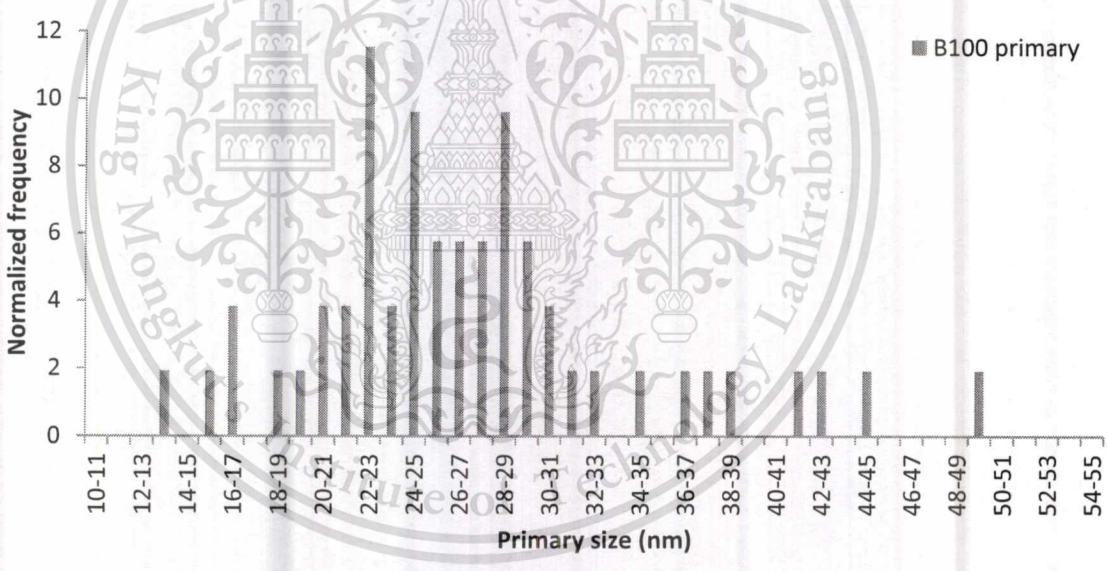


**Figure 4.11a** B100's primary particle's size distribution

This material is reserved for educational use only, not allowed for commercial use.
Forbidden to modify the content, and cite the document when use.

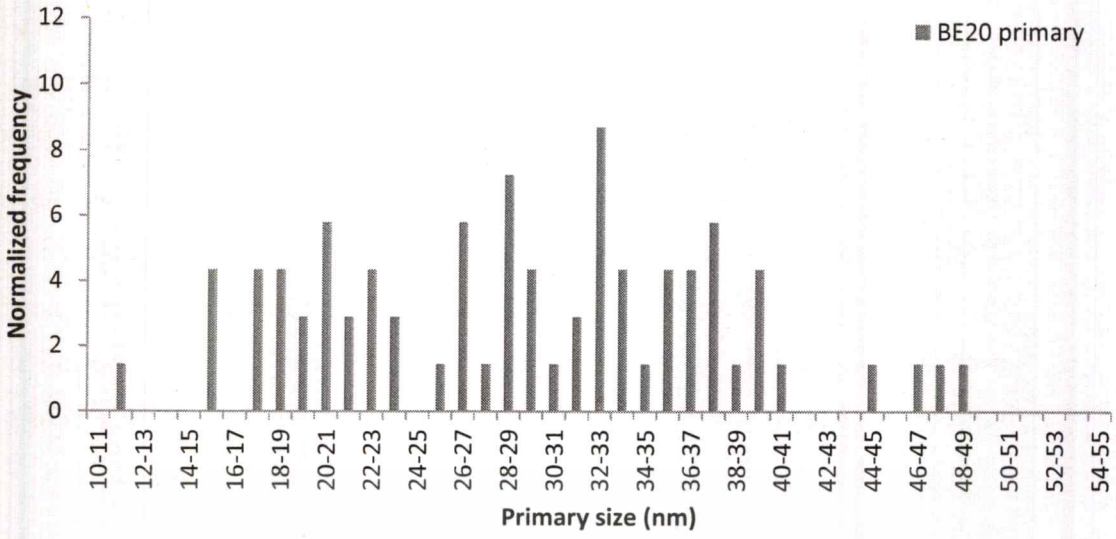


**Figure 4.11b** BE20's primary particle's size distribution

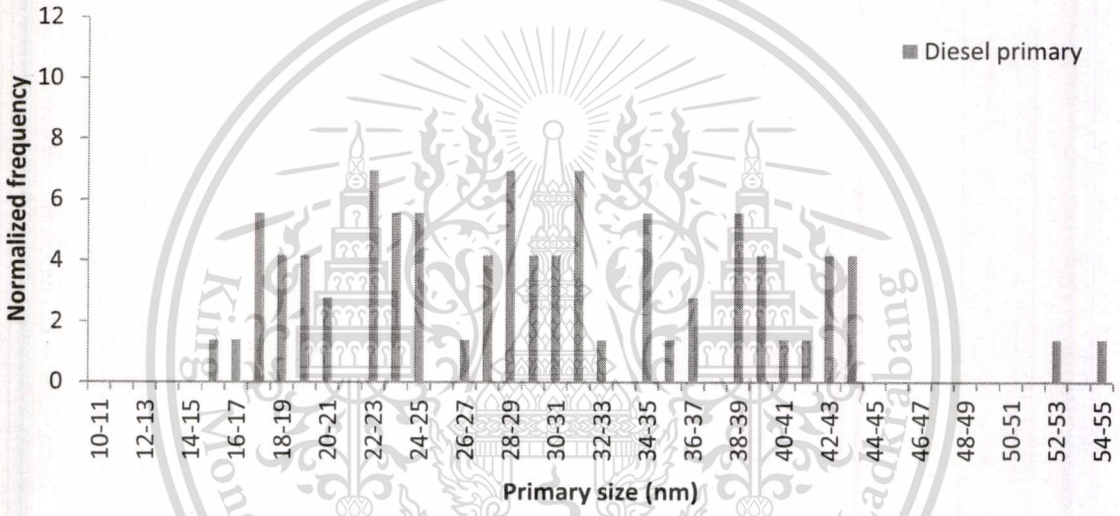


**Figure 4.11c** Diesel's primary particle's size distribution

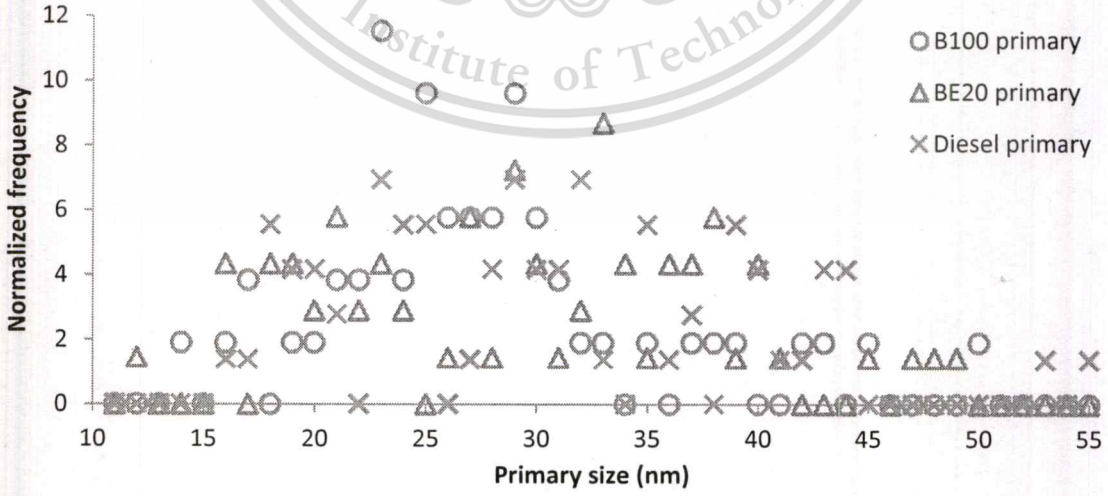


**Figure 4.11d** Combined fuel's primary particle's size distribution

This material is reserved for educational use only, not allowed for commercial use.
Forbidden to modify the content, and cite the document when use.

Other than the aspect of particle size, further PM characteristics that effect on oxidation reactivity should be investigated. Figure 4.12 propose a conceptual diagram about particle's surface area with different geometry. It is usual that particles with less sphericity i.e. non-circular, tends to has more surface area. This concept then was brought to investigate the B100, BE20, and diesel's primary particles. Figure 4.13 represents plots between equivalent diameters of the particles and their perimeters. It is obvious that all particles are not completely spherical because coefficients of the plot or slopes are more than pi or 3.14 for all cases. However, the effects of geometry difference for each PM type are negligible. So it is not supposed to influence particle's surface area.

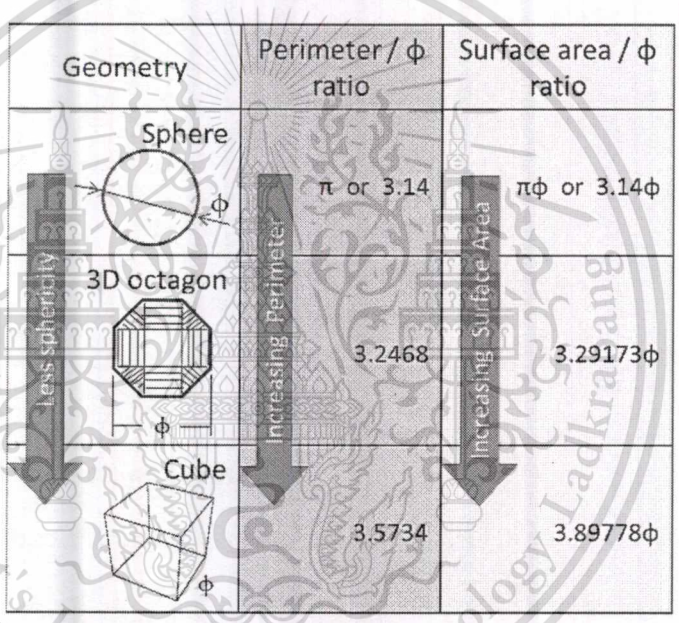


**Figure 4.12** Relationship between particle size, perimeter, and surface area for different geometry

This material is reserved for educational use only, not allowed for commercial use.
Forbidden to modify the content, and cite the document when use.

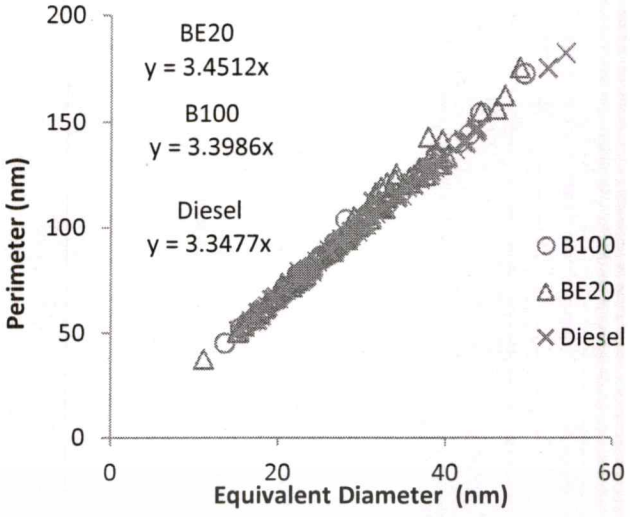


**Figure 4.13** Relationship between particle's diameter and perimeter of BE20, B100, and diesel's primary particle

4.5.2 Particulate matter nanostructure

More insight on particulate matter is necessary to consider deeper to nanostructure level. Figure 4.14 show high magnification TEM images of B100, BE20, and diesel's primary particles or soot particles respectively.

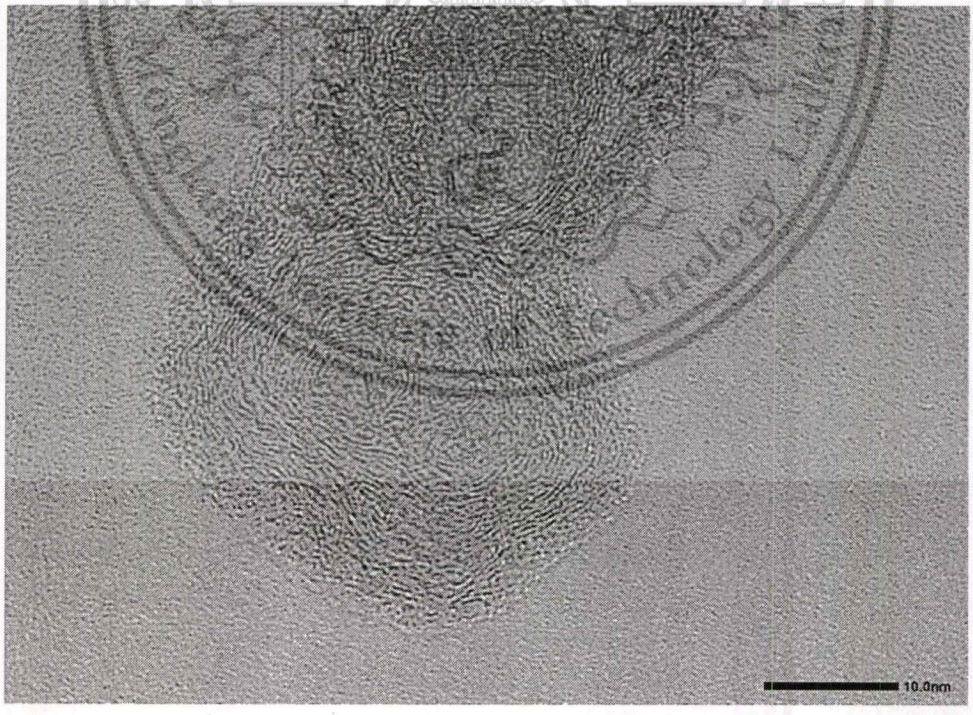


Figure 4.14a B100's Primary particles

This material is reserved for educational use only, not allowed for commercial use.
Forbidden to modify the content, and cite the document when use.

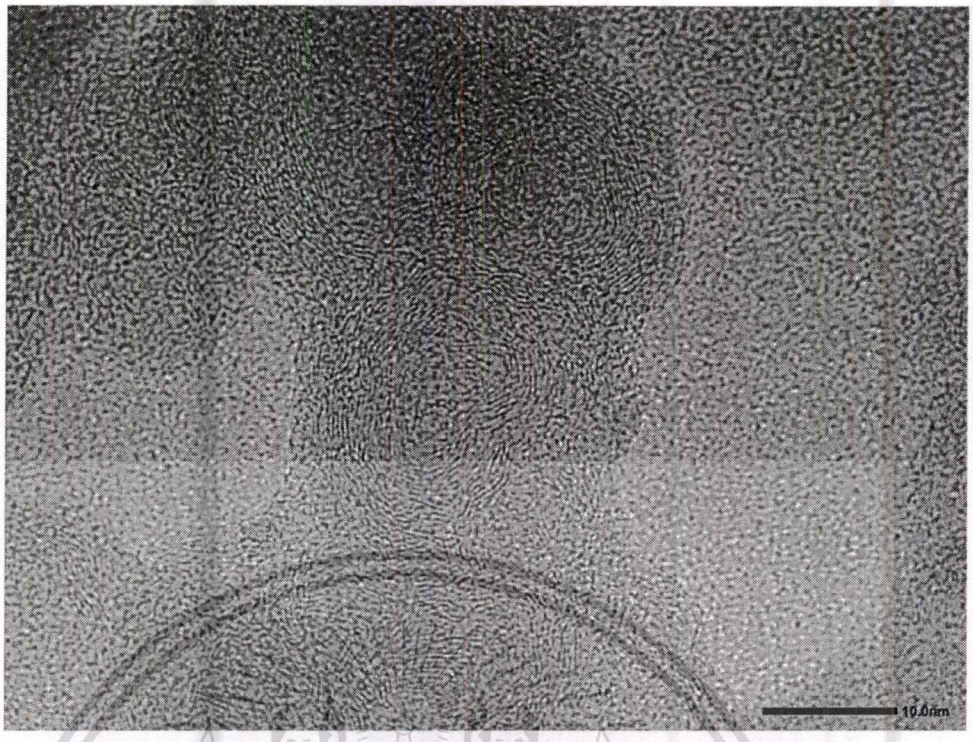


**Figure 4.14b** BE20's Primary particles


**Figure 4.14c** Diesel's Primary particles

This material is reserved for educational use only, not allowed for commercial use.
Forbidden to modify the content, and cite the document when use.

**In nanostructure level, it is more convenient to refer primary particles as soot particles** because we focus on action of carbon on PM characteristics. From the images, it can be seen that soot particles consist of many carbon crystallites. On each crystallite, it is Graphene sheet structure which is formed by molecules of hexagon-like carbon - 6 (C-6) is the possible smallest size. Such molecules are agglomerated to be the large ring of carbon then becomes a graphene sheet or crystallite platelet. These crystallites were processed by image processing method so that they can be quantitatively analyzed. Figure 4.15 show cropped images of B100, BE20, and diesel's soot particle in interested areas of carbon crystallite (approximately 10 nm x 10 nm.) Figure 4.16a – Figure 4.16c show black and white images of crystallites with noise already filtered. Figure 4.16d – Figure 4.16f show skeletonized images of the black and white images in order that crystallite length can be determined quantitatively.

King Mongkut's Institute of Technology Ladkrabang

This material is reserved for educational use only, not allowed for commercial use.
Forbidden to modify the content, and cite the document when use.

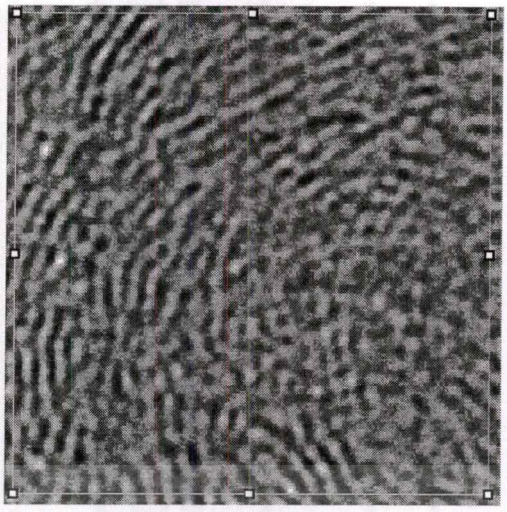

**Figure 4.15a** B100's crystallite cropped image

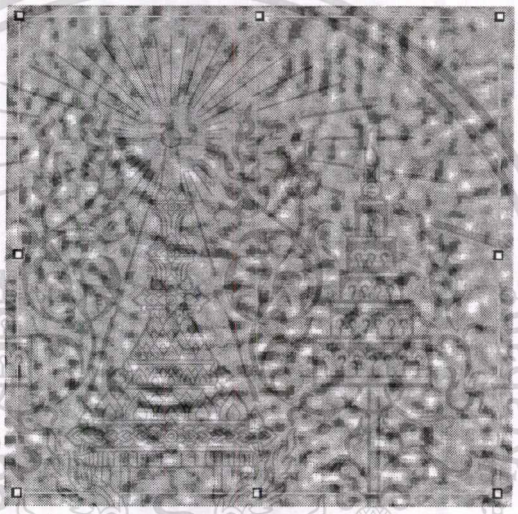

**Figure 4.15b** BE20's crystallite cropped image

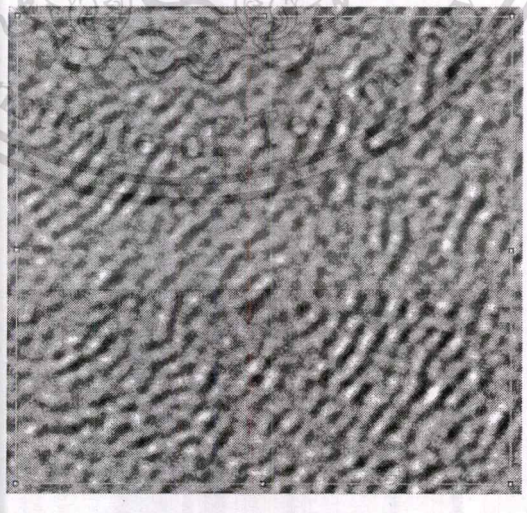

**Figure 4.15c** Diesel's crystallite cropped image

This material is reserved for educational use only, not allowed for commercial use.
Forbidden to modify the content, and cite the document when use.

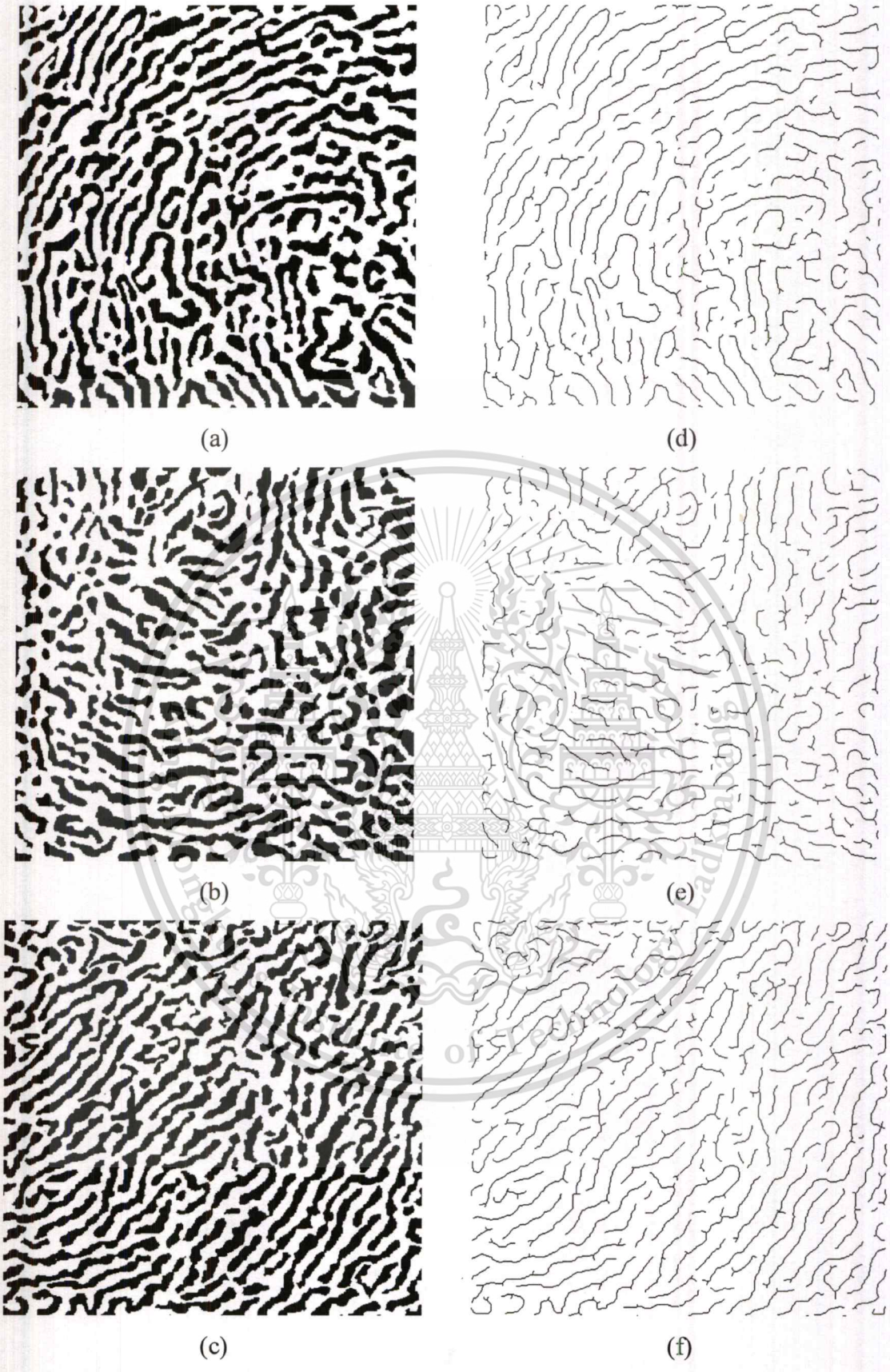


**Figure 4.16** Black and white images (a : B100 , b : BE20 , c : diesel) and Skeletonized images of crystallites (d : B100 , e : BE20 , f : diesel)

This material is reserved for educational use only, not allowed for commercial use.
Forbidden to modify the content, and cite the document when use.

From the skeletonized images, black lines represent carbon crystallites which refer to graphene sheets. To obtain more detail of the carbon crystallite, insight of carbon atom arrangement in the graphene sheet is necessary. According to conceptual model of Lipkea, the carbon crystallite was assumed that it consists of 2-5 carbon platelets with a pair of graphene sheet. Distance between the graphene sheets is about 0.35–0.36 nm. However, according to the measurement of adjacent skeletonized lines, the distance was found at 0.3 – 0.4 nm. Hence, skeletonized images in this case are appropriate to consider as 1 crystallite line per 1 graphene sheet. While longer the line, it has more possibility to contain more number of carbon hexagon rings in the graphene.

This concept also agrees with modern transmission electron microscopy. S.Akhtar [44] explained how to interpret TEM image of graphene flakes as shown in Fig. 4.17. The inter-planar spacing between the graphene planes is about 0.335 nm. The graphene layers at a folding become parallel to the incident electron beam in the TEM where each layer exhibits a dark line with ~ 0.335 nm spacing in the high resolution (HR) image.

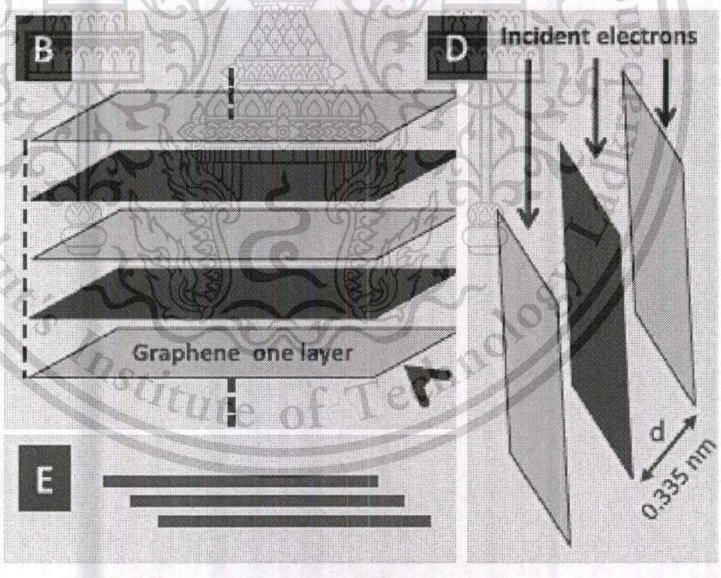


**Figure 4.17** Schematic illustration of bulk graphite and one graphene layer [44]

This material is reserved for educational use only, not allowed for commercial use.
Forbidden to modify the content, and cite the document when use.

Figure 4.18a – Figure 4.18d show size distribution of crystallite length of B100, BE20, and diesel's soot particle respectively. BE20's soot tends to have shortest crystallites compared with B100 and diesel's soot. Most crystallite are in the range of 0.4 – 2.0 nm. For B100, most crystallite is under 2.8 nm, while crystallite over 3.5nm can be moderately found for diesel.

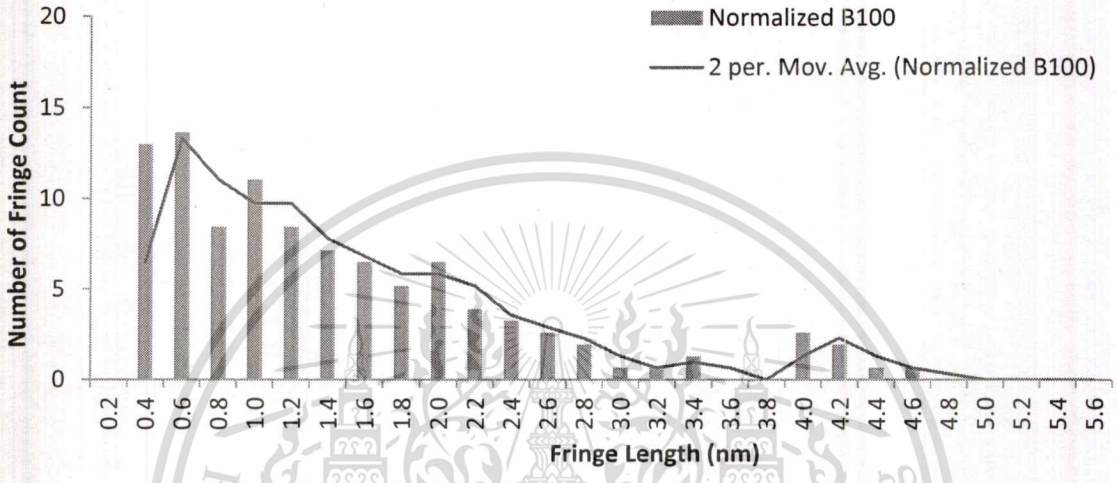


**Figure 4.18a** B100's crystallite size distribution

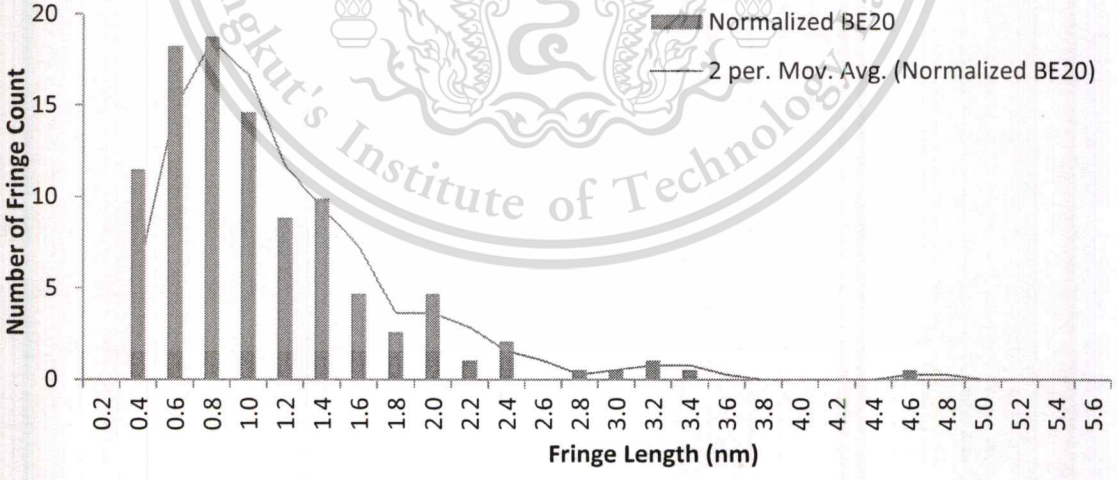


**Figure 4.18b** BE20's crystallite size distribution

This material is reserved for educational use only, not allowed for commercial use.
Forbidden to modify the content, and cite the document when use.

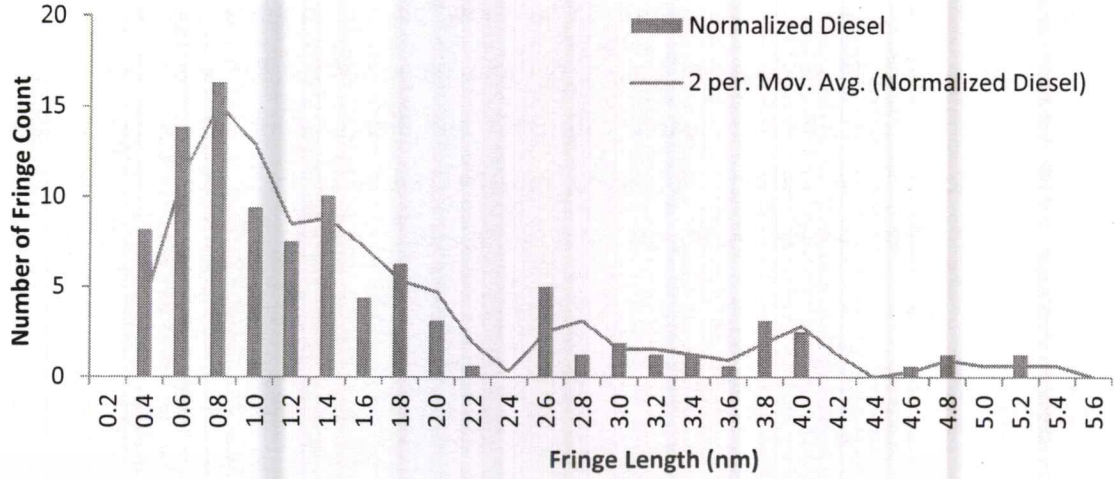


**Figure 4.18c** Diesel's crystallite size distribution

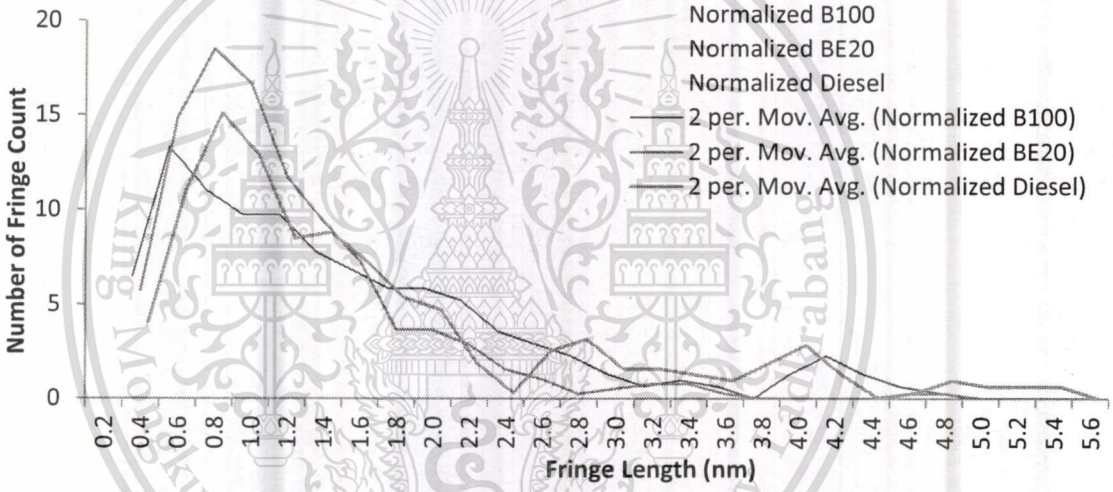


**Figure 4.18d** Combined fuel's crystallite size distribution

As recalled from the soot and char molecular model from V. Fernandez-Alos in Fig 2.31, carbon atom arrangement model was developed in this research. The model begins with theoretical distance of adjacent carbon atoms in the hexagonal ring of 1.421 A or 0.1421 nm. Therefore, referring simple hexagonal geometry can determine possible minimum crystallite length due to minimum structure of C-6 atoms at approximately 0.26 nm. As hexagonal structure grows up, dimension of the rings i.e. crystallite length can be determined as visualized image as shown in Fig. 4.19. Since conceptual graphene sheets are shaped as smooth layer, the skeletonized lines with small branches are out of consideration. Eventually, simulating and gathering enough data of the hexagonal structure, relationships between crystallite

This material is reserved for educational use only, not allowed for commercial use.
Forbidden to modify the content, and cite the document when use.

length and number of carbon atoms in the corresponding graphene sheet can be predicted as a model shown in Fig. 4.20

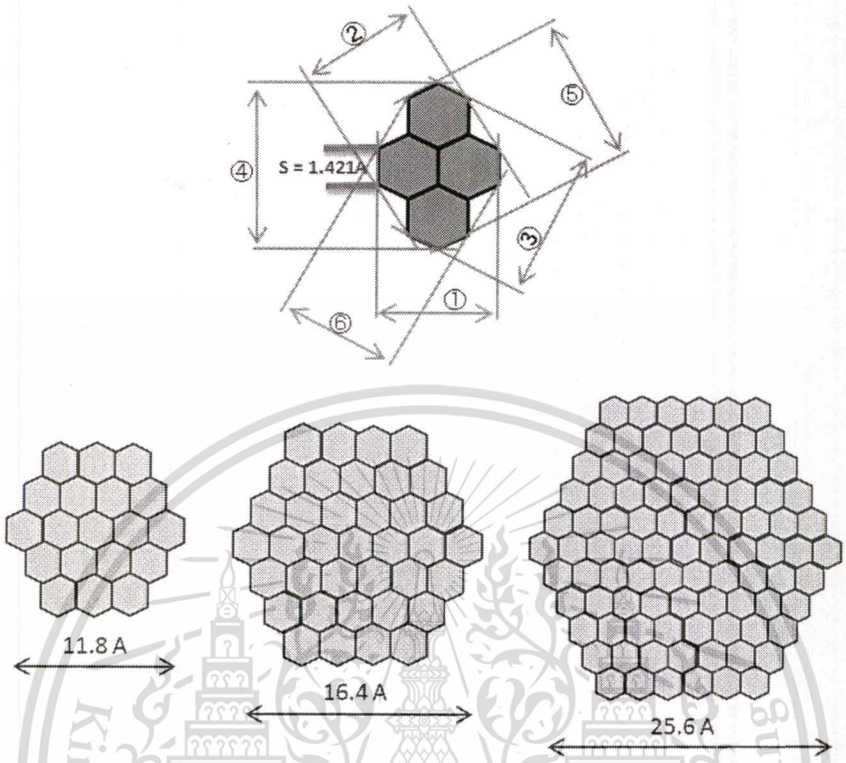


**Figure 4.19** Carbon hexagonal ring dimension measurement

Crystallite data from the skeletonized images actually represent a capture of soot particles in two dimensions i.e. cannot interpret the image in depth dimension. Therefore, to determine carbon atom density, it is necessary to consider another dimension deep into the captured image. Figure 4.21 propose a model to determine a controlled volume from the 2-dimension captured image. Each crystallite platelet or graphene sheet is assumed to form a circular sheet because of chemical bonding stability (similar to V. Fernandez-Alos's assumption about equivalent fringe's width and depth [38]). In order to estimate an accurate volume, the graphene sheets are simplified into rectangular shape. Integration of all sheets becomes a closed volume which is ready for carbon atom density calculation.

This material is reserved for educational use only, not allowed for commercial use.
Forbidden to modify the content, and cite the document when use.


**Figure 4.20** Prediction model of carbon crystallite length and carbon atom

This material is reserved for educational use only, not allowed for commercial use.
Forbidden to modify the content, and cite the document when use.

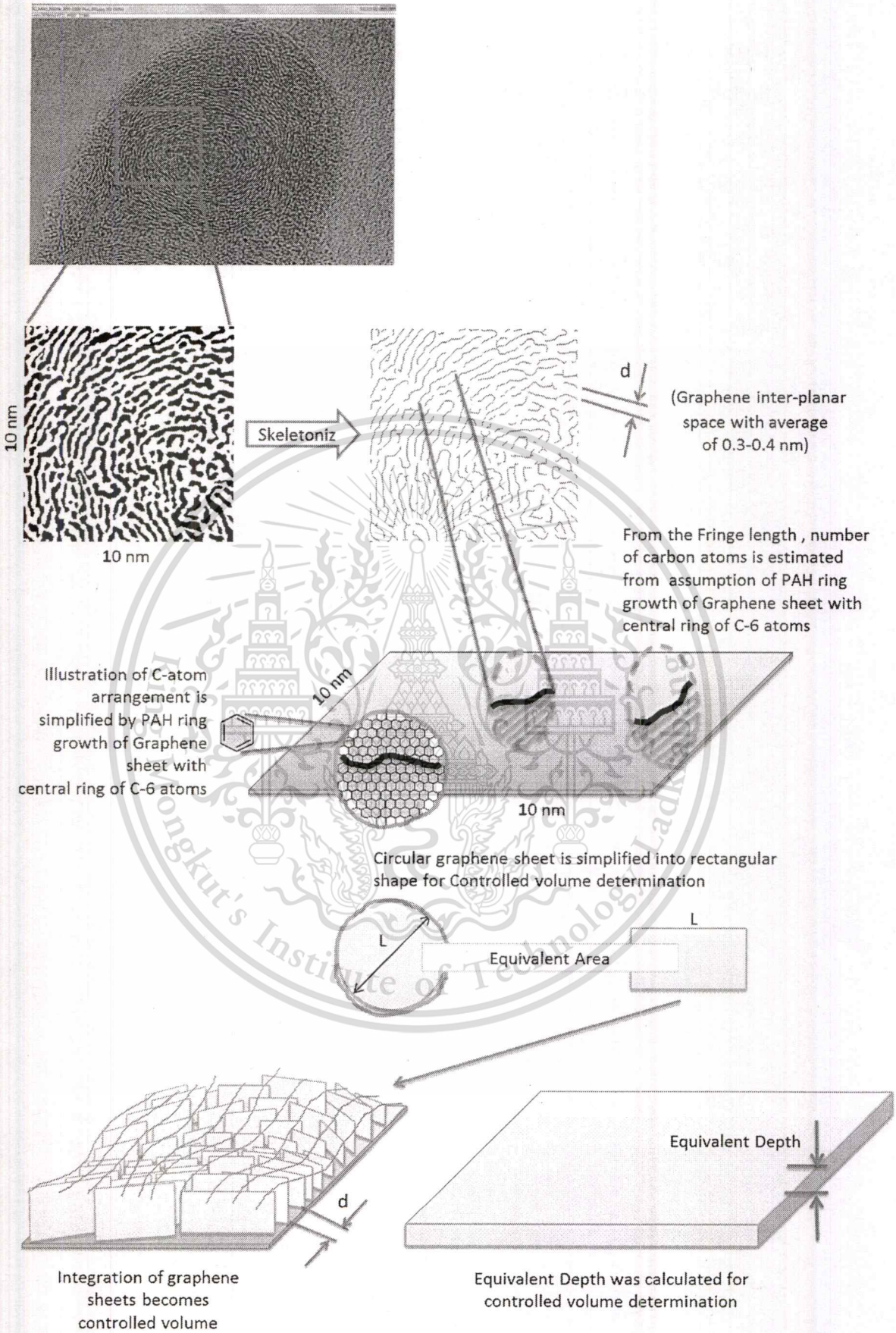


**Figure 4.21** Conceptual model of carbon crystallite length and carbon atoms

This material is reserved for educational use only, not allowed for commercial use.
Forbidden to modify the content, and cite the document when use.

Table 4.1 shows calculation results of carbon atom density compared among B100, BE20, and diesel's soot particle. Carbon density of diesel's soot is apparently higher than B100's and BE20's which agrees with the Black and White image from the image processing. Also, all calculation results of soot density conform to actual values of industrial graphite and carbon black properties.

**Table 4.1** Comparison of carbon atom and soot density of BE20, B100, and Diesel soot

| Items | BE20 | B100 | Diesel | Graphite | Carbonblack |
|---|---|---|---|---|---|
| Total crystallite length (nm/image) | 189.13 | 208.38 | 227.45 | | |
| Total C atoms | 9786.92 | 14700.46 | 17695.83 | | |
| Control volume (nm^3) | 110.86 | 162.27 | 171.61 | | |
| Carbon atom density (atom/nm^3) | 88.28 | 90.59 | 103.12 | | |
| Soot density (g/cm^3) | 1.76 | 1.81 | 2.06 | 1.7-1.8 [a] | 1.8 – 2.1 [b] |

a : http://www.chemicalbook.com/ProductMSDSDetailCB3109508_EN.htm ;
http://www.inchem.org/documents/icsc/icsc/eics0471.htm

b : Poco Graphite - An Entegris Company

This material is reserved for educational use only, not allowed for commercial use.
Forbidden to modify the content, and cite the document when use.

## 4.6 Oxidation kinetics

The particulate matter from B100 and BE20 was analyzed by isothermal TGA method to investigate oxidation behavior of the particulate matter from diesel and biodiesel engine. Since PM collected from the experiment is not pure soot, it might include some metal wear or irrelevant substance. In addition, even ramp-up temperature zone is feed by nitrogen gas to prevent oxidation reaction, humidity or volatile substance might include in the sample. Therefore, initial data until reach of isothermal temperature and data after steady mass are ignored. PM mass conversion is plotted with respect to time as shown in Fig. 4.22. Diesel's particulate matter from previous research was also analyzed as reference for this research. Mass conversions of all PM types are in similar trends. That is to say, higher temperature condition, PM mass reduces faster. BE20's PM seems to oxidize faster than B100'PM as shown at same temperature of 475°C it take a bit more time to oxidize. While diesel's PM seems difficult to oxidize as incomplete conversion at 550°C.

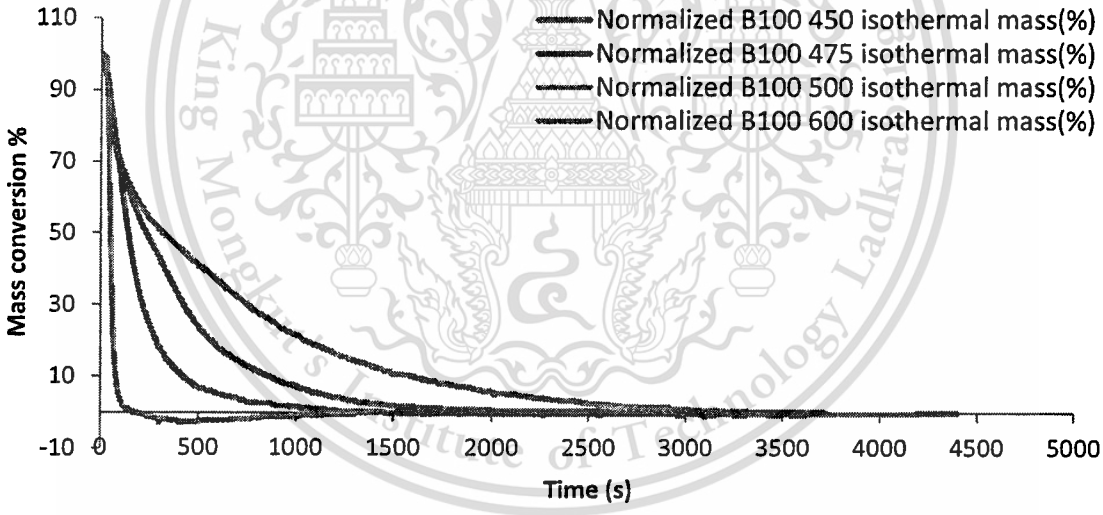


**Figure 4.22a** Normalized mass conversion of B100's particulate matter at 450°C, 475°C, 500°C, and 600°C

This material is reserved for educational use only, not allowed for commercial use.
Forbidden to modify the content, and cite the document when use.

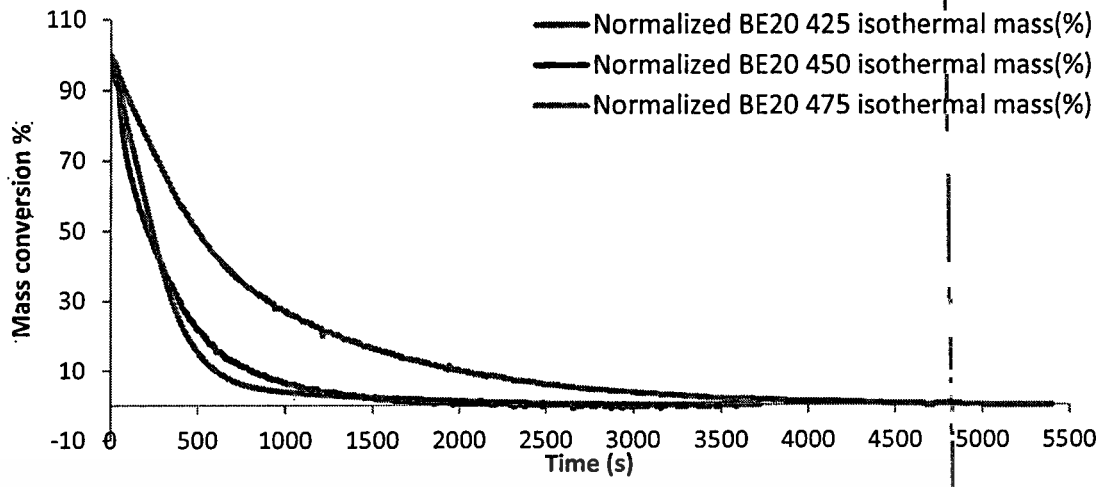


**Figure 4.22b** Normalized mass conversion of BE20's particulate matter at 425°C, 450°C, and 475°C

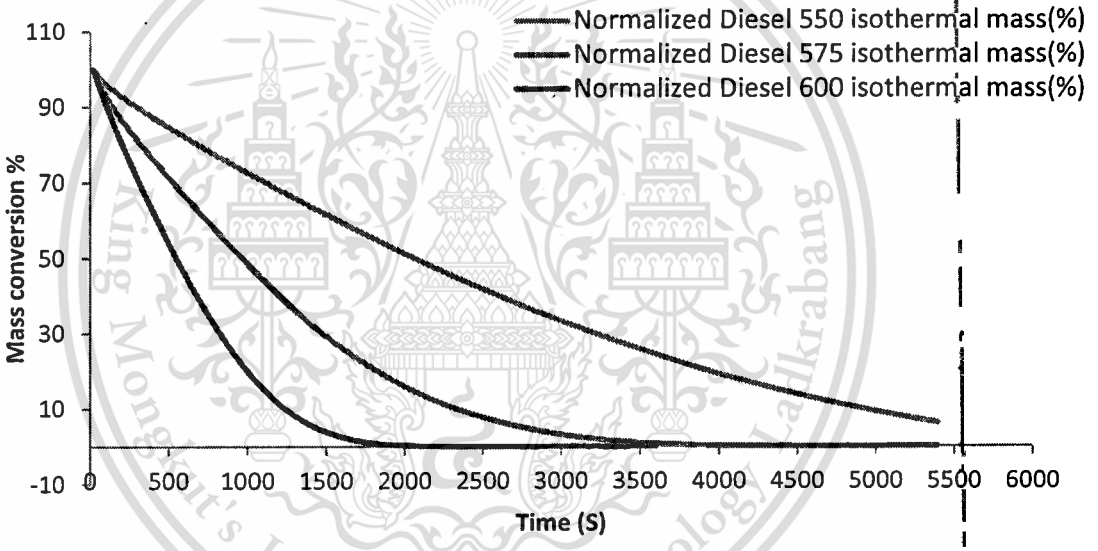


**Figure 4.22c** Normalized mass conversion of Diesel's particulate matter at 550°C, 575°C, and 600°C

Chemical kinetics of TGA results was analyzed by relations in Eqn.4.1

$$C(PM) + O_2 \rightarrow CO_2 \qquad (4.1)$$

This material is reserved for educational use only, not allowed for commercial use.
Forbidden to modify the content, and cite the document when use.

Global chemical reaction rate equation is described as relationships in Eqn.4.2

$$-\frac{d[C]}{ct} = kC^n {O_2}^m \tag{4.2}$$

Arrhenius equation express rate constant as Eqn. 4.3

$$k = Ae^{(\frac{-E_a}{RT})} \tag{4.3}$$

Modification of Eqn. 4.2 and Eqn. 4.3 yields

$$\ln\left[-\frac{d[C]}{ct}\right] = -\frac{E_a}{RT} + lnA + n \cdot \ln[C] + m \cdot \ln[O_2] \tag{4.4}$$

Where ;

n is order of reaction wrt [C] (physical factor)

m is order of reaction wrt [O2] (physical factor)

k is rate constant which depend on A , Ea , R , T

A is particle collision frequency factor (physical factor)

$E_a$ is activation energy (chemical factor)

R is gas constant

T is reaction temperature (K)

4.6.1 Activation energy

Activation energy ($E_a$) is the minimum energy which is required to initiate and complete a chemical reaction. The lower activation energy means the better reactivity. From the mass conversion graphs, rate of conversion was selected at constant slope zone for accurate $E_a$ estimation. From Eqn. 4.4, it is equivalent to **Arrhenius linear equation** of Y = mX + C, where Y axis is $\ln\left[-\frac{d[C]}{ct}\right]$, m is $-\frac{E_a}{R}$ , X is inverse temperature, and C is responsible for the remaining terms; $lnA + n \cdot \ln[C] + m \cdot \ln[O_2]$. Therefore, the data on conversion rate can be plotted as a graph in Fig.4.23 and activation energy can be calculated as in Table 4.2.

The results of the calculated activation energy are actually can be explained by the graphs in Fig. 4.22. For BE20's PM, $E_a$ is comparative low. That is why mass conversion speed or PM oxidation rate is almost independent on changing

This material is reserved for educational use only, not allowed for commercial use.
Forbidden to modify the content, and cite the document when use.

temperature at 450°C to 475°C. In contrast, mass conversion speed of diesel's PM are very dependent on temperature. Therefore, $E_a$ is comparative high.

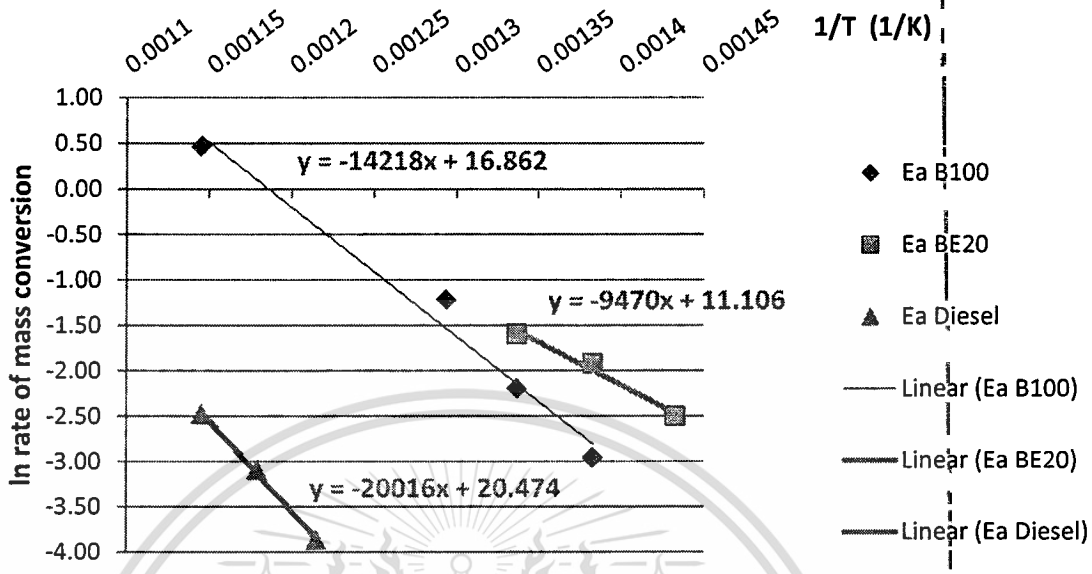


**Figure 4.23** Arrhenius plot of B100, BE20, and diesel particulate matter at isothermal TGA condition

**Table 4.2** Calculated activation energy of BE20, B100, and Diesel's PM

| | BE20 | B100 | Diesel |
|---|---|---|---|
| Activation Energy , kJ/mol | 78.7 | 118.2 | 166.4 |

4.6.2 Reaction order of particulate matter (n)

Reaction order of particulate matter can be obtained similarly to the method of activation energy. However, X-axis becomes *ln* function of decreasing mass of the PM. Slope of graphs become n or reaction order as shown in Fig. 4.24

This material is reserved for educational use only, not allowed for commercial use.
Forbidden to modify the content, and cite the document when use.

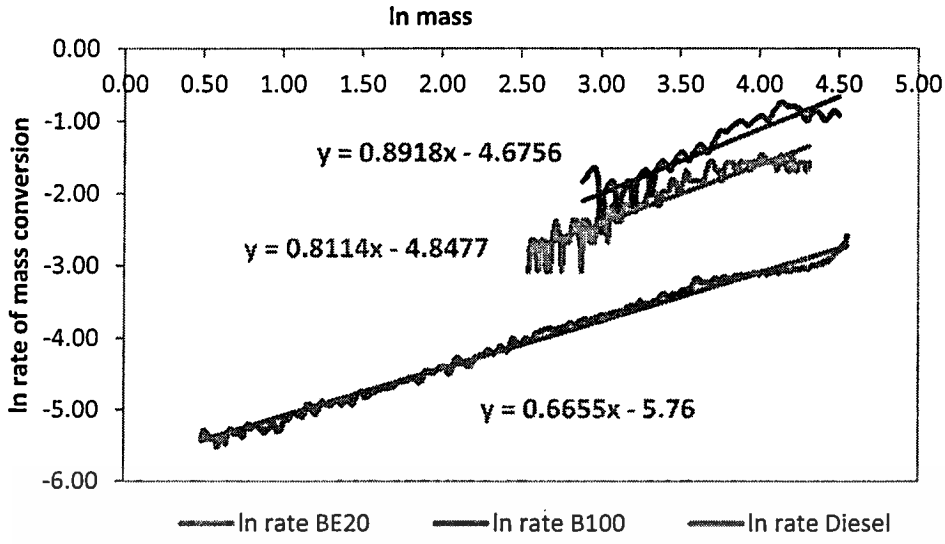


**Figure 4.23** Arrhenius plot of B100, BE20, and diesel particulate matter at isothermal TGA condition

**Table 4.2** Reaction order of BE20, B100, and Diesel's PM

| | BE20 | B100 | Diesel |
|---|---|---|---|
| Reaction order (slope of plot) | 0.81 | 0.89 | 0.67 |

This material is reserved for educational use only, not allowed for commercial use.
Forbidden to modify the content, and cite the document when use.

# CHAPTER 5

# CONCLUSIONS AND RECOMMENDATIONS

Ethanol has unique fuel properties compared with palm biodiesel or conventional diesel for application on conventional diesel engines. This research found that a little ratio of ethanol on biodiesel effects on engine combustion characteristics and particulate matter properties. First effect is reduction in particulate matter emission. High oxygen content and combustion behavior of retarded combustion play key role in more complete combustion. Second effect is PM nanostructure. With image processing of the soot particles, relationship between carbon crystallite morphology in soot's primary particles and chemical reactivity was found. Shorter crystallite morphology in ethanol fuel causes reduced in activation energy. That means soot are easier in oxidation reaction.

King Mongkut's Institute of Technology Ladkrabang

This material is reserved for educational use only, not allowed for commercial use.
Forbidden to modify the content, and cite the document when use.

# REFERENCES


Preechar Karin, Hiroshi Oki, Katsunori Hanamura, Chinda Charoenphonphanich, Nanostructures and Oxidation Kinetics of Diesel Particulate Matters, The Second TSM International Conference on Mechanical Engineering, 19-21 October, 2011, Krabi

Zhu, L., Cheung, C., Zhang, W., & Huang, Z. (2011). Combustion, performance and emission characteristics of a DI diesel engine fueled with ethanol–biodiesel blends. Fuel, 90(5), 1743-1750. doi:10.1016/j.fuel.2011.01.024

Ramadhas AS, Jayaraj S, Muraleedharan C. Use of vegetable oils as I.C. enginefuels – a review. Renew Energy 2004; 29:727–42

Graboski MS, McCormick RL. Combustion of fat and vegetable oil derived fuelsin diesel engines. Prog Energy Combust Sci 1998;24:125–64

Hulwan, Dattatray Bapu, and Satishchandra V. Joshi. "Performance, emission and combustion characteristic of a multicylinder DI diesel engine running on diesel–ethanol–biodiesel blends of high ethanol content." Applied Energy 88, no. 12 (2011): 5042-055. doi:10.1016/j.apenergy.2011.07.008.

Kraipat Cheenkachorn, Monpilai H.Narasingha, Jutahawan Pupakornnopparut , Biodiesel as an Additive for Diesohol, Asian Journal on Energy and Environment, 2006, 7(01), 267-276, ISSN 1513-4121

Prbakaran, B., and Dinoop Viswanathan. "Experimental investigation of effects of addition of ethanol to bio-diesel on performance, combustion and emission characteristics in CI engine." Alexandria Engineering Journal (2016)

Tutak, W., Jamrozik, A., Pyrc, M., & Sobiepański, M. (2017). A comparative study of co-combustion process of diesel-ethanol and biodiesel-ethanol blends in the direct injection diesel engine. Applied Thermal Engineering, 117, 155-163. doi:10.1016/j.applthermaleng.2017.02.029

G.K. Prashant, D.B. Lata, P.C. Joshi, Investigations on the effect of ethanol blend on the combustion parameters of dual fuel diesel engine, Appl. Therm. Eng. 96 (2016) 623–631.

Heywood, J.B. (1998). Internal Combustion Engine Fundamental, McGraw-Hill series in mechanical engineering, Singapore.

Karin, P., Borhanipour, M., Songsaengchan, Y., Laosuwan, S., Charoenphonphanich, C., Chollacoop, N., & Hanamura, K. (2015). Oxidation kinetics of small CI engine's biodiesel particulate matter. International Journal of Automotive Technology, 16(2), 211-219. doi:10.1007/s12239-015-0023-4




This material is reserved for educational use only, not allowed for commercial use.

Forbidden to modify the content, and cite the document when use.

Karin, P., Boonsakda, J., Siricholathum, K., Saenkhumvong, E., Charoenphonphanich, C., & Hanamura, K. (2016). Morphology and oxidation kinetics of CI engine's biodiesel particulate matters on cordierite Diesel Particulate Filters using TGA. International Journal of Automotive Technology, 18(1), 31-40. doi:10.1007/s12239-017-0003-y

Ishiguro, T., Takatori, Y. and Akihama, K. (1997). Microstructure of diesel soot particles probed by electron microscopy: First observation of inner core and outer shell. Combustion and Flame 108, 1, 231–234.

Vander Wal, R. L., Yezerets, A., Currier, N. W., Kim, D. H. and Wang, C. H. (2007). HRTEM study of diesel soot collected from diesel particulate filters. Carbon 45, 1, 70–77.

Kittelson, D. B. (1998). Engines and nanoparticles: A review. J. Aerosol Science 29, 5-6, 575–588.

King Mongkut's Institute of Technology Ladkrabang



This material is reserved for educational use only, not allowed for commercial use.
Forbidden to modify the content, and cite the document when use.

**Asst.Prof.Dr.Preechar Karin**

**Position and Affiliation**

Assistant Professor, Automotive Engineering Program
International College, King Mongkut's Institute of Technology Ladkrabang
1 Chalongkrung Road, Ladkrabang, Bangkok, 10520
Tel: +66-329-8260-1 Fax: +66-2-329-8262 Mobile: +66-85-128-5024
Email: kkpreech@staff.kmitl.ac.th, preechar.ka@kmitl.ac.th

**Work Experience**

- 2010-Present — Assistant Professor of Automotive Engineering Program, International College, King Mongkut's Institute of Technology Ladkrabang
- 2007-2010 — Research Assistant, Multidisciplinary Education and Research Center for Energy Science, Tokyo Institute of Technology, Japan
- 2007-2010 — Honors Scholarship for Privately Financed International Students (JASSO), Rotary Yoneyama Memmorial Foundation Inc., Japan
- 1997-2006 — Vehicle Design Engineer, Isuzu Technical Center of Asia Co.,Ltd., Isuzu Motor Ltd., Japan

**Education**

- D.Eng. (Mechanical Engineering), Tokyo Institute of Technology, Japan

**Research Experience**

- The Thailand Research Fund (TRF), Renewable Bio-oxygenated Fuel Particle Emission Trapping and Oxidation Behaviors inside Ceramic Micro-porous of Diesel Particulate Filters (2014-2016)
- The Thailand Research Fund (TRF), Renewable Bio-oxygenated Fuels Particulate Matter Trapping and Oxidation Behaviors (2012-2014)
- ASEA-UNINET Staff Exchange, One Month Scholarship, Engine After-treatment Technology for Particle Emissions Reduction (1-31 May 2013)
- International College, King Mongkut's Institute of Technology Ladkrabang, Physical and Chemical Characterization of Diesel Particulate Matter (March-September 2011)

**Management Experience**

- Committee and Secretary of Automotive Engineering Program, International College, King Mongkut's Institute of Technology Ladkrabang (2010-Present)
- Program Director of Automotive Engineering Program, TAIST-Tokyo Tech (King Mongkut's Institute of Technology Ladkrabang, King Mongkut's University of Technology Thonburi, National Science and Technology Development Agency and Tokyo Institute of Technology (2010-Present)
- Committee and Secretary of Thai Society of Mechanical Engineers (TSME) (2015-Present)
- Committee of Thai Society of Automotive Engineers (TSAE) (2014-2015)



This material is reserved for educational use only, not allowed for commercial use.
Forbidden to modify the content, and cite the document when use.

**International Journal Publications**

- P. Karin, J. Boonsakda, K. Siricholathum, E. Saenkhumvong, C. Charoenphonphanich and K. Hanamura, "Morphology and Oxidation Kinetics of CI Engine's Biodiesel Particulate Matters on Cordierite Diesel Particulate Filters using TGA", International Journal of Automotive Technology, Vol. 18, No. 1, pp. 31–40, 2017.
- P. Karin, C. Supanamok and K. Hanamura, "Impact of Soot on Metal Wear Characteristics using Laser Diffraction Spectroscopy", Journal of Research and Applications in Mechanical Engineering, Transactions of the TSME Vol. 4, No. 2, pp.126-134, 2016.
- P. Karin, M. Borhanipour, Y. Songsaengchan, S. Laosuwan, C. Charoenphonphanich, N. Chollacop and K. Hanamura, "Oxidation Kinetics of Small CI Engine's Biodiesel Particulate Matter", International Journal of Automotive Technology, Vol. 16, No. 2, pp. 211–219, 2015.
- P. Karin, Y. Songsaengchan, S.Laosuwan, C. Charoenphonphanich, N.Chollacop and K.Hanamura, "Physical Characterization of Biodiesel Particle Emission by Electron Microscopy", SAE International; 2013-32-9150.
- P. Karin, Y. Songsaengchan, S.Laosuwan, C. Charoenphonphanich, N.Chollacop and K.Hanamura, (2013) "Nanostructure Investigation of Particle Emission by Using TEM Image Processing Method", Energy Procedia, Elsevier, Vol.34, pp.757-766, 2013.
- P. Karin, Y. Songsaengchan, S.Laosuwan, C. Charoenphonphanich, N.Chollacop and K.Hanamura, (March, 2013) "Nanostructure of Renewable Oxygenated Fuels Particulate Matter", ASEAN Engineering Journal, AUN/SEED-Net, Vol.3 No.1, pp. 72-83.
- P. Karin, H. Oki, K. Hanamura and C. Charoenphonphanich, (October, 2012) "Nanostructures and Oxidation Kinetics of Diesel Particulate Matters", The Journal of Research and Applications in Mechanical Engineering (JRAME), Vol.1 No.2, pp. 3-8.
- H. Oki, P. Karin and K. Hanamura, (2011) "Visualization of Oxidation of Soot Nanoparticles Trapped on a Diesel Particulate Membrane Filter", SAE International Journal of Engines, SAE International, Vol. 4 no. 1 pp.515-526.
- P. Karin and K. Hanamura, (2010) "Particulate Matter Trapping and Oxidation on Catalyst-Membrane", SAE International Journal of Fuels and Lubricants, SAE International, Vol.3 No.1 pp.368-379.
- P. Karin and K. Hanamura, (2010) "Microscopic Visualization of Particulate Matter Trapping and Oxidation Behaviors in a Diesel Particulate Catalyst-Membrane Filter", Transactions of Society of Automotive Engineers of Japan, Society of Automotive Engineers of Japan Inc, Vol.41, No.4, pp.853-858.
- P. Karin and K. Hanamura, (2010) "Microscopic Visualization of PM Trapping and Regeneration in a Diesel Particulate Catalyst-Membrane Filter (DPMF)", Transactions of Society of Automotive Engineers of Japan, Society of Automotive Engineers of Japan Inc, Vol. 41, No. 1, pp.103-108.
- P. Karin, L. Cui, P. Rubio, T. Tsuruta and K. Hanamura, (2009) "Microscopic Visualization of PM Trapping and Regeneration in Micro-Structural Pores of a DPF Wall", SAE International Journal of Fuels and Lubricants, SAE International, Vol.2 No.1, pp.661-669.
- K. Hanamura, P. Karin, L. Cui, P. Rubio, T. Tsuruta, T. Tanaka and T. Suzuki, (2009) "Micro- and macroscopic visualization of particulate matter trapping and regeneration processes in wall-flow diesel particulate filters", International Journal of Engine research, Professional Engineering Publishing, Vol.10, No.5/2009, pp.305-321.
- L. Cui, P. Rubio, P. Karin, T. Tsuruta and K. Hanamura, (2009) "Microscopic Visualization of Particulate Matter Trapping and Regeneration in Microstructural Pores on Diesel Particulate Filter Wall", Transactions of Society of Automotive Engineers of Japan, Society of Automotive Engineers of Japan Inc, Vol. 40, No. 1, pp.153-158.



This material is reserved for educational use only, not allowed for commercial use.
Forbidden to modify the content, and cite the document when use.

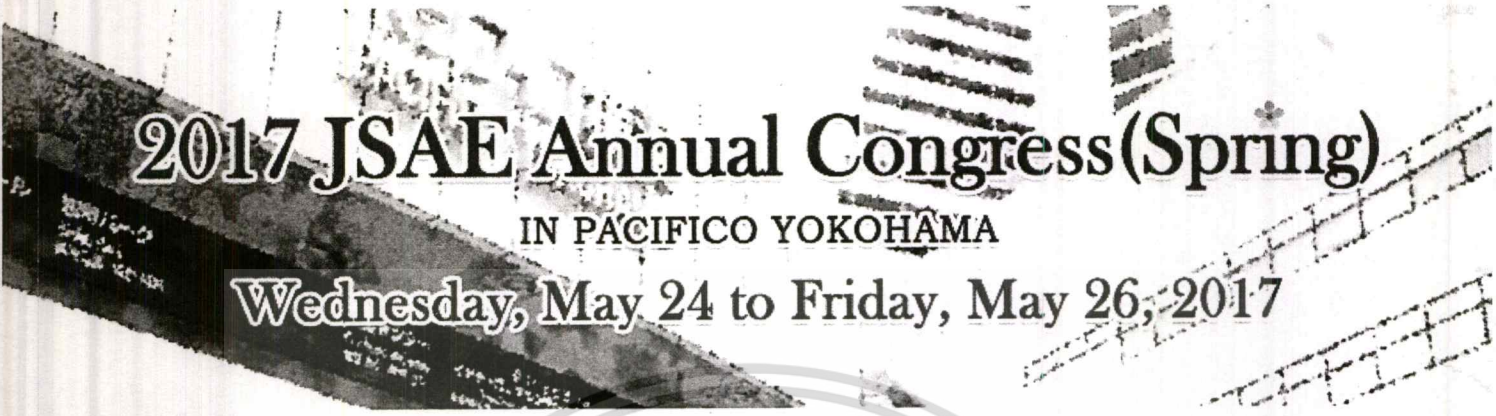



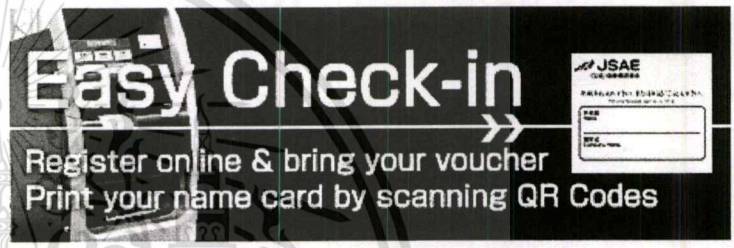


## TOPICS

2017.05.18 up Final program is now available. NEW

2017.03.10 up Early Bird Registration is now open.

2016.10.07 up Presentation registration is now open.

2016.8.01 up 2017 JSAE Annual Congress (Spring)

Period : Wednesday, May 24 to Friday, May 26, 2017 Venue : PACIFICO YOKOHAMA

Technical Paper Presentation of JSAE Annual Congress is open to (and welcomes) international speakers/audiences:

- Technical Session is organized regardless of the presentation language.
- The language of Technical Paper Presentation material is in English.


COPYRIGHT © SOCIETY OF AUTOMOTIVE ENGINEERS OF JAPAN, INC. ALL RIGHTS RESERVED.

This material is reserved for educational use only, not allowed for commercial use.
Forbidden to modify the content, and cite the document when use.

講演番号 168

文献番号 20175168

# Impact of Diesel Engine Combustion Characteristics on Particulate Matter's Morphology and Nanostructure from Ethanol-blended Biodiesel

**Park Watanawongskorn[1)*], Preechar Karin[1)], Chinda Charoenphonphanich[2)], Jiramed Boonsakda[1)], Katsunori Hanamura[3)], and Nuwong Chollacoop[4)]**

*1) International College, King Mongkut's Institute of Technology Ladkrabang, Chalongkrung Rd., Ladkrabang, Bangkok, 10520, Thailand (E-mail: park.wa@gmail.com)*
*2) Faculty of engineering, King Mongkut's Institute of Technology Ladkrabang*
*3) Department of Mechanical Engineering, Tokyo Institute of Technology*
*4) National Metal and Materials Technology Center, National Science and Technology Development Agency*

**ABSTRACT**: Many biodiesel researchers have been revealed that biodiesel plays a key role in Particulate Matter (PM) reduction due to impact of effective oxygen function compared with diesel fuel. To reduce further PM emission, oxygenated fuel such as ethanol could be one of possible options. This research focused on effects of ethanol on PM's quantity and morphology by blending with biodiesel. The PM quantity from engine operation was inspected altogether with PM's nanostructure by SEM and TEM technique. Results from this research could be utilized for Diesel Particulate Filter development for ethanol-blended biodiesel fuel.

**KEY WORDS**: **Heat engine, Particulate Matter(PM), Diesel engine, Ethanol, Biodiesel**

## 1. INTRODUCTION

Diesel engines are considered as one of the highest thermal efficiency engines among internal combustion engines (ICE)[(1)]. However, a major disadvantage is particulate matter (PM) emission which is harmful to human body and environment.

Biofuels, such as biodiesel or ethanol, have been often discussed as alternatives for diesel fuel replacement since they are obtained from renewable sources and their benefits in emission reduction. Biodiesel consists of alkyl monoesters of fatty acids derived from vegetable oil or animal fats. Due to its similar physical properties to diesel fuel, there is no need to modify the engine when the engine is fueled with the blends[(2-4)]. Ethanol is a low cost oxygenated fuel with high oxygen content. Use of ethanol in diesel fuel can contribute significant reduction of particulate matter (PM) emission for motor vehicles[(5)]. However, its considerable weakpoint is miscibility with diesel fuel. Kraipat et al.[(6)] studied about an emulsifier needed to homogenize the blend and found that biodiesel could be a good agent. The three-phase diagram showed that less than ten percent of biodiesel by volume fraction promote stability of the mixture.

In terms of engine performance and emission, many researchers have investigated effects of biodiesel-ethanol-diesel fuel on diesel engines. B. Prbakaran et al.[(7)] investigated effects of ethanol addition to biodiesel by blending with the maximum blend ratio of 50% ethanol. Operated with a single-cylinder diesel engine, brake thermal efficiency of the blends was similar to diesel base fuel. There was a decrease of nitrogen oxides and smoke emission, while maximum heat release rate and maximum pressure for the blends at higher load were increased. Prashant et al.[(8-9)] conducted investigations of a 4-cylinder diesel engine powered by diesel-ethanol blend. They showed that ignition delay increased for 40% ethanol fraction at low load. However, with higher load, ignition delay was found to be decreasing. The peak pressure rise was increasing at all cases. Darratray Bapu Hulwan et al.[(5)] studied performance, emission, and combustion characteristics of a multicylinder diesel engine from diesel-ethanol-biodiesel blends. The experiment was conducted with adjustable injection-timing fuel system. The report showed that at high ethanol blend ratio it is necessary to advance injection timing due to limited Cetane index. At high ratio of ethanol, smoke reduced remarkably at medium and high load for both low and high engine speed. An according research from Lei Zhu et al.[(2)] showed a test of ethanol-biodiesel blended fuel in a 4-cylinder diesel engine. They found that ethanol-biodiesel blends caused increase in maximum pressure and heat release rate and retarded further far away from top dead center.

Diesel particulate matters consist of a solid fraction and a soluble organic fraction (SOF). Primary particles of the PMs, composed of carbon and metallic ash, are coated with SOF and sulfate. The mean diameter of primary particles is usually in the range of 20-80 nm. Agglomerated particles are an assembly of primary particles and aggregates whose total surface area does not differ appreciable from the sum of specific surface areas of primary particles. Agglomerated particle size is normally 80-300 nm[(1,10)]. Scanning Electron Microscope (SEM) and Transmission


This material is reserved for educational use only, not allowed for commercial use.
Forbidden to modify the content, and cite the document when use.

Electron Microscope (TEM) observation of PMs have been conducted by several researchers[11]. A primary soot particle has two distinct parts; an inner core and an outer shell[12-13]. Generally, a primary particle from ICE has only one core with concentric fringe pattern which is hard to be distinguished as inner core or outer shell. Some primary particles were found to have a hollow interior and the outer shell exhibiting evidence of graphitization, with a higher crystalline than the non-hollowed particles[12,14]. Size distributions of diesel engine's PMs have been categorized as PM10, diameter (D) < 10 micron; fine particles, D < 2.5 micron; ultrafine particles, D < 0.1 micron; and nanoparticles, D < 0.05 micron or 50 nm.[12,15].

According to some recent researches about PM's quantity and morphology from biodiesel combustion, results showed that PM's quantity and average primary nanoparticle sizes have some relationships with engine speed and engine load. Biodiesel's PMs emitted about half in quantity and a little smaller in primary particle size, compared with diesel's PMs[12]. As a result of biodiesel and ethanol's benefits mentioned as above, especially ethanol combustion characteristics, the aim of this research is to study effects of combustion characteristics on PM's quantity emission, morphology, and nanostructure, by using ethanol-blended biodiesel fuel. Base biodiesel fuel was compared with a fraction of ethanol blended with biodiesel. The test was performed on a conventional diesel engine. PM quantity and morphology were investigated by an opacity smoke meter and electron microscopy for better understanding.

## 2. EXPERIMENTAL SETUP AND METHOD

### 2.1 Engine and Combustion Analyzer setup

The experiment was carried out on a 1-cylinder natural aspirated, direct injection, displacement of 709 $cm^3$ , compression ratio of 18:1, diesel engine. Fuel injection system was not modified. Engine specification was represented in Table1. The engine was coupled with an eddy-current dynamometer and a control system to adjust engine speed and engine load as shown in Fig. 1. Fuel supply system was set with a weight scale to measure fuel consumption. Exhausted gas temperature was measured at the exhausted port by a thermocouple.

Table 1
Engine specification.

| Items | Details |
|---|---|
| Engine type | 1-cylinder, Natural aspirated, Direct injection, Compression Ignition |
| Bore x Stroke | 97mm x 96mm |
| Displacement | 709$cm^3$ |
| Compression ratio | 18:1 |
| Rated power | 9.2kW @ 2400rpm |
| Injection timing | 19° CA bTDC |
| Injection pressure | 22MPa |

For parameter analysis in the combustion chamber, pressure versus crank angle data were measured by a piezoelectric sensor

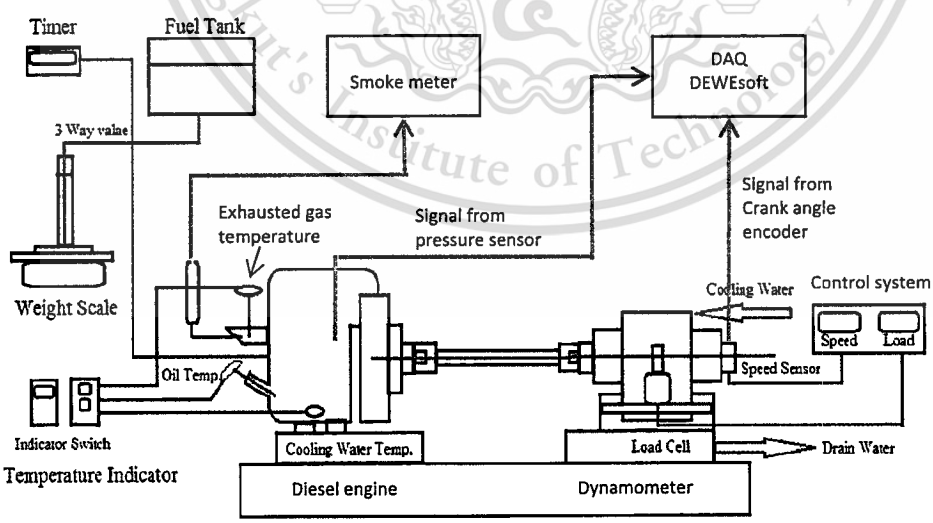


Fig. 1 Schematic diagram of experimental set up

This material is reserved for educational use only, not allowed for commercial use.
Forbidden to modify the content, and cite the document when use.

(Kistler 6052C31, 250Bar, sensitivity: ±0.5%) and a crank angle encoder (CA-RIE-360, resolution: 360 pulses/rev.). Signals of the cylinder pressure were recorded with one-degree resolution of crank angle. For further statistical analysis, two hundred engine cycles were recorded with three repeats. The pressure signals then were amplified with the data acquisition equipment (DEWESoft SIRIUSi-HS-CA) to obtain heat release rate, $dQ_n/d\Theta$ which can be estimated by deriving the formula in Reference[10].

$$\frac{dQn}{d\theta} = \frac{\gamma}{\gamma-1}p\frac{dV}{d\theta} + \frac{\gamma}{\gamma-1}V\frac{dp}{d\theta} \quad (1)$$

Here $\gamma$ is the ratio of specific heats, Cp/Cv. An appropriate range for $\gamma$ for diesel heat release analysis is 1.3–1.35. The wall heat transfer and blow by losses are not considered to find the heat released due to combustion of fuel inside cylinder. This helps to eliminate additional approximation in the analysis of heat release.

PM's quantity was measured by an opacity diesel smoke meter (OKUDA DSM-240, 0-100%, ±3% accuracy) which optically evaluate soot collected on paper filters by light reflection method.

### 2.2 Experimental fuel

The fuels used in this experiment include biodiesel (B100) and ethanol-biodiesel blend. The blended fuels contain 10% and 20% by weight of ethanol, and are identified as BE10 and BE20 respectively. The biodiesel was produced from palm-olein (B100-TIS2313-2549). The ethanol was used as Anhydrous ethanol 99.8%. Base fuels properties are shown in Table 2. For the blended fuel, properties of calorific value, heat of evaporization, carbon content, hydrogen content, oxygen content, stoichiometric air-fuel ratio, and density were estimated by interpolation and calculation.

### 2.3. Experimental method

Engine performance curve, brake specific fuel consumption (BSFC), brake thermal efficiency (BTE), and exhausted gas temperature (EGT) were measured to see overview effects of ethanol compared with biodiesel. In-cylinder pressure and net heat release rate from selected engine operating conditions were then recorded to see combustion characteristics.

PM's quantity was measured at the exhausted port as well as PM powder was collected by using an in-house metal-net particle collector to investigate morphology and nanostructures by using scanning electron microscopy (FE-SEM: Hitachi SU5000), and transmission electron microscopy(TEM: JEOL JEM-2100Plus)

Table 2
Fuel properties.

| Properties | Biodiesel | Ethanol | BE10 | BE20 |
|---|---|---|---|---|
| Chemical formula | $C_{14.9}H_{29.9}O_{1.9}$ | $C_2H_6O$ | - | - |
| Cetane index | 66.1 | 8.0 | - | - |
| Calorific Value (kJ/kg) | 39525 | 28329 | 38405 | 37285 |
| Heat of evaporization (kJ/kg) | 300 | 840 | 354 | 408 |
| Viscosity @ 40°C ($mm^2/s$) | 4.5 | 1.2 | - | - |
| Carbon (% mass) | 74.5 | 52.2 | 72.3 | 70.0 |
| Hydrogen (% mass) | 12.5 | 13.0 | 12.5 | 12.6 |
| Oxygen (% mass) | 13.0 | 34.8 | 15.2 | 17.4 |
| Stoichiometric Air fuel ratio | 12.3 | 9.0 | 11.9 | 11.6 |
| Density @ 25°C ($kg/m^3$) | 875.3 | 789.0 | 866.7 | 858.0 |

## 3. RESULTS AND DISCUSSION

### 3.1 Engine performance

The engine performance curve of biodiesel and ethanol blended biodiesel is plotted in Fig. 2. Engine load decreases as increasing engine speed for all fuels. The ethanol blended fuel produces lower load due to lower calorific value as well as lower stoichiometric air-fuel ratio i.e. leaner combustion compared with biodiesel. The engine load shows significant drop at higher speed and more ethanol blended ratio.

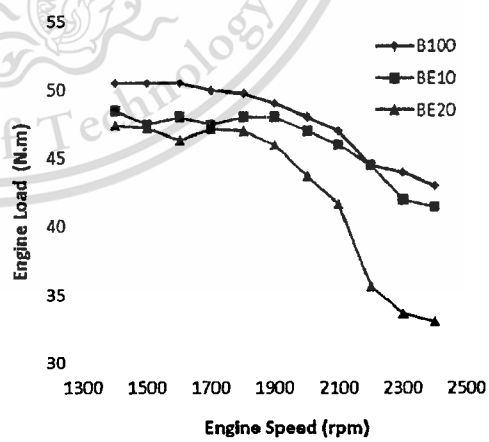


Fig. 2 Engine performance curve

This material is reserved for educational use only, not allowed for commercial use.
Forbidden to modify the content, and cite the document when use.

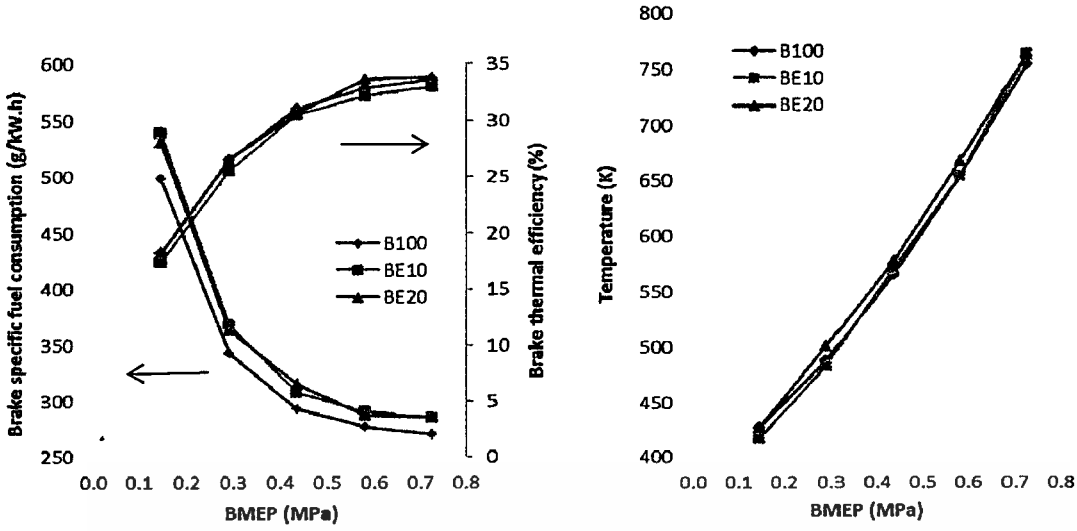


Fig. 3 Brake specific fuel consumption, Brake thermal efficiency, and Exhausted gas temperature at engine speed of 2000 rpm

**3.2 Brake specific fuel consumption (BSFC), Brake thermal efficiency (BTE), and Exhausted gas temperature (EGT)**

Brake specific fuel consumption (BSFC), Brake thermal efficiency (BTE), and Exhausted gas temperature (EGT) are shown in Fig. 3. BSFC of the ethanol blended fuels, are higher than that of biodiesel at all load conditions due mainly to the lower calorific value of ethanol. Thus, the amount of fuel supply into the engine must be greater. The trend shows decrease in the BSFC as the engine load increase. It can be explained as; when the engine load increases, combustion temperature which is implied from the rise of EGT increases as well. Reactivity of fuel and oxygen activates conversion of combustion heat to mechanical work much more than amount of energy from the fuel input. That is why the BSFC decreases as the engine load increases.

BTE plots show that as the engine load increases, the engine produces more thermal efficiency for all fuels. The BTE of BE20 and B100 is close to each other because the higher BSFC of BE20 compensates its lower calorific value, compared with B100.

**3.3 Combustion characteristics**

In-cylinder pressure variation with respect to crank angle are shown in Fig. 4a and heat release rate in Fig. 4b. The engine load was varied in the range of 0.2 MPa, 0.4 MPa, and 0.6 MPa at constant engine speed of 2400 rpm. Peak pressures of all fuels increase with the increasing engine load. Considering at the ethanol blended fuels, at low load of 0.2MPa, the peak pressure occurs after the biodiesel's peak for 10 to 15 crank angle degrees. At the low load condition, low combustion temperature causes ethanol blended fuel which has higher heat of evaporization as well as low cetane index delays in start of combustion. Therefore, the peak pressure occur further away from top dead center. At higher engine load, the increase of combustion temperature cause better fuel vaporization which leads to less combustion delay in the ethanol blended fuel and the peak pressures increase as well.

Heat release rate plots show that combustion processes of all fuels start with premixed combustion phase followed by diffusion combustion phase. At low engine load, the fuel with more ethanol content which is BE20 has more significant ignition delay which effects on retarded premixed combustion phase, while a higher peak of the heat release can be observed. The reason is that low temperature in the low load condition causes the ethanol blended fuel need more time for fuel atomization due to higher heat of vaporization of ethanol as explained above. After enough fuel atomization and mixing with oxygen, rapid combustion produces high peaks of heat release rate as shown in the Fig. 4b. However, at the higher engine load, higher combustion temperature make better fuel vaporization and fuel atomization as well. There is reduction in retarded combustion for the ethanol blended fuels as well as stronger premixed combustion leads to higher peak of heat release rate. Although the ethanol blended fuels have more delay in premixed combustion, their combustion processes tends to finish earlier than biodiesel which agrees with a little lower EGT in Fig. 3. That means the diffusion combustion time for the ethanol blend is reduced since better fuel atomization, mixing, and more oxygen content in the fuels promote more complete combustion.

This material is reserved for educational use only, not allowed for commercial use.
Forbidden to modify the content, and cite the document when use.

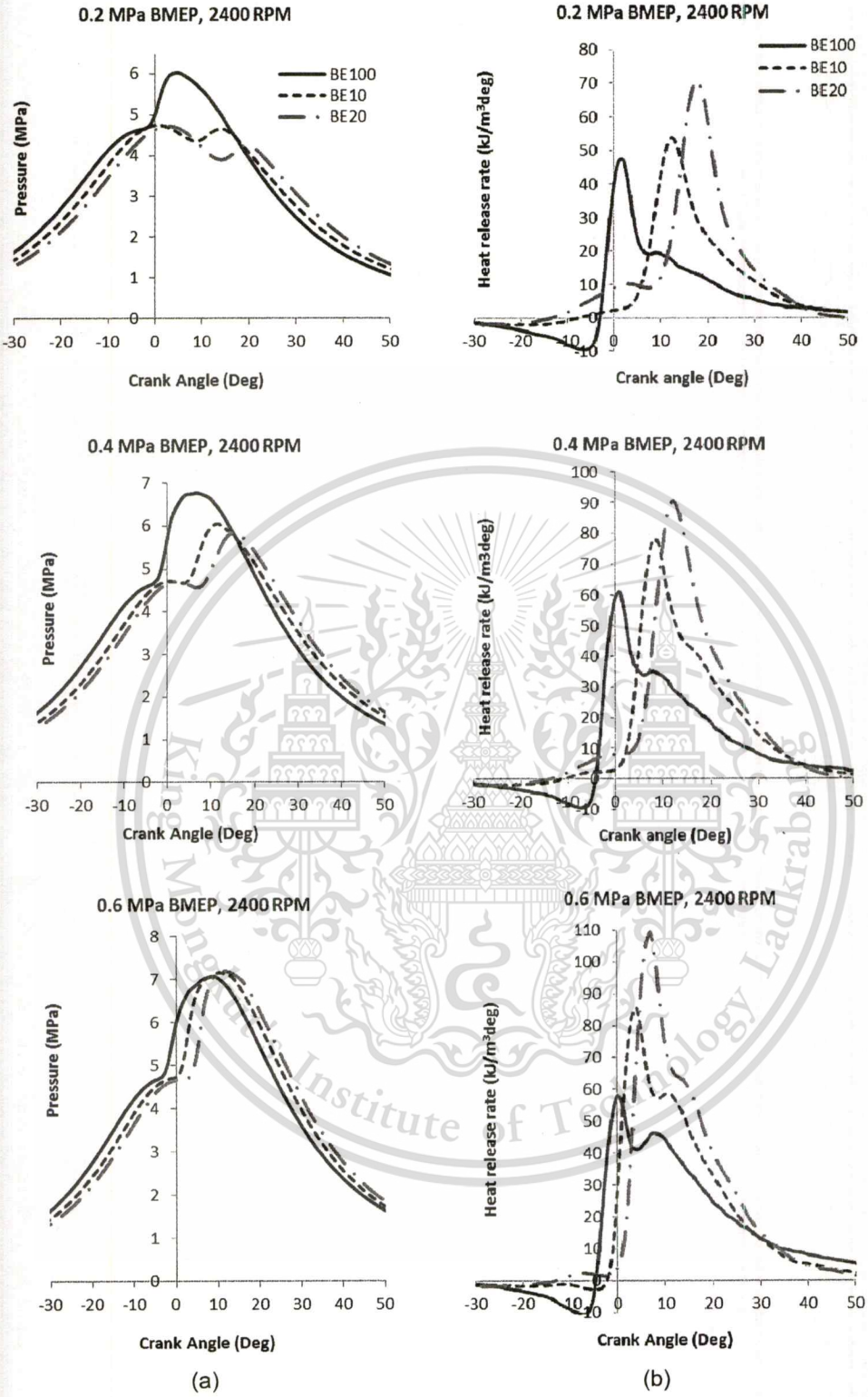


Fig. 4 (a) In-cylinder pressure, (b) Heat release rate versus crank angle at engine speed of 2400 rpm

This material is reserved for educational use only, not allowed for commercial use.
Forbidden to modify the content, and cite the document when use.

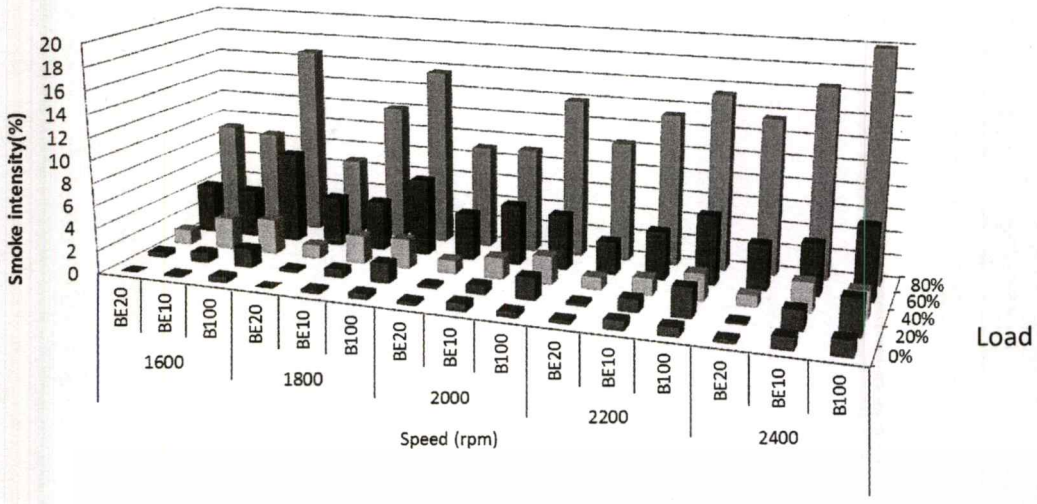


Fig. 5 Smoke intensity

**3.4 PM's quantity emission**

Figure 5 shows measurement results of smoke intensity which is an indirect method to estimate PM's quantity. The intensity is strongly dependent on the engine load. The more engine load, the greater smoke intensity due to more fuel supply for combustion. The ethanol blended fuels produce less smoke than the biodiesel at almost all engine operating conditions because retarded combustion characteristics provide enough time for fuel atomization and high peak of heat relaease tends to promote better fuel-oxygen's reactivity.

**3.5 PM's morphology and nanostructure**

Morphology and nanostructure of the PM were investigated by electron microscopy. Some PM's types were found on the paper filters such as fine particles or PM 2.5, D < 2.5 micron, and ultrafine particles, D < 100 nm. Fig. 6 shows a sample of a fine particle from BE10 fuel.

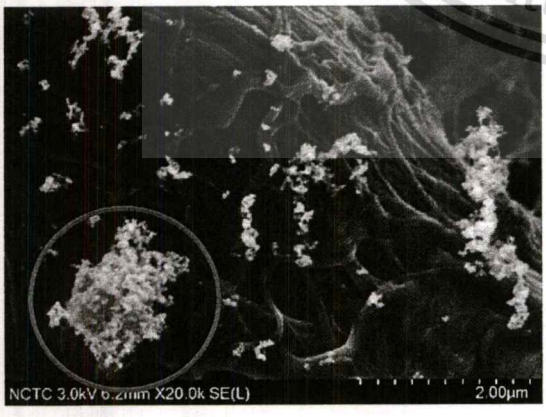


Fig. 6 SEM image of BE10's PM 2.5 at 0.6 MPa and 2000 rpm

SEM images of biodiesel's and BE20's agglomerated particles are presented in Fig. 7 and Fig. 8 respectively. Biodiesel's agglomerated particles tends to gather densely on the paper filter, compared with BE20's agglomerated particles.


Fig. 7 SEM image of biodiesel's agglomerated particles on paper filter at 0.6 MPa and 2000 rpm


Fig. 8 SEM image of BE20's agglomerated particles on paper filter at 0.6 MPa and 2000 rpm

This material is reserved for educational use only, not allowed for commercial use.
Forbidden to modify the content, and cite the document when use.

Visualized by TEM images, each agglomerated paticle consists of many uniformed primary nanoparticles. Figure 9 and Figure 10 show TEM image of biodiesel's and BE20's agglomerated particle in the engine condition of 0.6 MPa load and 2000 rpm. respectively. It can befound that average size of the agglomerated particles has no significant difference among biodiesel's and ethanol blended biodiesel's PM.

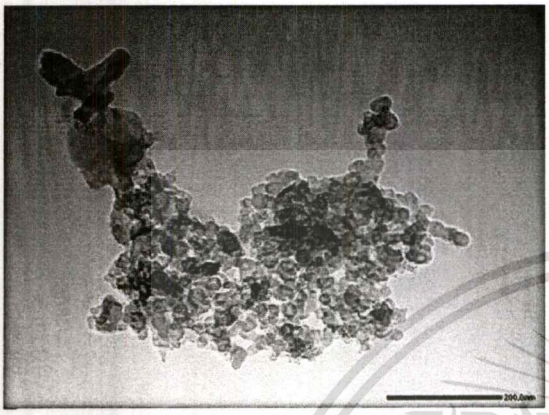

Fig. 9 TEM image of biodiesel's agglomerated particles at 0.6 MPa and 2000 rpm

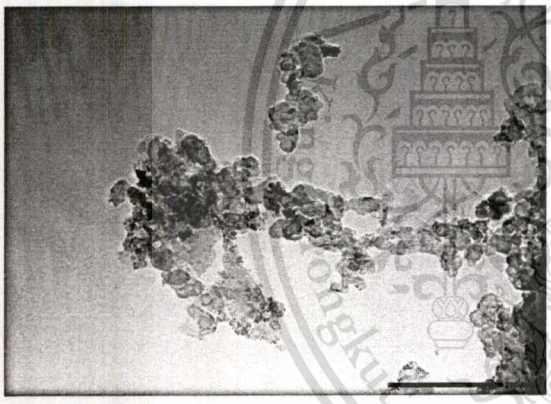

Fig. 10 TEM image of BE20's agglomerated particles at 0.6 MPa and 2000 rpm

Moreover, primary nanoparticles of biodiesel's and ethanol blended's PM was observed with further TEM's magnification so that inner core and outer shell of the primary nanoparticles can be clearly seen. Figure 11 and Figure 12 show TEM image of biodiesel's and BE20's primary nanoparticle respectively. Morphology of biodiesel's primary particle has clear cut and smooth contour compared with ethanol's. Carbon crystallite traces are also clear. While contour of BE20's primary nanoparticle is not smooth and appears incomplete spherical form. It is possible that PM's oxidation from ethanol blended fuel's combustion is stronger around primary particles compared with biodiesel fuel.

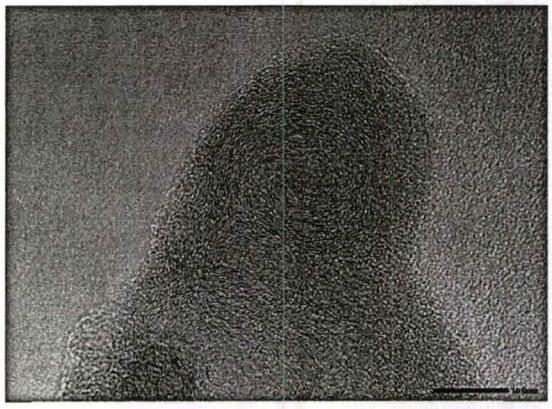

Fig. 11 TEM image of biodiesel's primary particle at 0.6 MPa and 2000 rpm

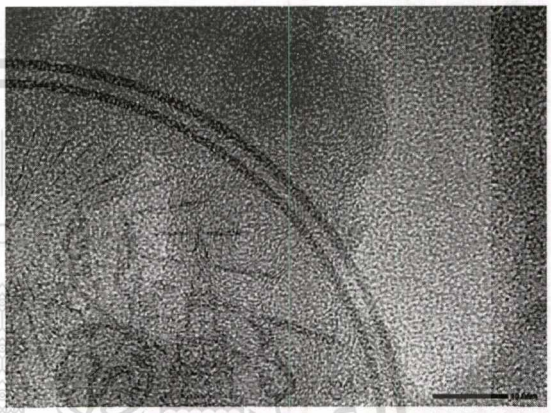

Fig. 12 TEM image of BE20's primary particle at 0.6 MPa and 2000 rpm

## 4. CONCLUSION

The research started with a review of physical fuel properties in order to forecast combustion behavior of the ethanol-blended biodiesel. Then the engine performance test was conducted. Ethanol blended fuel contributed higher BSFC since the nature of lower calorific value compared with biodiesel while BTE has no significant difference. Combustion analysis showed a considerable delayed combustion of the ethanol blended fuel due to lower cetane index and more heat of evaporization. As a result of ignition delay, fuel have more preparation for better atomization leading to rapid premixed combustion with high peak of heat release rate. Early finish in diffusion combustion phase also emphasizes the rapid combustion behavior of the ethanol blended fuel. Combustion behaviors might effect on PM's quantity reduction. However, opacity smoke meter is not the most accurate way to measure PM's quantity since some PM particles that covered by hydrocarbon cannot be detected by the smoke meter.

This material is reserved for educational use only, not allowed for commercial use.
Forbidden to modify the content, and cite the document when use.

PM's morphology and nanostrucuture were successfully investigated by SEM and TEM techniques. Nanostructure of agglomerated particles has no significant difference among biodiesel and ethanol blended biodiesel. However, there were trails of incomplete morphology of BE20's primary nanoparticle. These can be implied that ethanol blended fuel has more potential in PM's oxidation reactivity.

## ACKNOWLEDGEMENT

The authors gratefully acknowledge the academic support from Thailand Advanced Institute of Science and Technology and Tokyo Institute of Technology (TAIST-Tokyo Tech) by National Science and Technology Development Agency (NSTDA) and the financial support from Thailand Graduate Institute of Science and Technology (TGIST), Thailand Research Fund(TRF), and KMITL International College.

## REFERENCES

(1) Preechar Karin, Hiroshi Oki, Katsunori Hanamura, Chinda Charoenphonphanich, Nanostructures and Oxidation Kinetics of Diesel Particulate Matters, The Second TSM International Conference on Mechanical Engineering, 19-21 October, 2011, Krabi

(2) Zhu, L., Cheung, C., Zhang, W., & Huang, Z. (2011). Combustion, performance and emission characteristics of a DI diesel engine fueled with ethanol–biodiesel blends. Fuel, 90(5), 1743-1750. doi:10.1016/j.fuel.2011.01.024

(3) Ramadhas AS, Jayaraj S, Muraleedharan C. Use of vegetable oils as I.C. enginefuels – a review. Renew Energy 2004; 29:727–42.

(4) Graboski MS, McCormick RL. Combustion of fat and vegetable oil derived fuelsin diesel engines. Prog Energy Combust Sci 1998;24:125–64

(5) Hulwan, Dattatray Bapu, and Satishchandra V. Joshi. "Performance, emission and combustion characteristic of a multicylinder DI diesel engine running on diesel–ethanol–biodiesel blends of high ethanol content." Applied Energy 88, no. 12 (2011): 5042-055. doi:10.1016/j.apenergy.2011.07.008.

(6) Kraipat Cheenkachorn, Monpilai H.Narasingha, Jutahawan Pupakornnopparut , Biodiesel as an Additive for Diesohol, Asian Journal on Energy and Environment, 2006, 7(01), 267-276, ISSN 1513-4121

(7) Prbakaran, B., and Dinoop Viswanathan. "Experimental investigation of effects of addition of ethanol to bio-diesel on performance, combustion and emission characteristics in CI engine." Alexandria Engineering Journal (2016)

(8) Tutak, W., Jamrozik, A., Pyrc, M., & Sobiepański, M. (2017). A comparative study of co-combustion process of diesel-ethanol and biodiesel-ethanol blends in the direct injection diesel engine. Applied Thermal Engineering, 117, 155-163. doi:10.1016/j.applthermaleng.2017.02.029

(9) G.K. Prashant, D.B. Lata, P.C. Joshi, Investigations on the effect of ethanol blend on the combustion parameters of dual fuel diesel engine, Appl. Therm. Eng. 96 (2016) 623–631.

(10) Heywood, J.B. (1998). Internal Combustion Engine Fundamental, McGraw-Hill series in mechanical engineering, Singapore.

(11) Karin, P., Borhanipour, M., Songsaengchan, Y., Laosuwan, S., Charoenphonphanich, C., Chollacoop, N., & Hanamura, K. (2015). Oxidation kinetics of small CI engine's biodiesel particulate matter. International Journal of Automotive Technology, 16(2), 211-219. doi:10.1007/s12239-015-0023-4

(12) Karin, P., Boonsakda, J., Siricholathum, K., Saenkhumvong, E., Charoenphonphanich, C., & Hanamura, K. (2016). Morphology and oxidation kinetics of CI engine's biodiesel particulate matters on cordierite Diesel Particulate Filters using TGA. International Journal of Automotive Technology, 18(1), 31-40. doi:10.1007/s12239-017-0003-y

(13) Ishiguro, T., Takatori, Y. and Akihama, K. (1997). Microstructure of diesel soot particles probed by electron microscopy: First observation of inner core and outer shell. Combustion and Flame 108, 1, 231–234.

(14) Vander Wal, R. L., Yezerets, A., Currier, N. W., Kim, D. H. and Wang, C. H. (2007). HRTEM study of diesel soot collected from diesel particulate filters. Carbon 45, 1, 70–77.

(15) Kittelson, D. B. (1998). Engines and nanoparticles: A review. J. Aerosol Science 29, 5-6, 575–588.

This material is reserved for educational use only, not allowed for commercial use.
Forbidden to modify the content, and cite the document when use.

# The 23rd Small Engine Technology Conference

# Call for Papers

SETC 2017 JAKARTA

Society of Automotive Engineers of Japan, Inc. | SAE INTERNATIONAL | IATO SAE-INDONESIA | Patronage of FISITA


**VENUE : JAKARTA CONVENTION CENTER**
**PERIOD : November 15 to 17, 2017**

**DUE DATES**
Abstracts due : January 31, 2017
Draft manuscripts due : April 14, 2017
Final manuscripts due : July 31, 2017

**FOREWORD**

SAE, Society of Automotive Engineers of Japan, Inc., is pleased to announce that the 23rd Small Engine Technology Conference (SETC2017) will be held in Jakarta, Indonesia from November 15 to 17, 2017.

The conference is jointly organized by JSAE and SAE International with the support of Society of Automotive Engineers Indonesia (IATO) and Japan Land Engine Manufacturers Association (LEMA). We kindly ask prospective researchers and engineers in a diversified field of technologies and products with power source to submit electronic abstracts.

The conference offers up-to-date and new information in the development of technologies concerned in an exchange of participants from the globe. The events include technical visits, keynote speech, plenary session, exhibition and poster sessions besides ceremonial events of opening and awards & closing. Lunch & coffee-break for networking, welcome reception and banquet will be served as well.

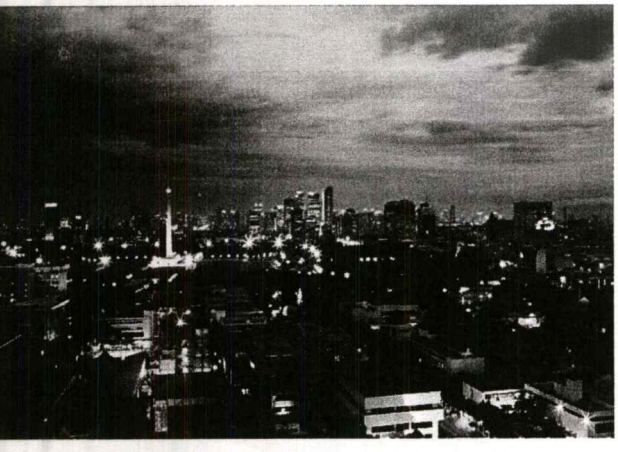

Central District of Greater Jakarta City

**MAIN SUBJECT AREAS**

- **Product Categories** focused in this conference are:

  **Vehicles with power source** such as ATV, Motorcycles, Scooters, Personal Mobility, Marine, Snowmobiles, Recreational Vehicles, Utility Vehicles, Power Assist Devices, Power Assist Bicycles and Unmanned Vehicles.
  *Automobiles, Large Vessels, Large Aircraft, Locomotives and Spaceships are inapplicable.

  **Machines with power source** such as Snow Removal Equipment, Portable Power Generators, Agricultural Equipment, Garden Equipment, Hand Tools and Powered Exoskeleton.
  Technologies applicable for the products above are to be presented in this conference.

- **Technological Areas** focused in this conference are:

  **Combustion Engines** such as 4 stroke Engines, 2 stroke Engines, SI Engines, Diesel Engines, HCCI Engines, Unconventional Engines and Competition Engines.

  **New Energy Sources** such as Hybrid Drives, Electric Drives, Fuel Cells and Solar Cells.

  **Components** such as Chassis, Suspensions, Brakes, Transmissions, Drivetrains, Electrical Systems, Electronic Systems, Fuel Supply Systems and Wheels & Tires.

  **Development Technologies** such as Numerical Simulations, Measurements and Production Technologies.

  **Fuels, Lubricants, and Tribology** such as Alternative Fuels, Fuel Reformations, Additives, Friction Loss and Wear.

  **Vehicle Technologies** such as Dynamics, Handling, Drivability, Safety Technology & Functional Safety and Human Factors & Ergonomics.

  **Environmental Impacts** such as Noise, Vibration, Emissions, Aftertreatment and Life Cycle & Recyclability.

  **Materials** such as Composites, Metal Alloys, Heat & Surface Treatment, New Material and Material Processing.

This material is reserved for
Forbidden to modify the content, and cite the document when use.

. **Language**: English. No simultaneous translation will be provided

. **Submission of Abstracts**

We kindly ask prospective researchers and engineers in a diversified field of technologies and products with power source to submit electronic abstracts of 300 to 500 words on-line via SETC website (URL: http://www.setc-jsae.com/) linked to JSAE Paper Entry System. You will receive an automatic reply upon the submission.

The abstract should include:

- Tentative paper title
- Author (and co-authors) with full name, affiliation, mailing address, e-mail address, telephone and fax numbers.

Each abstract should clearly state:

- The main issues and conclusions
- The process by which the conclusions were reached
- The significance of the work to progress of the relevant engineering area.

Abstract to be received on-line from December 2016.

. **Papers/Presentations**

The papers should be written and presented at the conference, which should be applications oriented. No paper will be accepted without a presentation.

- The papers should be prepared in hard metric (SI) units.
- Material of a purely descriptive nature or containing commercialism should be omitted.
- Final manuscripts should make a contribution to the state-of-the-art technology or present a comprehensive review, be of high technical quality with conclusions supported by technical data.
- A presenting author when his/her final manuscript accepted, is asked to make on-line advanced registration via SETC website linked to the registration system and also to bring his/her own PC for presentation to the venue.
- Your technical paper could be selected for SAE Journal.

. **Exhibition and Poster Session**

OEMs, suppliers and academia will be given an opportunity to exhibit products and technical information during the conference at the venue. Poster session in conjunction with technical session will be also provided to graduate & undergraduate university students, and their researchers.

. **Advertisements and Sponsorship**

Advertisement banner and preliminary & final program will be offered.

Also, the conference sponsorship program will be planned. Information will be available at the SETC website late 2016.

## REPUBLIC OF INDONESIA

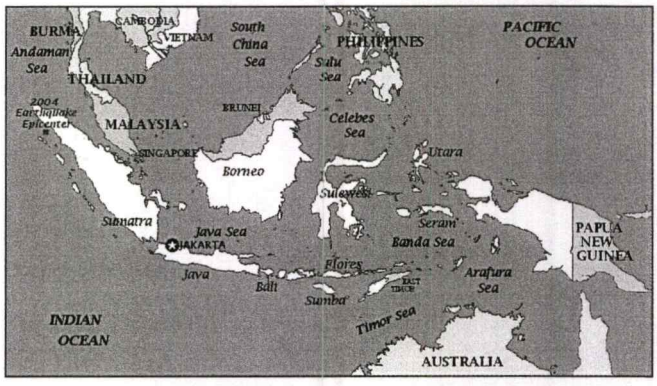


### REPUBLIC OF INDONESIA AT GLANCE

Indonesia is a country in Southeast Asia. Located between the Indian and Pacific Ocean, it is the largest archipelagic state in the world, consisting of more than 18,000 islands. Moreover, Indonesia possesses the 2nd longest coastlines in the world, measuring of 54,716 km. The major islands are Java, Sumatra, Borneo (Kalimantan), Papua and Celebes (Sulawesi). With an estimated population of more than 256 million people, Indonesia is the world's fourth most populous country as well as the most populous Muslim majority country.

### GREATER JAKARTA CITY

Jakarta is the capital city of the Republic of Indonesia which serves as the center of government, as well as the epicenter for finance, business and trade. As the biggest city in Indonesia, Jakarta acts as the main hub for international air connections in the archipelago. The city has many deluxe hotels that offer first class services in rooms, function halls and superb cuisine, whether for individuals or for large delegations. In addition, Jakarta is also famous for offering one of the best shopping venues in South East Asia with numerous modern shopping centers for your consumer needs.

### ACCESS

If you fly to Jakarta using international airline, you will arrive in Terminal 2 or 3 of Jakarta Soekarno-Hatta International Airport. The airport is located on Cengkareng, a district northwest of the city. The distance from the airport to the venue at Jakarta Convention Center is about one to two hours depending on traffic condition. There are several ways that you can get from the airport to Jakarta. The easiest and most convenient is taking a taxi. You'll see plenty of taxi drivers as soon as you leave the arrival terminal.

### INFORMATION ON THE WEB:

INDONESIAN TRAVEL GUIDE:
http://www.indonesia.travel/

JAKARTA TRAVEL GUIDE:
http://www.indonesia-tourism.com/jakarta/

VENUE – JAKARTA CONVENTION CENTER:
http://www.jcc.co.id

**SETC2017 SECRETARIAT**
**Society of Automotive Engineers of Japan, Inc. E-mail: setc2017@jsae.or.jp**
**Website: http://www.setc-jsae.com/**

Forbidden to modify the content, and cite the document when use.

JSAE 20179094 / SAE 2017-32-0094

# Impact of Biodiesel on Small CI Engine Combustion Behavior and Particle Emission Characteristic

**Preechar Karin, Park Watanawongskorn, Jiramed Boonsakda**
**Eakkawut Saenkhumvong, Sippakorn Rungsritanapaisan, Settavit Srivarocha**
**Chinda Charoenphonphanich**
King Mongkut's Institute of Technology Ladkrabang

**Nuwong Chollacoop**
National Science and Technology Development Agency

**Katsunori Hanamura**
Tokyo Institute of Technology

Copyright © 2017 SAE Japan and Copyright © 2017 SAE International

## ABSTRACT

Diesel engines are high thermal efficiency because of high compression ratio but produce high concentration of particulate matter (PM) because of direct injection fuel diffusion combustion. PM must be removed from the exhaust gas to protect human health. This research describes biodiesel engine performance, efficiency and combustion behavior using combustion pressure analyzer. It was clearly observed that PM emitted from CI engines can be reduced by using renewable bio-oxygenated fuels. The morphology and nanostructure of fossil fuel and biofuel PMs were investigated by using a Scanning electron microscopy (SEM) and Transmission electron microscopy (TEM). The morphology of biodiesel and diesel doesn't have much different in the viewpoint of particulate matter trapping using DPF micro surface pores. The agglomerated ultrafine particles and primary nanoparticles sizes of diesel and biodiesel engine's PM are approximately 50-500 nm and 20-50 nm, respectively. The primary particle of biodiesel engine's PM is smaller than that of fossil diesel. The average of diesel and biodiesel PM's carbon platelets is in the range of 0.2-5.2 nm.

## INTRODUCTION

Diesel engines are considered as one of the highest thermal efficiency engines among internal combustion engines (ICE) [1]. However, a major disadvantage is particulate matter (PM) emission which is harmful to human body and environment. Biofuels, such as biodiesel or ethanol, have been often discussed as alternatives for diesel fuel replacement since they are obtained from renewable sources and their benefits in emission reduction. Biodiesel consists of alkyl monoesters of fatty acids derived from vegetable oil or animal fats. Due to its similar physical properties to diesel fuel, there is no need to modify the engine when the engine is fueled with the blends [2-4]. In terms of engine performance and emission, many researchers have investigated effects of biodiesel fuel on diesel engines. M.M. Hasan *et al.* [5] investigated effects of biodiesel by blending with the maximum blend ratio of 30% biodiesel. Operated with a single-cylinder diesel engine, brake thermal efficiency of the blends was similar to diesel base fuel. There was a decrease of nitrogen oxides and smoke emission, while maximum heat release rate and maximum pressure for the blends at higher load were increased. Mohanad *et al.* [6-7] conducted investigations of a 4-cylinder diesel engine powered by rapeseed biodiesel blend. They showed that ignition delay increased for higher cetane number. Sakthivel *et al.* [8] studied performance, emission, and combustion characteristics of a diesel engine, injection timing is a major parameter that sensitively affects the engine performance, emission and durability. The brake thermal efficiency for B20 was higher compared to diesel in the entire load. The ignition delay and combustion duration were shorter for biodiesel than diesel which results in lower heat release rate, peak pressure and rate of pressure rise. Retardation of injection timing caused decrease in emission and combustion parameters like Oxides of Nitrogen ($NO_x$), Hydrocarbon (HC) and Carbon Monoxide (CO), peak pressure, ignition delay, combustion duration and heat release rate which increased with advancement in injection timing. An according research from Guven *et al.* [9] showed that biodiesel blends caused decrease in maximum pressure and heat release rate and retarded further far away from top dead center.

Diesel particulate matters consist of a solid fraction and a soluble organic fraction (SOF). Primary particles of the PMs, composed of carbon and metallic ash, are coated with SOF and sulfate. The mean diameter of primary particles is usually in the range of 20-80 nm. Agglomerated particles are an assembly of primary particles and surface area does not differ appreciable from the sum of specific surface areas of primary particles. Agglomerated particle size is normally 80-300 nm [10]. Scanning Electron Microscope (SEM) and Transmission Electron Microscope (TEM) observation of PMs have been conducted by several researchers [11]. A



This material is reserved for educational use only, not allowed for commercial use.
Forbidden to modify the content, and cite the document when use.

primary soot particle has two distinct parts; an inner core and an outer shell [12-13]. Generally, a primary particle from ICE has only one core with concentric fringe pattern which is hard to be distinguished as inner core or outer shell [14]. Size distributions of diesel engine's PMs have been categorized as PM10, diameter (D) < 10 micron; fine particles, D < 2.5 micron; ultrafine particles, D < 0.1 micron; and nanoparticles, D < 0.05 micron or 50 nm. [15].

# METHODOLOGY

Table 1. Engine specification.

| Items | Details |
|---|---|
| Engine type | 1-cylinder, Natural aspirated, Direct injection, Compression Ignition Engine |
| Bore x Stroke | 97 mm x 96mm |
| Displacement | 709 cm3 |
| Compression ratio | 18:1 |
| Rated power | 9.2 kW @ 2400 rpm |
| Injection timing | 19° CA bTDC |
| Injection pressure | 22 MPa |

Table 2. Fuel properties.

| Properties | Diesel | Biodiesel |
|---|---|---|
| Chemical formula | $C_{14.2}H_{28}$ | $C_{14.9}H_{29.9}O_{1.9}$ |
| Carbon (% mass) | 85.1 | 74.5 |
| Hydrogen (% mass) | 14.0 | 12.5 |
| Oxygen (% mass) | 0.9 | 13.0 |
| Auto ignition temp (°C) | 288 | 294 |
| Calorific value (kJ/kg) | 46,180 | 39,525 |
| Heat of vaporization (kJ/kg) | 250 | 300 |
| Viscosity @ 40°C ($mm^2/s$) | 3.0 | 4.5 |
| Density @ 25°C ($kg/m^3$) | 844.8 | 875.3 |
| Stoichiometric air fuel ratio | 14.7 | 12.3 |
| Distillation (°C) | | |
| T10 | 214.3 | 336.2 |
| T30 | 250.3 | 339.7 |
| T50 | 281.5 | 341.4 |
| T70 | 312.5 | 345.4 |
| T90 | 352.3 | 351.2 |

The experiment was carried out on a 1-cylinder natural aspirated, direct injection, displacement of 709 cm3, compression ratio of 18:1, diesel engine. Fuel injection system was not modified (mechanical fuel injection system). Engine specification was represented in Table 1. The engine was coupled with an eddy-current dynamometer and a control system to adjust engine speed and engine load. Fuel supply system was set with a weight scale to measure fuel consumption. For parameter analysis in the combustion chamber, pressure versus crank angle data were measured by a piezoelectric sensor (Kistler 6052C31, 250Bar, sensitivity: ±0.5%) and a crank angle encoder (CA-RIE-360, resolution: 360 pulses/rev.). Signals of the cylinder pressure were recorded with one-degree resolution of crank angle. For further statistical analysis, two hundred engine cycles were recorded with three repeats. The pressure signals then were amplified with the data acquisition equipment (DEWESoft SIRIUSi-HS-CA) to obtain heat release rate.

The fuels used in this research include commercial diesel and biodiesel (B100). The commercial diesel contains approximately 5% biodiesel due to the regulation while the biodiesel was produced from palm-olein (B100-TIS2313-2549). Fuels properties are shown in Table 2. Biodiesel is more homogeneous molecules which shown by vaporize temperature. It is very narrow and very high around 610 to 620 Kelvin. This implies that biodiesel has higher heat of vaporization. Engine performance curve, brake specific fuel consumption (BSFC) and brake thermal efficiency (BTE) were measured to see overview effects of biodiesel compared with commercial diesel. In-cylinder pressure, net heat release rate, and accumulative heat release from selected engine operating conditions were then recorded to see combustion characteristics.

PM's quantity was measured by an opacity diesel smoke meter (OKUDA DSM-240, 0-100%, ±3% accuracy) which optically evaluate soot collected on paper filters by light reflection method. PM powder was collected by using an in-house metal-net particle collector to investigate morphology and nanostructures by using scanning electron microscopy (FE-SEM: Hitachi SU5000), and transmission electron microscopy (TEM: JEOL JEM-2100Plus)

# RESULTS AND DISCUSSION

## *Combustion Characteristics*

The engine performance curve of diesel and biodiesel is plotted in Fig. 1 (a). Engine load decreases as increasing engine speed for all fuels. Brake specific fuel consumption (BSFC) and Brake thermal efficiency (BTE) are shown in Fig. 1 (b) and (c), respectively. BSFC of the biodiesel are higher than that of diesel at all load conditions due mainly to the lower calorific value. Thus, the amount of fuel supply into the engine must be greater. The trend shows decrease in the BSFC as the engine load increase. It can be explained as; when the engine load increases, combustion temperature which is implied from the rise of Exhaust gas temperature (EGT) as shown in Fig. 1 (d) increases as well. Reactivity of fuel and oxygen activates conversion of combustion heat to mechanical work much more than amount of energy from the fuel input. That is why the BSFC decreases as the engine load increases. BTE plots show that as the engine load increases, the engine produces more thermal efficiency for both fuels. The BTE of biodiesel is higher than diesel at all load condition because the fuel properties such as more oxygen fraction could promote complete combustion which biodiesel could reach optimum BTE at less load compared with diesel.



This material is reserved for educational use only, not allowed for commercial use.
Forbidden to modify the content, and cite the document when use.

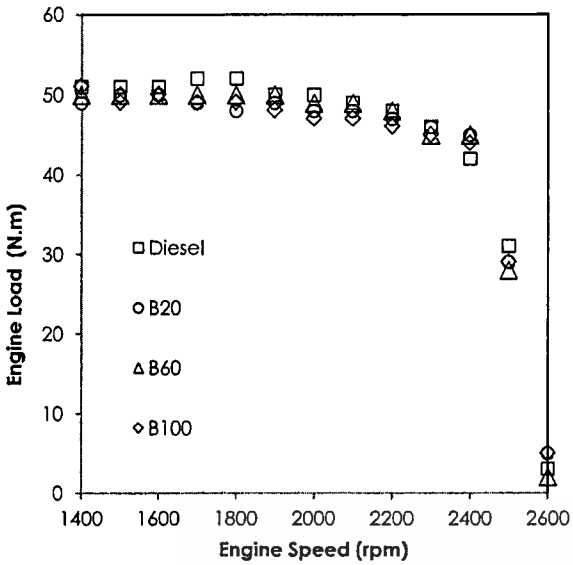


(a) Engine performance

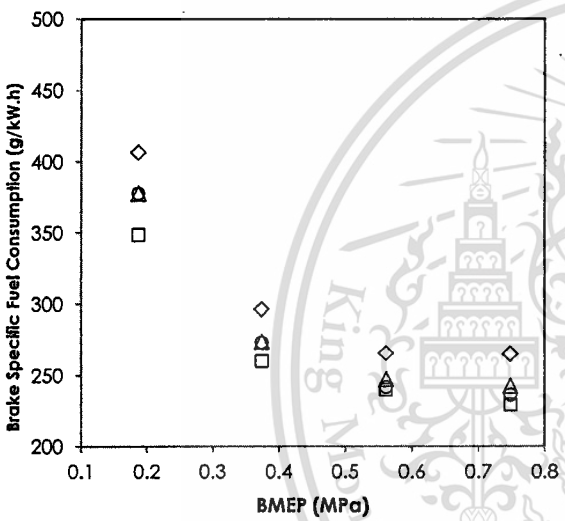


(b) Fuel consumption

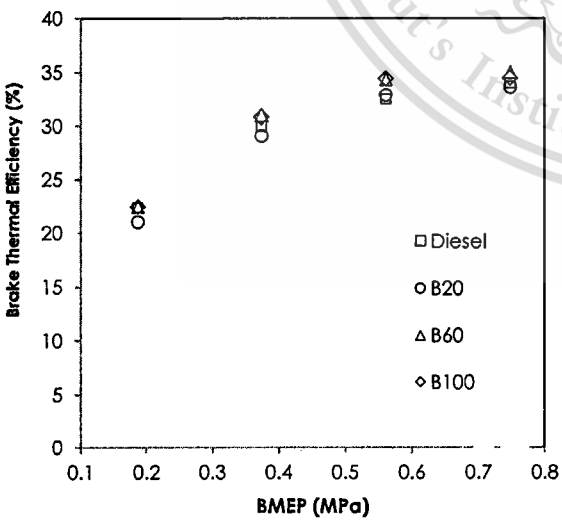


(c) Brake thermal efficiency

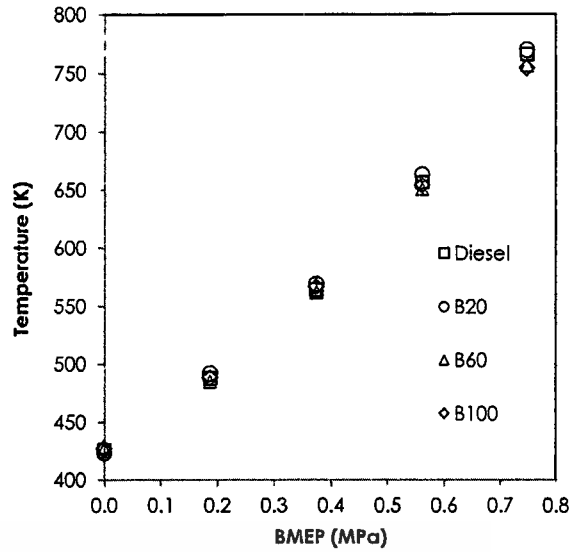


(d) Exhaust gas temperature

Figure 1. (a) Engine performance, (b) Brake specific fuel consumption (BSFC), (c) Brake thermal efficiency (BTE), and (d) Exhaust gas temperature (EGT) at the engine speed of 2000 rpm.

In-cylinder pressure variation with respect to crank angle is shown in Fig. 2, and heat release rate in Fig. 3. The engine load was varied in the range of 0.2 MPa, 0.4 MPa, and 0.6 MPa at constant engine speed of 2400 rpm. Peak pressures of all fuels increase with the increasing engine load. Considering the biodiesel at 0.2 MPa and 0.4 MPa BMEP load, the pressure rises of biodiesel before reaching peak pressure occurs prior to the diesel. This is the effect of higher oxygen fraction in fuel promote faster combustion. At higher engine load, the increase of combustion temperature cause better fuel vaporization for both fuels, so there is no significant in pressure rise with respect to crank angle.

Heat release rate plots show that combustion processes of all fuels start with ignition delay, premixed combustion phase, and followed by diffusion combustion phase. At same start of injection of 19° CA bTDC in the condition of 0.2 MPa and 0.4 MPa BMEP load, biodiesel has shorter ignition delay, while a higher peak of the heat release can be observed on diesel on all load conditions. From fuel properties of biodiesel, density and auto ignition temperature was negative impact with shorter ignition delay, so oxygen fraction is that mainly effects of shorter ignition delay than diesel fuel. The reason is that low temperature in the low load condition with higher oxygen fraction causes the biodiesel start combustion earlier. However, longer ignition delay in diesel causes enough fuel atomization and mixing with oxygen, so it produces higher peaks of heat release rate. In addition, it is also well-known that the high bulk modulus of the biodiesel makes the injection timing earlier in the case of mechanical injection system, which may advance the auto-ignition timing.



This material is reserved for educational use only, not allowed for commercial use.
Forbidden to modify the content, and cite the document when use.

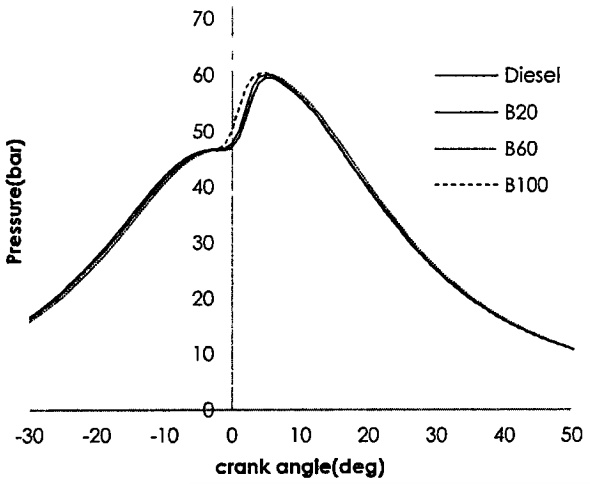


(a) 0.2 MPa BMEP

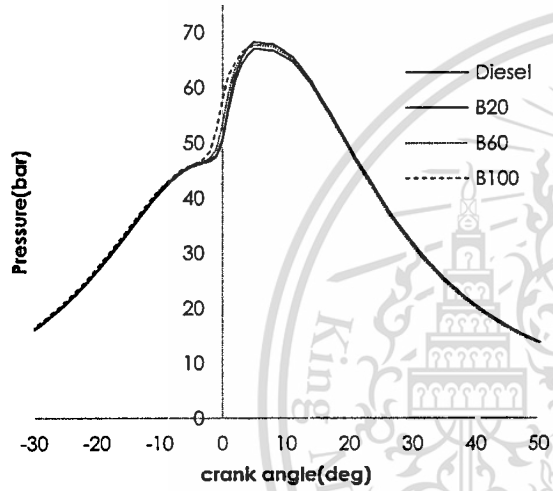


(b) 0.4 MPa BMEP

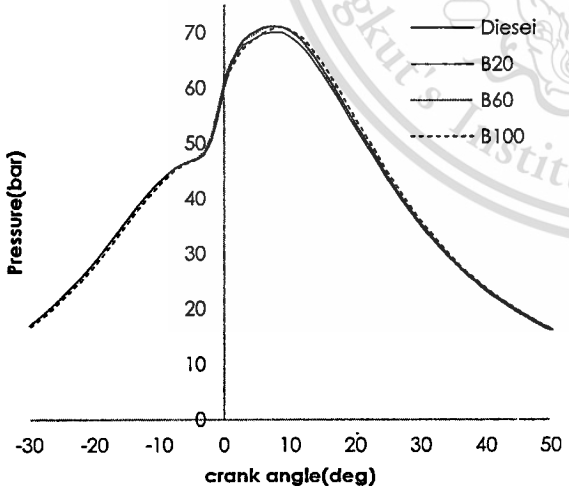


(c) 0.6 MPa BMEP

Figure 2. In-cylinder pressure versus crank angle at engine speed of 2400 rpm, (a) 0.2 MPa BMEP, (b) 0.4 MPa BMEP and (c) 0.6 MPa BMEP.

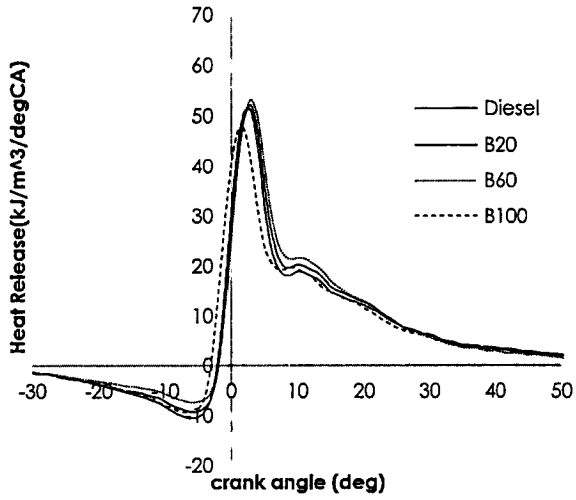


(a) 0.2 MPa BMEP

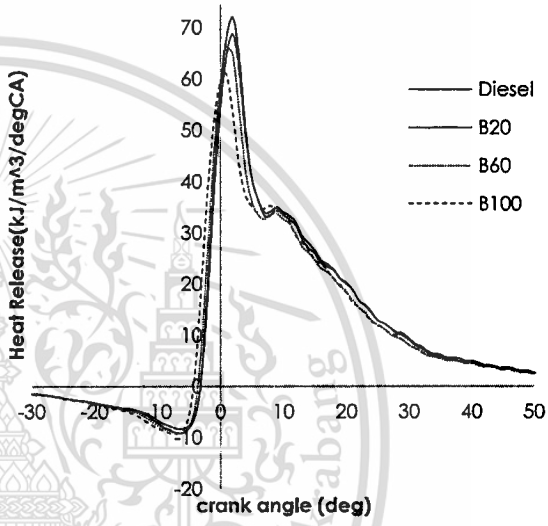


(b) 0.4 MPa BMEP

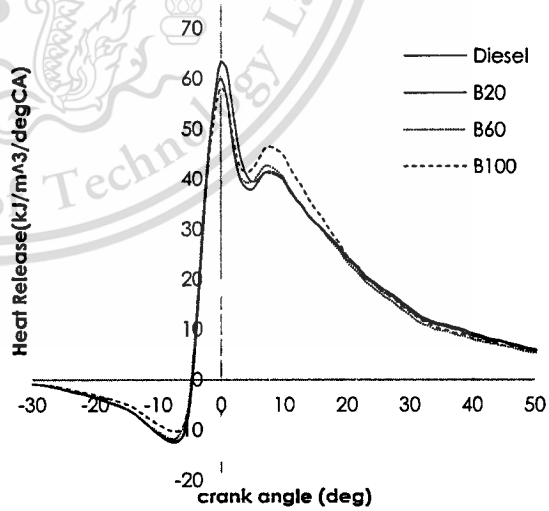


(c) 0.6 MPa BMEP

Figure 3. Heat release rate versus crank angle at engine speed of 2400 rpm, (a) 0.2 MPa BMEP, (b) 0.4 MPa BMEP and (c) 0.6 MPa BMEP.



This material is reserved for educational use only, not allowed for commercial use.
Forbidden to modify the content, and cite the document when use.

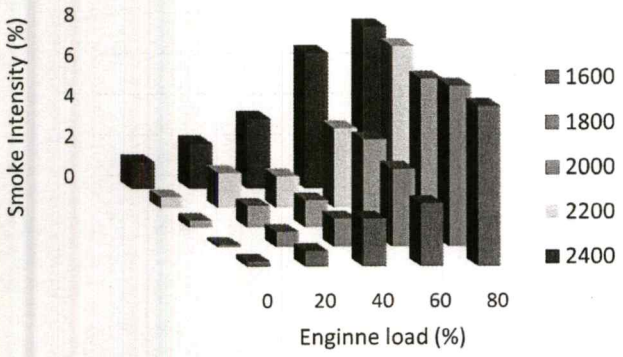


(a) Diesel engine's particulate matter

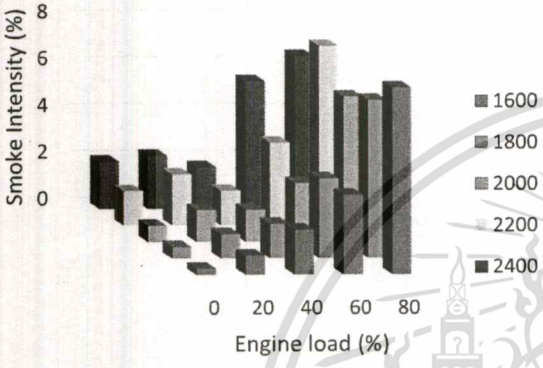


(b) B20 engine's particulate matter

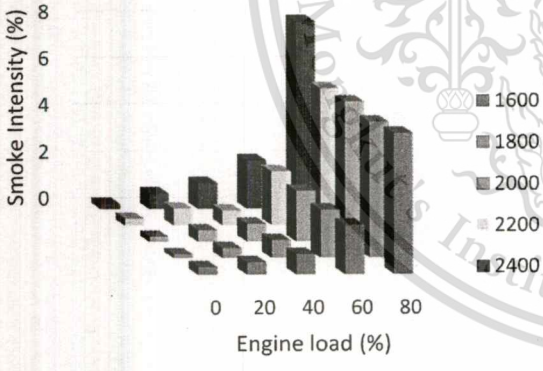


(c) B60 engine's particulate matter

Figure 4. Quantity of (a) diesel (b) B20 (c) B60 and (d) B100 engine's PM using opacity smoke meter in each engine load and engine speed operation condition.

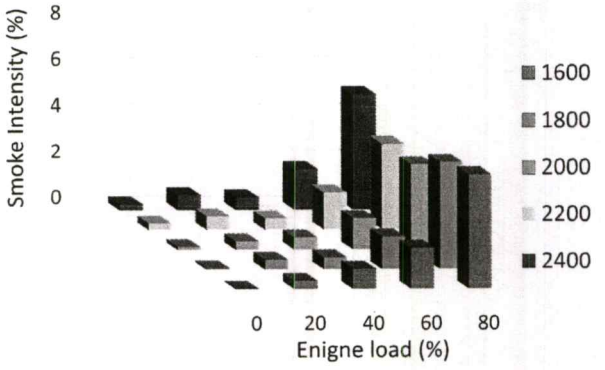


(d) B100 engine's particulate matter

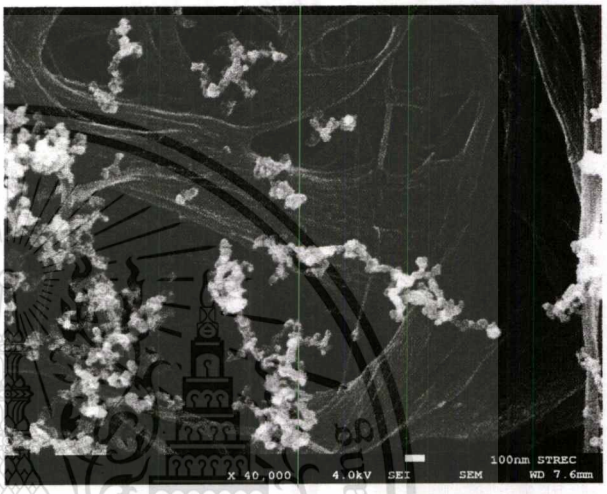


Figure 5. SEM image of diesel engine's fine particle emission in the condition of 80% load engine operation.

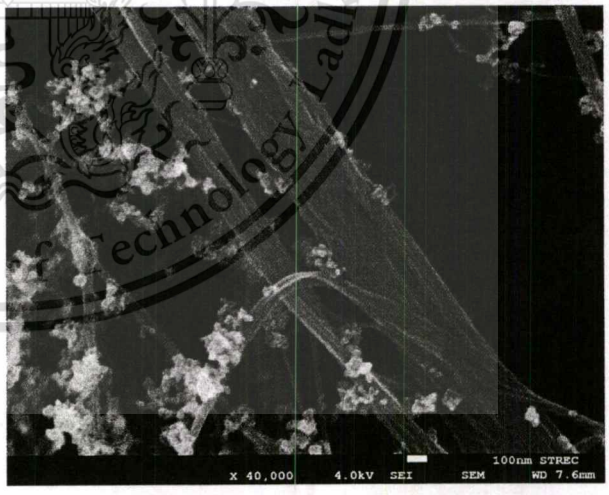


Figure 6. SEM image of B100 engine's fine particle emission in the condition of 80% load engine operation.



This material is reserved for educational use only, not allowed for commercial use.
Forbidden to modify the content, and cite the document when use.

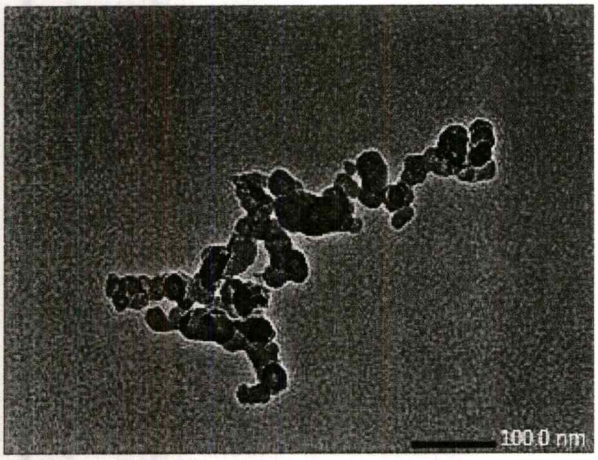


Figure 7. TEM image of diesel ultrafine particle emission in condition 80% load operation.

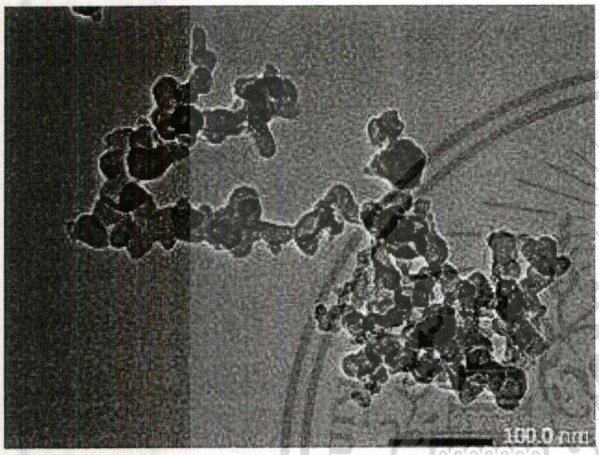


Figure 8. TEM image of B100 ultrafine particle emission in condition 80% load operation.

### *Particle Emission Characteristics*

Figure 4 shows measurement results of smoke intensity which is an indirect method to estimate PM's quantity. The intensity is strongly dependent on the engine load. The more engine load, the greater smoke intensity due to more fuel supply for combustion. In this research, much amount of particle was used to determine the integrity of combustion process. The biodiesel produces less smoke than the diesel at almost all engine operating conditions because oxygenated fuel promote more complete combustion and better fuel-oxygen's reactivity.

Morphology and nanostructure of the PM were investigated by electron microscopy. Some PM's types were found on the paper filters such as fine particles and ultrafine particles. Ultrafine particles of diesel and biodiesel engine's PM consist of many single nanoparticles. Figure 5 and 6 show fine particle of diesel and biodiesel in the condition of 80% (engine torque of 38 Nm) load engine operation, respectively.

Agglomerated ultrafine particles of diesel and biodiesel engine's PM was also clearly observed using TEM as shown in Fig. 7 and 8, respectively. The average agglomerated ultrafine particle diameter size are in the range of 50-500 nm. Primary nanoparticles of diesel and biodiesel engines was also clearly observed using TEM as shown in Fig. 9 and 10, respectively. The average primary nanoparticle diameter size are in the range of 20-50 nm. Each carbon platelet in the inner core and outer shell of primary nanoparticle was also clearly observed by TEM.

Moreover, TEM image is used for numerate platelet number that aggregate layered in the particle. Each of platelet is consisted properly by carbon atom from incomplete combustion product. Figures 11, 12 and 13 are the images of original 10 $nm^2$ focused area, after post processing of two colors and after post processing of skeleton carbon platelet length estimation of diesel fuel. Figures14, 15 and 16 are the images of original 10 $nm^2$ focused area, after post processing of two colors and after post processing of skeleton carbon platelet length estimation of biodiesel, respectively. From the skeleton images, the carbon platelets inside the PM were measured by image processing program. The skeleton carbon platelets, which have 1-unit pixel width for each platelet, were measured for the white area in the image to be a carbon platelet length. The estimated of platelet sizes distribution in each condition are shown in Fig.17 and 18. The average of diesel and B100 PM carbon platelets is in the range of 0.2-5.2 nm.

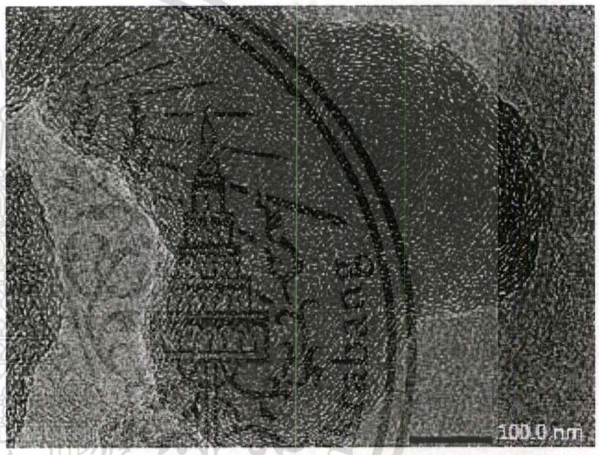


Figure 9. TEM image of diesel primary nanoparticle emission in condition 80% load operation.

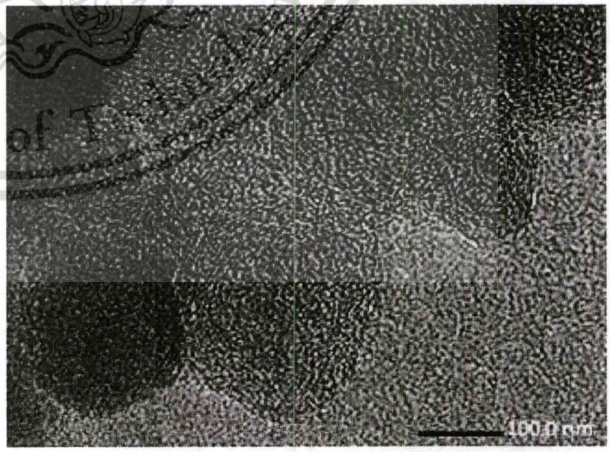


Figure 10. TEM image of B100 primary nanoparticle emission in condition 80% load operation.



This material is reserved for educational use only, not allowed for commercial use.
Forbidden to modify the content, and cite the document when use.

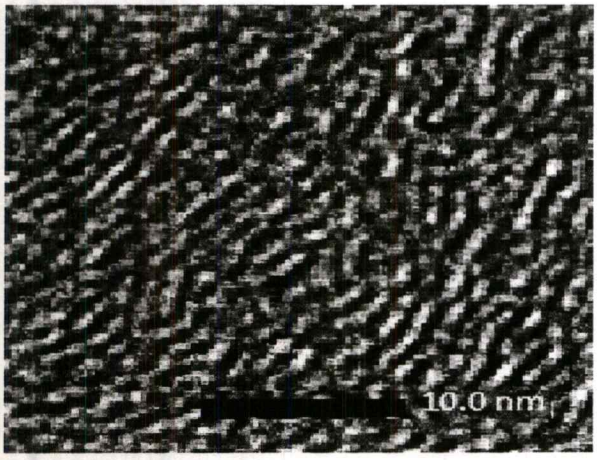


Figure 11. TEM images of engine 80% load operation diesel single PMs.

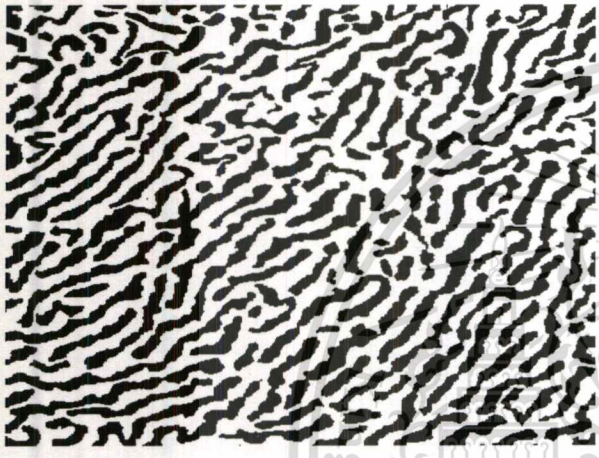

Figure 12. Two colors TEM images post process of engine 80% load operation diesel single PMs 10nm$^2$ focused area.

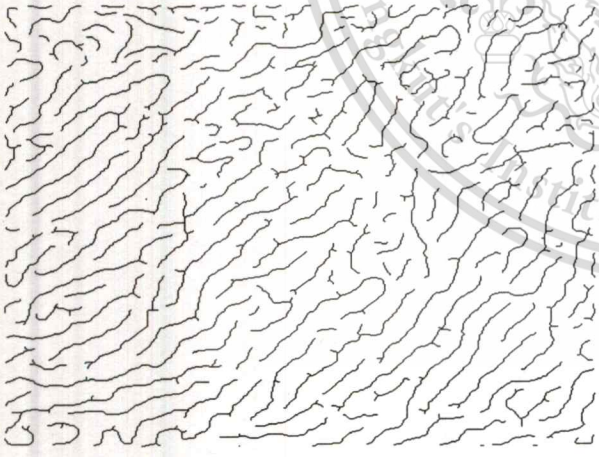

Figure 13. Skeleton TEM images post process of engine 80% load operation diesel single PMs 10nm$^2$ focused area.

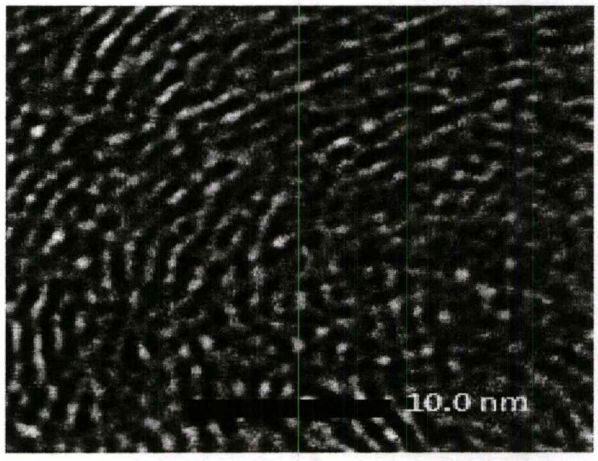


Figure 14. TEM images of engine 80% load operation B100 single PMs.

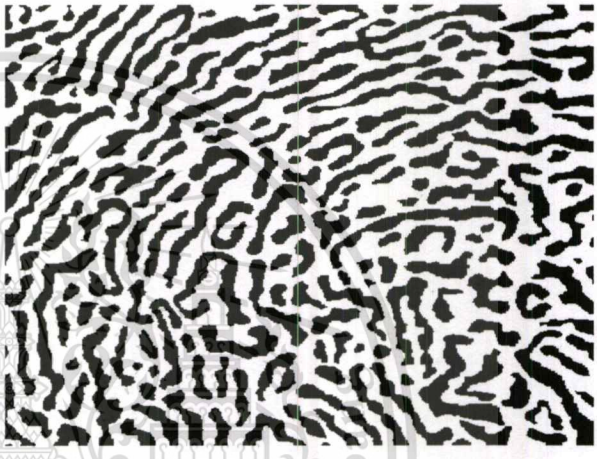

Figure 15. Two colors TEM images post process of engine 80% load operation B100 single PMs 10nm$^2$ focused area.

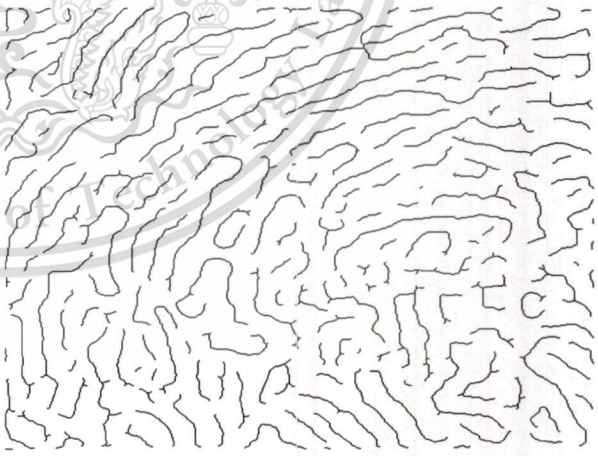

Figure 16. Skeleton TEM images post process of engine 80% load operation B100 single PMs 10nm$^2$ focused area.



This material is reserved for educational use only, not allowed for commercial use.
Forbidden to modify the content, and cite the document when use.

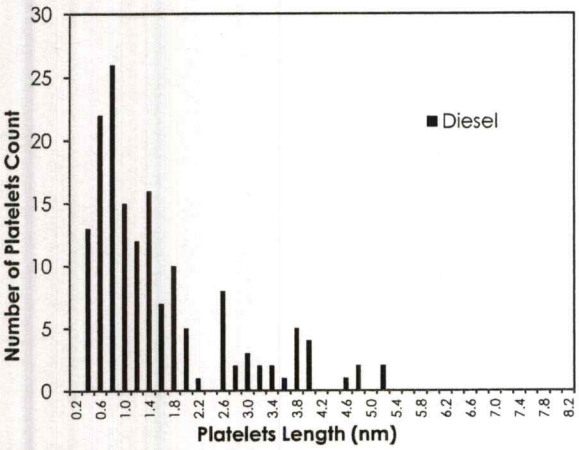


Figure 17. Platelet sizes distribution of diesel PM's carbon platelets.

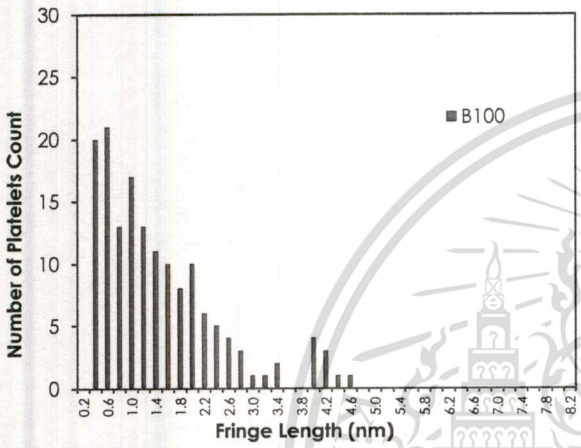


Figure 18. Platelet sizes distribution of B100 PM's carbon platelets.

## CONCLUSIONS

The amount of particulate matter emitted from CI engine depend on several variables. The result shows the parameter which has the highest effect on PM quantity is engine load, concentration of biodiesel and engine speed respectively. When increase concentration of biodiesel in fuel, PM reduce because oxygen concentration in fuel increase. Higher concentration of oxygen makes more complete combustion and higher thermal efficiency. The quantities of particulate matter emitted from biodiesel engine are approximately a half of diesel engine's particulate matter. Morphology of CI engine's PM10, PM2.5, ultrafine particle and nanoparticle was characterized using SEM and TEM successfully. The morphology of biodiesel and conventional diesel doesn't have much different in the viewpoint of particulate matter trapping using DPF micro surface pores.

## REFERENCES

1. J. B. Heywood, Internal Combustion Engine Fundamental, *McGraw-Hill series in mechanical engineering*, Singapore, (1998).

2. L. Zhu, C. Cheung, W. Zhang, and Z. Huang, Combustion, performance and emission characteristics of a DI diesel engine fueled with ethanol–biodiesel blends. *Fuel*, 90 (5), 1743-1750, (2011).

3. A. S. Ramadhas, S. Jayaraj and C. Muraleedharan, Use of vegetable oils as I.C. engine fuels – a review. *Renew Energy*, 29, 727–42, (2004).

4. M. S. Graboski and R. L. McCormick, Combustion of fat and vegetable oil derived fuels in diesel engines. *Prog Energy Combust Sci*, 24, 125–64, (1998).

5. M.M. Hasan and M.M. Rahman, Performance and emission characteristics of biodiesel–diesel blend and environmental and economic impacts of biodiesel production, *Renewable and Sustainable Energy Reviews*,74, 938–948, (2017).

6. M. Aldhaidhawi, R. Chiriac and V. Badescu, Ignition delay, combustion and emission characteristics of Diesel engine fueled with rapeseed biodiesel. *Renewable and Sustainable Energy Reviews,* 73, 178-186, (2017).

7. G.K. Prashant, D.B. Lata and P.C. Joshi, Investigations on the effect of ethanol blend on the combustion parameters of dual fuel diesel engine, *Applied Thermal Engineering*. 96, 623–631, (2016).

8. G. Sakthivel and N. Saravanan and M. Ilangkumaran, Influence of injection timing on performance, emission and combustion characteristics of a DI diesel engine running on fish oil biodiesel, *Energy*, 116, 1218-1229, (2016).

9. G. Gonca and E. Dobrucali, Theoretical and experimental study on the performance of a diesel engine fueled with diesel-biodiesel blends, *Renewable Energy*, 93, 658-666, (2016).

10. P. Karin, H. Oki, K. Hanamura and C. Charoenphonphanich, Nanostructures and Oxidation Kinetics of Diesel Particulate Matters, *Journal of Research and Applications in Mechanical Engineering*, 1(2), 3-8, (2012).

11. P. Karin, M. Borhanipour, Y. Songsaengchan, S. Laosuwan, C. Charoenphonphanich, N. Chollacoop and K. Hanamura, Oxidation kinetics of small CI engine's biodiesel particulate matter. *International Journal of Automotive Technology*, 16(2), 211-219, 2015.

12. P. Karin, J. Boonsakda, K. Siricholathum, E. Saenkhumvong, C. Charoenphonphanich and K. Hanamura, Morphology and oxidation kinetics of CI engine's biodiesel particulate matters on cordierite Diesel Particulate Filters using TGA. *International Journal of Automotive Technology*, 18(1), 31-40, (2017).

13. T. Ishiguro, Y. Takatori and K. Akihama, Microstructure of diesel soot particles probed by electron microscopy: First observation of inner core and outer shell. *Combustion and Flame* 108(1), 231–234, (1997).

14. R. L. Vander Wal, A. Yezerets, N. W. Currier, D. H. Kim and C. H. Wang, HRTEM study of diesel soot collected from diesel particulate filters, *Carbon,* 45(1), 70–77, (2007).

15. D. B. Kittelson, Engines and nanoparticles: A review. *J. Aerosol Science*, 29(5-6), 575–588, (1998).

## ACKNOWLEDGMENTS

The authors gratefully acknowledge the support from Bangchak Corporation Public Co., Ltd., FOCUSLAB Ltd., Thailand Research Fund (TRF), KMITL and NSTDA.



This material is reserved for educational use only, not allowed for commercial use.
Forbidden to modify the content, and cite the document when use.